R. & M. No. 3688

MINISTRY OF DEFENCE (PROCUREMENT EXECUTIVE)

AERONAUTICAL RESEARCH COUNCIL
REPORTS AND MEMORANDA

An Investigation of Annular Aerofoils for Turbofan Engine Cowls

By C. YOUNG
Aerodynamics Dept., R.A.E., Farnborough

LONDON: HER MAJESTY'S STATIONERY OFFICE
1972
PRICE £3·27 NET

An Investigation of Annular Aerofoils for Turbofan Engine Cowls

By C. YOUNG

Aerodynamics Dept., R.A.E., Farnborough

Reports and Memoranda No. 3688*
December, 1969

Summary.

Three annular aerofoils suitable for use as short fan cowls on turbofan engines of high bypass ratio have been tested at zero incidence over a range of subsonic Mach numbers and also in static conditions. Comparisons are presented with experimental results from a conventional type of 'pipe' rig, and with predictions from a linearised and a non-linearised theory. The results show that the effect of the cowl afterbody is fairly small and can be calculated theoretically. Both types of theoretical methods give good predictions of the surface pressure distribution, but the comparison between theoretical and measured mass flow through the cowl deteriorates as Mach number increases.

LIST OF CONTENTS

Section.

1. Introduction
2. Theoretical Calculation of Pressures on Annular Aerofoils
   - 2.1. Linearised theories
   - 2.2. Non-linear theories
   - 2.3. Compressible flow
3. New Cowl Shapes and Test Rig
   - 3.1. Design of cowl shapes
   - 3.2. Design of cowl rig
4. Experimental Results
   - 4.1. Range of test conditions
   - 4.2. Incidence and blockage corrections

* Replaces R.A.E. Tech. Report 69285—A.R.C. 32 241.

4.3. Intake velocity ratio and mass flow ratio

4.4. Drag measurements

4.5. Cowl surface pressure distributions

4.6. Static tests

4.7. Pressure recovery

5. Comparison with Conventional Test

6. Comparison with Theory

7. Conclusions

Acknowledgements

List of Symbols

References

Appendix I. Balance measurements

Appendix II. Mass flow ratio calculation

Tables 1–4

Illustrations—Figs. 1 to 67

Detachable abstract cards

---

1. *Introduction.*

Jet engine cowls have normally been designed and tested on the assumption that the intake and exit flows can be treated separately and that the external flow field depends only on the intake velocity ratio and not on the internal geometry. The development of engines of high bypass ratio has led to a number of designs utilising short fan cowls, for which these basic assumptions can be questioned. Such short fan cowls can be regarded as annular aerofoils in which the circulation developed around the cowl plays an important part in determining both the internal and external flow fields.

The investigation described in this Report forms part of a wider programme of research into the aerodynamics of cowls for engines of high bypass ratio and is particularly concerned with two related problems:

(1) How far is the conventional method of testing the intake as an isolated feature still valid for the new range of geometries?

(2) What use can be made of existing theories for the prediction of the flow around annular aerofoils in the design of improved cowl shapes for these engines?

The conventional type of experimental rig for testing intakes consists essentially of a pipe whose forward end is shaped to a specified contour, and through which the flow is controlled by some form of throttle. Surface pressures are measured around the intake and drag measurements are made using a

pitot-static rake mounted normal to the cowl surface at some convenient point. Typical of this rig are those used by NACA to develop the well known NACA-1 intake shape[1] and the rig designed by Rolls Royce for tests in the A.R.A. 9ft × 8ft transonic tunnel[2], with which comparisons are made in this Report.

In the conventional type of rig, the intake shape is followed by a length of constant diameter pipe and an afterbody. The cylindrical section is designed to be long enough to ensure that the intake and exit flows do not influence one another. The 'pipe' rig is therefore several diameters long. These dimensions are more appropriate to the older type of jet engine; but modern engines have separate fan cowls with length/diameter ratios as small as 1·2*. For such short cowls it seems likely that the flow over the front part of the cowl will be affected by the presence of an afterbody and the conventional type of tests may give misleading results. For the present series of tests, a different type of rig was designed, in which the complete fan cowl is represented as an annular aerofoil. This rig is described in Section 3.2, and a comparison of the results obtained for one intake shape which was also tested on the Rolls Royce B5 rig is made in Section 5.

Intake shapes for subsonic engine nacells have normally been designed empirically, and a large majority of these which have been used to date have been based on the NACA-1 series of shapes[1]. These intakes have been fitted to a variety of afterbody shapes also developed in isolation. Quite separately from this line of development, fairings for ducted airscrews have been developed as annular aerofoils, using design principles analogous to those used for two-dimensional aerofoils. The second and third cowls of this present series were designed in this way using a linearised theory as the design tool; this design method is discussed in Section 2.1 and the design of the cowls in Section 3.1. Comparisons of the measured pressure distributions with those predicted by this linearised theory, and by non-linearised theory are made in Section 6.

2. *Theoretical Calculation of Pressures on Annular Aerofoils.*

2.1. *Linearised Theories.*

A simple theory for calculating the flow around an infinitely thin annular aerofoil at zero incidence in incompressible flow was developed by Küchemann and Weber[3] in about 1942, by using a distribution of bound vortex rings on a quasi-cylinder representing the mean surface of the aerofoil. If v_x and v_r are the axial and radial velocity increments induced by these singularities, then the condition that the aerofoil surface $r(x)$ is a streamline is

$$\frac{dr(x)}{dx} = \frac{v_r(x, r)}{V_0 + v_x(x, r)}. \tag{1}$$

In Küchemann and Weber's theory, the bound vortex distribution was represented by the first three terms of the Birnbaum series, and the unknown vortex strengths found by satisfying equation (1) at three points along the mean surface of the aerofoil.

An extension of this theory was made by Bagley et al.[4] to deal with aerofoils of finite thickness. This was done by adding a distribution of source rings to the bound vortex rings and at the same time, linearising the boundary conditions. This was achieved by placing the singularities on the mean surface $r = R_0$ of the cylinder, by neglecting the $v_x(x, r)$ term in equation (1) and by evaluating the induced velocities on the mean cylinder instead of on the aerofoil surface. Equation (1) then becomes

$$\frac{dr(x)}{dx} = \frac{v_{qr}(x, R_o) \pm v_{vr}(x, R_o)}{V_0} \tag{2}$$

where $r = R_o + z_c \pm z_t$, z_c and z_t being the camber and semi-thickness of the profile, and v_{qr} and v_{vr} the radial velocity components due to the source and vortex distributions respectively.

Equation (2) can be split into 'thickness' and 'camber' parts: the second part was dealt with as in the

* The TF 39 engines for the Lockheed C-5A aircraft have a bypass ratio of 8 and have cowls of this length. More recent designs for civil aircraft have had longer cowls to reduce noise emission.

original theory of Küchemann and Weber, whilst the 'thickness' part of the problem was dealt with by analogy with Weber's treatment[5] of the twodimensional aerofoil. Also by analogy with twodimensional aerofoil theory, the singularity in the loading at the leading edge of the aerofoil was eliminated by using a Riegels factor, thus the linearised velocity distribution around the aerofoil becomes,

$$\frac{V}{V_0} = \frac{1}{\{1+(dz/dx)^2\}}\left[1+v_{qx} \pm v_{\gamma x}\right].$$

Annular aerofoils at an angle of incidence can also be treated by the method of Ref. 4.

This linearised treatment of the problem has been rationalised and further developed in the past few years notably by A. Roberts and others at BAC Weybridge. They use distributions of sources and vortices along the chordal cylinder of the aerofoil and satisfy the boundary condition at points on the same cylinder. A matrix formulation of the equations is used and a set of digital computer programs written which allow the boundary conditions to be satisfied at up to about 100 points. The Roberts programs can also be used to calculate the flow around a pair of concentric annular aerofoils of unequal chord.

The most important new feature introduced by Roberts is an additional vortex distribution which is used to represent the effect of a fan or screen within the annular aerofoil. Küchemann and Weber have shown in Ref. 3 how a fan or screen could be represented in a potential flow model by a vortex distribution on a semi-infinite cylinder extending downstream from the aerofoil into the wake. This is used in a modified form by Roberts. With the computer programs it is therefore possible to calculate the pressure distribution around a prescribed annular aerofoil for any range of values of the intake velocity ratio V_i/V_o (or the corresponding mass flow parameter, μ, defined in Section 4.3).

Fig. 1 shows the incremental velocities predicted by the Roberts method using 8 points and the method of Ref. 3 using only 3 points. The calculations were made for a 12 per cent RAE 103 thickness distribution with a circular arc camber line. The difference can be seen to be quite small.

2.2. *Non-Linear Theories.*

As a consequence of the increasing availability of digital computers, a large number of methods have appeared for calculating the incompressible flow around bodies with distributions of singularities (sources or vortices) on the body surface. All such methods use singularities placed at N points around the contour and calculate the velocity increments induced by these at N points where suitable boundary conditions are imposed. This results in a set of N linear simultaneous equations which can be solved to give the strengths of the singularities. The velocity distribution around the body is then found by summation of the contributions from all the singularities.

In principle, if N is made large enough, the method will give a solution which is exact, provided, of course, that the numerical processes involved are correct. However, most methods so far published are not entirely satisfactory especially when applied to shapes with thin trailing edges.

The method developed at R.A.E. will be described in a further paper. This uses a distribution of sources on the surface and vortex distributions on the camber surface of the cowl and downstream of the trailing edge. The strengths of the sources are determined by applying the boundary condition that the flow is tangential to the surface of the body. Two vortex distributions are used; one to control the flow through the cowl and the other to satisfy the Kutta condition.

The vortex distribution used to control the flow through the cowl extends from the leading edge of the cowl to infinity downstream. The distribution is placed on the camber surface over the chord length of the cowl and on a cylinder of constant diameter downstream of the trailing edge. The strength of the vortex distribution is calculated to give any specified mass flow ratio.

The vortex distribution used to satisfy the Kutta condition only extends over the chord length of the cowl and is also placed on the camber surface. The classical Kutta condition is that there should be smooth outflow at the trailing edge so that the pressure is uniform across the edge. This means that the velocities above and below the trailing edge are equal. In this respect, the isolated annular aerofoil is no different from the two-dimensional aerofoil, but when the annular aerofoil is used as an engine cowl, for example,

the total head of the internal stream is different to that of the external stream. Since the pressure should still be continuous across the trailing edge, there must be a finite velocity difference between the points inside and outside of the trailing edge. In the R.A.E. method, the velocity difference is set equal to the strength of the vortex distribution which extends downstream of the trailing edge.

The inclusion of a Kutta condition means that there are now $N+1$ linear simultaneous equations to solve for the N source strengths and the strength of the Kutta vortex.

2.3. *Compressible Flow.*

The subsonic compressible flow about any body can be calculated by relating it to the incompressible flow about a related body using a Prandtl-Glauert analogy.

For an annular aerofoil this means calculating the flow about an 'analogous' body obtained by multiplying all the radial dimensions of the body by a factor β, ($\beta = \sqrt{1-M_0^2}$). The axial and radial velocity increments thus obtained $\hat{v}_x$ and $\hat{v}_r$ from the incompressible calculation are related to the compressible flow velocity increments by the equations

$$\frac{v_x}{V_o} = \frac{1}{\beta^2}\frac{\hat{v}_x}{V_o}, \quad \frac{v_r}{V_o} = \frac{1}{\beta}\frac{\hat{v}_r}{V_o}.$$

3. *New Cowl Shapes and Test Rig.*

3.1. *Design of Cowl Shapes.*

The external shape of an engine intake is normally specified by two parameters, (see Fig. 10),

(a) d_i/d_m the ratio of the intake highlight diameter to the maximum cowl diameter, and

(b) l/d_m the ratio of the forebody length to the maximum cowl diameter, thus a '90/35' cowl has $d_i/d_m = 0{\cdot}90$ and $l/d_m = 0{\cdot}35$.

The effect of varying these parameters on the pressure distribution and drag characteristics of the NACA-1 intake shape has been widely investigated, but it is not known whether these results can be carried over to other shapes with any confidence. From this experience design 'rules' have been developed which are expressed in geometric terms.

The main requirements from the intake are as follows. In the cruise condition when the cowl is operating in a free stream Mach number of about 0·85 and at a mass flow ratio of about 0·75, the requirement is that the flow over the other surface of the cowl should be devoid of shock waves. This generally means that the cowl should have a fairly large nose radius and thus be thick, but considerations of cowl weight and total drag conflict with this requirement and in most practical applications a thin cowl is preferred. However, should an engine failure occur, then most of the air that would normally be accepted by the engine has to flow around the outside of the cowl—this is commonly referred to as spilling. In general, the suction peaks near the leading edge of the cowl are smaller the larger the nose radius and hence the spillage limit is better when the cowl is thick.

The design compromise is further complicated by the fact that the second parameter, l/d_m, also has a considerable effect. For a given d_i/d_m, the nose radius is reduced as the forebody length, l/d_m is increased, so the spillage limit is poorer. At the other end of the range, the drag-rise Mach number is increased by lengthening the forebody. However, for a fixed chord length there is a limit to how far the crest can be moved back before adverse pressure gradients on the afterbody become too great and the boundary layer separates.

A compromise must therefore be found between the cruise condition and the engine failure case. Naturally the static performance of the intake must also be taken into consideration and this may put an additional limit on the nose radius that can be used. Summing up then, the basic requirement is for a cowl with the minimum weight that will work over a wide range of Mach numbers and mass flow ratios without shock waves or flow separations.

All that has been said so far applies to the outer surface of the cowl and since cowl drag has been defined as the external drag only (*see* Section 4.4) the shape of the outer surface has received far more attention than the inner surface. However, the same amount of care must be exercised over the design of the inner surface if flow separation and the resulting decrease in pressure recovery is to be avoided.

The main parameters for the inner surface are,

(a) the contraction-ratio, i.e. the ratio of highlight area to throat area, and

(b) the position of the throat.

The value of the contraction-ratio required for a specific engine is generally laid down by the engine manufacturer, and is fixed by the amount of flow distortion that can be permitted at the engine face, especially in the cross flow condition. Contraction-ratio values of between 1·2 and 1·35 are now standard for most engines of high bypass ratio. Once the contraction-ratio had been fixed it has been normal practice to fit a 2:1 ellipse or other simple shape between the highlight and the throat. Evidence to suggest that an ellipse is the best shape is slight, and the experimental results for cowl 1, which are presented in Section 4.5, show that such a shape leads to excessively large suction peaks near the throat and suggest that better shapes could be found. Ideally it would be expected that the flow would be accelerated from zero at the stagnation point to the velocity required at the engine face without any over-acceleration. This can be done if rapid changes in curvature at the throat are avoided but unless the throat can be moved further back, the contraction-ratio must be kept low. For example, on cowl 2, which does avoid over-acceleration, the contraction-ratio is only 1·22.

The afterbody of the cowl is also usually designed separately, and again empirical design rules are generally used. The main design aim here is to avoid the large drag penalty associated with boundary layer separation if the curvature of the surface is excessive.

For short cowls it seems unlikely that satisfactory shapes can be designed by patching together the separate forebody, afterbody and internal shapes, and so when designing cowls 2 and 3 the whole cowl shape was designed as one, i.e. from a specified thickness distribution a camber line was found which would give the required pressure distribution. In this way, problems of assembling the various pieces did not arise and the surface curvature was kept continuous around the highlight and crest of the cowl.

Cowl 1 was intended to provide a direct comparison between the present rig and a pipe rig, so it has the same forebody shape as one tested in the A.R.A. 9ft × 8ft transonic tunnel on the B5 pipe rig.

The forebody was a 85/45 shape designed at A.R.A. for a somewhat longer cowl. Ordinates were specified from the crest, through the highlight point to the throat. These were scaled up from the highlight diameter of 5·95 in (0·151 m) used on the B5 rig to 12 in (0·305 m) used on the present rig. The cowl profile was completed to the trailing-edge by fitting a cubic spline curve and a straight line to the outer surface and a circular arc and straight line to the inner surface. The ordinates for the complete cowl are given in Table 1.

Some difficulty was experienced in fitting a satisfactory afterbody to the forebody shape. The problem arose because the surface curvature of the cowl in the region where the forebody is blended into the cylindrical section of the B5 rig has to be kept deliberately low. When the shape was scaled up for a complete cowl with the length to diameter ratio chosen for the tests, the profile crest was found to be as far back as 53 per cent chord. The combination of a prescribed low curvature and such a position of the crest made it very difficult to fit an afterbody without a severe trailing-edge angle. It is not surprising therefore, that the pressure distribution shown in Fig. 3, calculated by linearised theory shows an increased suction level near the crest. This does emphasise that great care is required when fitting separately designed forebody and afterbody shapes to form complete cowls. The pressure distributions calculated at two Mach numbers and mass flow ratios are shown in Figs. 2 and 3.

The design of cowls 2 and 3 was started by choosing a suitable thickness distribution based on two-dimensional experience. Preliminary calculations were made using a 12 per cent R.A.E. 103 thickness distribution but it became obvious that a distribution with a larger nose radius was required; therefore, for cowls 2 and 3 new thickness distributions with circular leading edges were designed. Camber lines were then designed which, in combination with the chosen thickness distribution gave a specified pressure distribution on the outer surface. At this stage the computer program described in Section 2.1 was not

complete, but the matrices appropriate to an eight-point calculation were available and these were used for a manual calculation. As a check on the smoothness of the eight-point solution the pressures on the same profile in twodimensional flow were calculated using Weber's method at 16 points.

Cowl 2 was designed to have a sonic roof top pressure distribution at a Mach number of 0·75 and a mass flow ratio of 0·8. This pressure distribution was chosen because it had worked well for wings and was similar to that originally specified for the NACA-1 shape. The cowl forebody is considerably shorter and slightly thinner than the A.R.A. 85/45 cowl; in terms of the usual parameters it has $d_i/d_m = 0{\cdot}87$ and $l/d_m = 0{\cdot}32$. It was hoped that the increase of spillage effects due to decreasing the nose radius and thickness would be adequately compensated by the reduction in length.

The internal surface of this cowl as calculated is not entirely satisfactory. The contraction-ratio is low, only 1·22, and the surface has slight waviness. Attempts were made to smooth the surface but it was found that this caused considerable distortion to the predicted outer surface pressure distribution. No alterations were therefore made. The theoretical pressure distribution at the design conditions and at a reduced velocity ratio and Mach number are shown in Figs. 4 and 5. The ordinates of the cowl are given in table 2.

For cowl 3 it was decided to return to a value of the contraction-ratio more representative of current practice. A value of 1·26 was eventually chosen while keeping d_i/d_m and l/d_m about the same as for cowl 2. The internal shape from the highlight to the crest is not a 2:1 ellipse and this has helped to keep the suction peak near the throat to a reasonable level. The cowl was designed to have a suction peak near the nose followed by a sonic roof top pressure distribution at the design Mach number of 0·78 and mass flow ratio of 0·8. The theoretical pressure distribution at two mass flow ratios and Mach numbers are shown in Figs. 6 and 7. The ordinates of the cowl are given in Table 3.

The profile shapes for the three cowls are plotted together in Fig. 8, and the slope against curvature distributions in Fig. 9. The important parameters are summarised in Table 4.

3.2. *Design of Cowl Rig.*

A simplified drawing of the cowl rig is shown in Fig. 10 and photographs of it installed in the wind-tunnel in Figs. 11a and 11b.

The rig was designed around an existing six component strain gauge balance mounted in the sting as shown. A solid sting was also manufactured for use when measuring the pressure distribution on the cowl. Both stings have elliptic noses and the dimensions have been kept as small as possible to keep the internal blockage to a minimum.

Three thin support struts connect the cowl to the balance so the drag force on the struts is measured in addition to the cowl forces. Each cowl is turned from Dural castings and was made in two sections so that connections to the static pressure tappings could be made. A total of thirty-three pressures on the cowl can be measured. The pressure tubes are carried from the cowl to the sting inside two of the three support struts whilst the third supports a rake of 17 pitot tubes and a static pressure tube which is offset from the rake to minimise interference effects. This internal rake is used for measuring the mass flow through the cowl.

The flow at the cowl exit is surveyed by a further pitot rake of 20 tubes spaced at 0·4 in (10·2 mm) intervals, and one static pressure tube also offset from the rake. This rake can be rotated through 360 degrees independently of the cowl to check for flow symmetry. The rake is clearly visible in Fig. 11b. The rear rake was intended to be used for measuring the external drag of the cowl but originally there were not enough tubes in the trailing-edge region to do this with any accuracy. A further rake of 6 pitot tubes was therefore added to the rake and was used for the high speed tests on cowl 1 and on cowls 2 and 3 over the whole Mach number range.

A large central plug could not be used to vary the flow through the cowl as in a 'pipe' rig because of the large bouyancy forces that would be generated. A screen was used instead. The screen takes the form of two 'fans', each with eighteen tapered arms of rectangular cross section. These are installed just aft of the three support struts. The front screen is fixed, and the rear screen can be rotated using part of the tunnel roll mechanism. It was hoped that this would provide a continuous variation of flow through the cowl, but it was found that when the screens were just overlapping a large swirl was produced which reacted back on the support struts causing rolling moments high enough to damage the balance. The screens

were therefore used either directly behind one another or with the rear screen displaced by 10 degrees. Figs. 12a and 12b show the screens in these positions. Three sets of mass flow ratios could therefore be covered with the rig, the third case being that with no screens installed. Another thin screen, with half the blockage of the other two was later manufactured and used in the tests on cowls 2 and 3.

One further modification was made after the first series of tests on cowl 1. To use the balance readings, the interference drag from the screens and centrebody has to be estimated. This is difficult as the aerodynamic blockage of the screens is not easy to estimate. A new nose for the centrebody was therefore manufactured with 8 pressure measuring holes installed in it.

4. *Experimental Results.*

4.1. *Range of Test Conditions.*

All the tests were made in the R.A.E. 8ft × 6ft transonic wind-tunnel during March and August 1968 and March 1969.

The first tests on cowl 1 were made on the balance sting and the range of Mach numbers possible was therefore limited by the capacity of the balance. At the highest mass flow ratio the maximum Mach number attainable was 0·7 because of the large drag associated with the shock wave at the throat of the cowl. When the screens are installed the drag force acting on them is balanced by a thrust on the cowl and this thrust was the limiting factor at the lower mass flows. Mach numbers above 0·78 could not therefore be obtained. The tests made in March 1969 extended the Mach number rznge to 0·86 with the cowl mounted on the solid sting.

Balance measurements on the other two cowls could be made up to a Mach number of 0·86 at all mass flow ratios, though for pressure measurements the cowl was mounted on the solid sting.

Transition was fixed on both surfaces of the cowls by bands of ballotini extending from 6·25 per cent to 10·4 per cent chord. On the outer surface 170* grade ballotini was used and on the inner surface, because of the lower velocities, the size was increased to 72** grade. Flow visualisation using ace-napthene on cowls 1 and 3, at a Mach number of 0·7, showed that transition did occur on the inner and outer surfaces of the cowl.

Tests on cowl 1 were mostly made at a tunnel pressure of 0·5 atmospheres but this was increased to 0·75 atmospheres for a limited range of Mach numbers, to investigate Reynolds number effects. The Reynolds number for cowls 2 and 3 was held constant at 2×10^6, based on chord length, over the whole Mach number range. The variation of Reynolds number with Mach number for cowl 1 is shown in Fig. 13.

4.2. *Incidence and Blockage Corrections.*

Most of the tests were confined to a nominal incidence of zero though tests on cowl 2 were also made at incidences of ± 1 degree. Earlier measurements in the 8ft × 6ft wind-tunnel suggested that there was a downwash at the test station varying from 0·4 degrees at $M = 0{\cdot}3$ to 0 degrees at $M = 0{\cdot}9$ but these values have not always been confirmed in other tests. The cowls were therefore set up an inclination of 0·2 degrees to the tunnel axis (at all Mach numbers). As a check on this setting, tests were made at $M = 0{\cdot}7$ and $\mu = 0{\cdot}76$ with the cowl set at incidences of ± 1 degree, and with the cowl rotated through 90 and 180 degrees from its standard position (with the pressure holes facing the roof of the working section). Results in Fig. 48 show some small differences in the measured pressures especially near the peak. Assuming that the variation of $C_{p_{min}}$ with α is linear, it appears that the cowl is misaligned to the main stream direction at that Mach number of about 0·2, $\pm 0{\cdot}1$ degrees indicating a somewhat greater downwash than was assumed initially.

During the later series of tests on cowl 1 (after some modifications had been made to the tunnel) some new downwash figures became applicable. These were checked by rotating the cowl and found to be fairly accurate. The tests on cowl 1 at Mach numbers of 0·7 and above were therefore made at a true zero incidence.

The change in Mach number due to the blockage of the model has been estimated by the usual methods[10]

---

* This means that the spherical grains of ballotini passed through a sieve with 0·0038 in (0·097 mm) square holes, but were retained in a sieve with 0·0048 in (0·122 mm) square holes.

** This means that the spherical grains of ballotini passed through a sieve with 0·0088 in (0·224 mm) square holes but were retained in a sieve with 0·0104 in (0·264 mm) square holes.

to be only about $-0{\cdot}005$ at a free stream Mach number of 0·8. No correction was therefore applied to any of the results.

4.3. *Intake Velocity Ratio and Mass Flow Ratio.*

The flow around an engine cowl is characterised by either of the two related quantities; the mass flow ratio, μ, or the intake velocity ratio, VR.

The mass flow ratio is defined as

$$\mu = \frac{A_o}{A_i} = \frac{\rho_i V_i}{\rho_o V_o}$$

where A is the stream tube area and the subscripts o and i refer to free stream conditions and conditions at the inlet respectively. In these tests the mass flow ratio was measured directly, using the rake of pitot tubes inside the cowl and its associated static pressure by the method outlined in Appendix II. As only one static tube is provided it is assumed that the radial variation of static pressure at this station is small. The inlet area is here defined as the highlight plane. If the area of the stagnation plane is used instead of the highlight area in the definition of the mass flow ratio, then the values of the lowest mass flow ratios quoted should be increased by about 10 per cent. At the higher values of mass flow ratio, the change is smaller since the stagnation point is nearer to the highlight.

The other quantity, the intake velocity ratio, VR, is also quoted on the figures and is defined as the ratio of the mean velocity at the highlight plane to the free stream velocity, V_i/V_o. Though this is not measured directly it can be evaluated from the mass flow ratio using the formula

$$\mu = \frac{V_i}{V_o}\left[\frac{\gamma-1}{2} M_0^2 \left[1-\left(\frac{V_i}{V_o}\right)^2\right]+1\right]^{5/2}.$$

4.4. *Drag Measurements.*

The definition of cowl drag has been given by the Definitions Panel of the Aeronautical Research Council[6]. Only the drag on the external surface is considered, where the external surface extends from the stagnation point to the trailing-edge.

The interest in cowl drag is centred on two areas; the drag at low mass flow ratio and low forward speed corresponding to the condition when an engine failure occurs, and the drag at high Mach numbers and a mass flow ratio of about 0·7 corresponding to conditions at cruise.

As the mass flow through the cowl is reduced, the thrust force which the cowl must support increases. The suction peaks at the nose increase leading to increasing adverse pressure gradients which cause thickening and eventually separation of the boundary layer on the cowl. The corresponding increase in pressure drag on the cowl is commonly referred to as 'spillage drag' since it is associated with the air 'spilling' outwards over the cowl as the entry streamtube area reduces.

A similar increase in pressure drag occurs as the free stream Mach number increases at a fixed mass flow ratio. Again, the external suction peaks increase, leading to boundary-layer thickening and separation, in this case associated with the appearance of shock waves, and again the cowl drag increases.

Drag measurements on cowl 1 using the rake could only be made in the second series of tests because the spacing of the pitot tubes on the original rake was too great. The wake traverse results shown in Fig. 14 are therefore limited to Mach numbers above 0·7.

At low Mach numbers the drag coefficient was estimated using flat plate turbulent skin friction coefficients. The drag values obtained in this way were lower than of those measured on the B5 rig at A.R.A. However, a direct comparison is not possible. The drag measuring rakes on the B5 rig are situated a few inches behind the afterbody so that the measured drag includes the skin friction drag of the cylindrical centre section and afterbody in addition to the forebody drag. The ratio of the surface area to frontal area on the B5 rig is about three times that of the R.A.E. cowl rig, so the two sets of results are substantially in agreement at low speed; the results at higher speed are compared in Section 5.

All the drag coefficients for cowls 2 and 3 were obtained using the rake with the six additional pitot tubes. A typical set of boundary layer profiles measured at the trailing-edge of the cowl at low speed are shown in Fig. 15. The result of a boundary layer calculation by Green's extension of Head's method[7] is shown in Figs. 16 and 17. These show that there is no significant difference between the cowls. This is not confirmed by the experimental results shown in Figs. 18 and 19 which imply that cowl 2 had a higher drag than cowl 3 at all Mach numbers. This is because it is extremely difficult to set up the extra pitot tubes in the position intended and some earlier results had shown that a displacement of the rake by 0·024 in (0·61 mm) (half the diamter of a pitot tube) from the trailing-edge, would more than double the drag level. The results in Figs. 18 and 19 therefore, should not be taken as absolute values though the differences in drag at different mass flows and Mach numbers should be correct.

It is doubtful if absolute drag levels could be measured on such a rig unless there was some way of setting up the pitot rake with extreme precision. The most reliable method of obtaining drag coefficients is probably to perform a boundary layer calculation on the measured pressure distribution.

The drag measured by the strain gauge balance is the sum of

(Internal and external skin friction drag) + (Internal and external pressure drag) + (strut drag).

The pressure drag term is the sum of the forces on the isolated cowl plus the forces due to interference of the struts, screens and centrebody. Estimates of the various terms are made in Appendix I where it is shown that the balance results are reasonably consistent with the wake traverse results.

4.5. *Cowl Surface Pressure Distributions.*

The pressure distributions for the three cowls over the range of Mach numbers and mass flow ratios covered in the tests are shown in Figs. 20 to 48. The effect of changing Reynolds number on the measured distribution is small as shown in Fig. 20 and all the other distributions on cowl 1 are at the lower Reynolds number.

Cowl 1 does have the suction peak near the crest predicted by the theory and this peak interacts in an unusual way with the shock on the forebody at high Mach numbers, which explains the dip in the drag coefficients shown in Fig. 14. At $M = 0{\cdot}82$, there is a shock at about 40 per cent chord, i.e. ahead of the crest, and the drag is just beginning to rise, but at $M = 0{\cdot}84$ this shock has disappeared and the height of the peak at 60 per cent chord has dropped considerably. The pressures measured on the rake behind the cowl indicate that there is probably an isentropic recompression back to the trailing edge or a very weak shock at this Mach number. With a further increase in Mach number to 0·86, the peak at 60 per cent chord has grown again and a shock has appeared on the afterbody with a corresponding increase of drag.

Pearcey has pointed out[8] that this link between two separate regions of transonic flow has been observed on two-dimensional aerofoils and quotes an example from Ref. 9. In this example, the flow over an aerofoil with a bulge at an angle of incidence of 4 degrees showed very similar behaviour. At a Mach number of 0·711, the flow pattern was similar to that on cowl 1 at a Mach number of 0·82. Two shocks were present, one at about 33 per cent chord, the other at about 40 per cent chord. At a Mach number of 0·717, the forward shock had disappeared and the rear shock had moved back slightly but there was not the marked reduction in suction level observed on the cowl. However, on the aerofoil there was no reduction in drag, which in fact increased quite rapidly at Mach numbers greater than 0·711.

Dips in the C_D v M curves are becoming increasingly common as more experiments are made on aerofoils and cowls with peaky pressure distributions, but drag reductions as large as those measured on cowl 1 are unusual and the drag results of cowls 2 and 3 are more typical.

The inner surface pressure distributions of cowl 1 at the high mass flow ratio shows a very high suction peak at the throat. At a Mach number of 0·7 this had developed into a shock wave causing internal flow separation and a consequent decrease in the mass flow ratio.

The other two cowls show quite similar supercritical behaviour although the shock wave on cowl 2 is further back in most cases. Cowl 2 does not have the sonic roof-top pressure distribution because the mass flow is lower than expected, though the inner surface distribution has the desired features.

In some figures the inner surface pressure distribution is plotted for one mass flow ratio only, in order to keep the presentation consistent; the shape of the distribution does not change as the mass flow is reduced.

4.6. *Static Tests.*

Cowls 2 and 3 have very different internal contraction shapes, and it was thought that this might lead to significant differences in their performance at zero forward speed. Consequently static tests were made on the rig shown in Figs. 49a and 49b.

Air was drawn through the cowl by a 275 horsepower centrifugal compressor. At the lowest speed at which it was possible to run the motor without overheating, the air velocity through the cowl, as measured by the pitot-static combination on the internal rake was 300 ft/s. Lower speeds were then obtained by throttling the fan exhaust system. Pressures were measured at points around the inlet using alcohol manometers.

The cowls were placed in a box so that the front of the box was at about 70-80 per cent chord; it was then hoped that in this position there would be no interference with the flow around the cowl lip. However, experiments with a piece of card fixed normal to the surface at 35 per cent chord and at right angles to the chord, suggested that the flow around the intake was very sensitive to disturbances, and the results may not be completely free of all interference from the box. As shown in Fig. 50, a 10in × 3in (25·4 cm × 7·62 cm) card caused reattachment of the boundary layer at the lip, and even when the card was reduced to a 1 in (2·54 cm) square it still affected the flow.

In view of this evidence it is doubtful whether much significance can be attached to the comparison between the results for the two cowls in Figs. 51 and 52. However, it may be noted that, at a velocity of about 200 ft/s in the throat, the length of the region of separated flow was more extensive on cowl 2 (which has the lower contraction-ratio).

On both cowls there was a tendency for the boundary layer to reattach intermittently but the lag in the manometer tubes did not permit a record to be made of the associated variation in the pressures.

Fixing transition on the outside of the cowl did not appear to make any significant difference.

4.7. *Pressure Recovery.*

The pressure recovery, defined as

$$\frac{\bar{H}}{H_o} = \frac{1}{H_o}\int H \frac{dA}{A},$$

could not be measured accurately in the tests because the boundary layer at the measuring station is so thin and only one of the pitot tubes gave a reading that differed from H_o. A simple estimate using a 1/7th power law profile passing through the measured value showed that the pressure recovery never falls below 99 per cent at all Mach numbers with the exception of cowl 1 at the highest mass flow ratio when a shock at the throat provoked separation.

5. *Comparison with Conventional Test.*

The comparisons between the pressures measured on the A.R.A. B5 forebody rig and the R.A.E. cowl rig are shown in Figs. 53 to 56.

At low Mach number the full cowl of the R.A.E. tests shows higher suction levels than on the forebody alone. This would be expected for two reasons. The addition of the afterbody produces a cambered profile; and thus increases the circulation; the displacement flow is also modified since the afterbody can be simulated by adding a distribution of sinks to the sources representing the forebody. An incompressible calculation shows that about 80 per cent of the measured difference is due to the increase in circulation. As the Mach number is increased the difference in suction levels increases and when supercritical flow is present the distributions are quite different in character.

The drag rise on the complete cowl is associated with the development of the rear shock wave, but this

development is interrupted between Mach numbers of 0·82 and 0·84 by the favourable intereaction between the forebody and afterbody shocks. The drag rise in the A.R.A. tests is due to the rearward movement of the single forebody shock and occurs when this shock has reached about 80 per cent of the forebody length. From this comparison alone it is difficult to say with certainty whether the drag rise of the complete cowl would be less than that on the intake alone. It is expected however, that a complete cowl with a more normal conventional afterbody pressure distribution will have a lower drag rise Mach number than the corresponding isolated intake because of the higher suction levels.

6. *Comparison with Theory.*

In this section, comparisons are presented of the measured pressure distributions with those predicted by two calculation methods.

The linearised theory used was that outlined in Section 2.1; for these comparisons, the full program utilising 20 points was used. Some results from the R.A.E. non-linearised program described in Section 2.2 are also presented.

The main difference between the two approaches is that in the linearised calculations the singularities are placed on a mean cylinder, whilst in the non-linearised case the singularities are placed on the body surface. The latter, therefore, would be expected to be more exact. Conditions at the trailing edge are satisfied automatically in the linearised calculation by appropriate choice of vortex distributions, but in the non-linearised method the problem is more difficult and has not been adequately solved in any method published so far. The new method overcomes all the difficulties by using two separate vortex distributions in addition to the singularities on the surface, so it is possible to change the flow through the cowl while satisfying the Kutta condition.

The results of the linearised calculation are shown in Figs. 57 to 62. The agreement between the experimental and predicted pressure distributions is remarkably good at low Mach numbers; even the leading edge suction peaks and the suction peak or the throat cowl 1 being predicted quite accurately.

At high Mach numbers the position is different. The outer surface agreement is generally fairly good considering that the velocities at the peaks are just supersonic. On the inner surface, however, the agreement is very poor; the discrepancy in pressure coefficient being as high as 0·5 in one case. The reason for this seems to be that the internal velocity ratio is wrong. Exhaustive checks on the computer program have failed to discover any error, so it appears that there is a deficiency in the mathematical model of the flow.

Figs. 63 to 67 show the results from the R.A.E. non-linearised calculation. The effect of the support sting was included in these calculations. The agreement is very good in all cases except perhaps over the first 1·5 per cent chord where the calculation overestimates the suction level. The calculations were made with only 70 points on the cowl surface and the agreement may improve if this number is increased.

7. *Conclusions.*

This investigation had two principal objectives. The first was to investigate the pressure distribution and drag characteristics of an intake shape incorporated into a short complete cowl and to compare these with the corresponding results for the intake shape fitted to a long pipe. The results show that the local velocities on the outer surface of the complete cowl are higher at all values of the intake velocity ratio and flight Mach number, and that this difference is due mainly to the additional circulation around the profile. This effect is not large and would be smaller for the longer cowls now favoured for turbofan engine nacelles.

The second main objective was to investigate the effectiveness of various theoretical methods for predicting pressure distributions on cowls and for designing cowls with prescribed pressure distributions. This is envisaged as a step towards replacing the present empirical design rules for cowl shapes by a more rational process based on design for the required flow pattern, similar to the design process now used for aerofoils, but this wider aspect is not considered in the present Report.

The theoretical methods are found to predict the pressure distribution on the cowl to a reasonable degree of accuracy. Of the available calculation methods that based on linearised theory is more satisfactory since problems at the trailing-edge are avoided at any mass flow ratio. However, the results presented show that modifications to both types of programs are required to improve the agreement on the inner surface.

Comparison of the measured pressure distributions with the drag measurements for cowls 2 and 3 show that the drag rise does not occur until the flow is substantially supercritical and a shock is present behind the crest. Consequently, it is not possible to draw any general conclusions relating the design (incompressible) pressure distribution with the drag characteristics, although it is probably significant that cowl 3 designed for a 'peaky' pressure distribution has a higher drag rise Mach number.

The spillage boundaries for these cowls was not determined in these tests though some low-speed tests with more blockage in the cowl may be made later. Static tests, however, did not show any significant differences even though the shapes tested were quite dissimilar.

Acknowledgements.

The author would like to express his appreciation of the help received from the Aircraft Research Association, Hawker Siddeley Aviation and Rolls Royce during this investigation.

LIST OF SYMBOLS

A	Stream tube area
c	Cowl chord length
C_D	Cowl drag coefficient
$C_{D_{pre}}$	Pre-entry drag coefficient
$C_{D_{skin}}$	Skin friction drag coefficient
C_p	Static pressure coefficient
C_p^*	Static pressure coefficient for local Mach number of unity
d	Cowl diameter
H	Total pressure
L	Forebody length
M	Mach number
p	Static pressure
r	Radial coordinate
R_o	Mean radius of cowl
t	Cowl thickness
v_x, v_r	Velocity increments in x, r directions
v_{qx}, v_{qr}	Velocity increments in x, r directions due to source distribution

v_{yx}, v_{yr}	Velocity increments in x, r directions due to vortex distribution
V	Total velocity
VR	Velocity ratio $= V_i/V_o$
x	Axial coordinate
z	Aerofoil thickness measured from cylinder of radius R_o
$z_c(x)$	Camber line shape
$z_t(x)$	Aerofoil thickness distribution
α	Angle of incidence
β	$\sqrt{1-M^2}$
δ^*	Displacement thickness of boundary layer
μ	Mass flow ratio
θ	Momentum thickness of boundary layer
ρ	Local radius of curvature

Subscripts

i	Inlet or highlight station
m	Maximum diameter station
o	Free-stream conditions
s	Measuring station (Appendix II)

REFERENCES

No.	*Author(s)*	*Title, etc.*
1	D. D. Baals, N. F. Smith and J. B. Wright	The development and application of high critical speed nose inlets. N.A.C.A. Report 920 (1948).
2	M. C. Hitchcock	The spillage drag of NACA-1 series intake cowlings. Bristol Siddeley Engines Ltd., PD 1429/1. February 1967.

REFERENCES—*continued*

3 D. Küchemann and J. Weber — *Aerodynamics of propulsion.* McGraw Hill, Chapter 3, pp. 49–52 (1952).

4 J. A. Bagley, N. B. Kirby and P. J. Marcer — A method of calculating the velocity distribution on annular aerofoils in incompressible flow. A.R.C. R. & M. 3146 (1958).

5 J. Weber .. .. .. — The calculation of the pressure distribution over the surface of two dimensional and swept wings with symmetrical aerofoil sections. A.R.C. R. & M. 2918 (1953).

6 Definitions Panel of the A.R.C. — Definitions of the thrust of a jet engine and of the internal drag of a ducted body. A.R.C. C.P. 190 (May 1954).

7 J. E. Green .. .. .. — Extension to compressible flow of Head's entrainment method of turbulent boundary layer prediction. R.A.E. Technical Report (to be published).

8 H. H. Pearcey .. .. .. — Private communication.

9 L. Howarth (Editor) .. .. — *Modern Developments in Fluid Dynamics—High Speed Flow.* Oxford, Vol. 2, Chapter XII, p. 637 (1953).

10 H. C. Garner (Editor) .. — Subsonic wind tunnel wall corrections. Chapter VI. Wall interference in tunnels with ventilated walls. Agardograph 109, October 1966.

11 D. H. Wilkinson .. .. — A numerical solution of the analysis and design problems for the flow past one or more aerofoils or cascades. A.R.C. R. & M. 3545, (1967).

APPENDIX I

Balance Measurements

In Section 4.4 it is stated that the various terms that comprise the balance measurements could be estimated; a comparison of these estimates and the measured values are given below.

The balance drag is made up as follows:—

Balance drag = Total skin-friction drag + pressure drag on the cowl + strut drag + interference drag from the screens and centrebody.

In inviscid flow, the interference drag is equal and opposite to the drag force measured on the centrebody and screen; in the calculations this was obtained by integrating the pressure distribution measured on the centrebody. The total skin-friction drag and the strut drag were estimated using the data in the R.Ae.S. data sheets. The total pressure drag was obtained by graphically integrating the pressure distribution

measured on the cowl; because of the sparseness of the pressure points on the inner surface, this term is probably the most unreliable.

The comparison is not continued for Mach numbers greater than 0·5 because, at the next highest Mach number, shock waves were present on the outer surface of the cowl.

It was expected that the agreement between the balance and estimated results would be best when the cowl was empty since the presence of the 'fans' tended to separate the flow and this is not accounted for in the present comparison. This is partially borne out by the figures below (Table A.1). Case 1 corresponds to the empty cowl, case 2 with the thin screen installed and case 3 with one 'thick' screen installed.

TABLE A.1.

M_o	$\frac{V_i}{V_o}$	Case	Estimated skin friction drag	Interference drag	Pressure drag	Strut drag	Estimated total drag	Balance drag
Cowl 2								
0·3	0·69	1	0·04570	−0·01323	−0·02422	0·0137	0·02195	0·02568
0·3	0·64	2	0·04614	−0·01892	−0·03568	0·0139	0·00544	0·01693
0·3	0·60	3	0·04631	−0·02192	−0·05152	0·0141	−0·01303	−0·01224
0·5	0·67	1	0·04424	−0·01564	−0·02690	0·0137	0·01540	0·02429
0·5	0·62	2	0·04474	−0·02112	−0·04208	0·0138	−0·00456	0·01096
0·5	0·58	3	0·04508	−0·02561	−0·05352	0·0141	−0·01995	−0·00507
Cowl 3								
0·3	0·73	1	0·04558	−0·00805	0·00102	0·0137	0·05225	0·03213
0·3	0·68	2	0·04592	−0·01417	−0·01680	0·0139	0·02885	0·02323
0·3	0·64	3	0·04620	−0·01919	−0·03252	0·0141	0·00859	0·00737
0·5	0·70	1	0·04407	−0·00897	−0·00352	0·0137	0·04528	0·02996
0·5	0·65	2	0·04446	−0·01737	−0·02156	0·0139	0·01943	0·02017
0·5	0·60	3	0·04474	−0·02323	−0·04276	0·0141	−0·00715	0·00256

APPENDIX II

Mass Flow Ratio Calculation

In Section 4.3 it was stated that the mass flow ratio was calculated using the 17 pitot tubes and the static pressure tube on the internal rake; the calculation method is outlined below.

If Q is the mass flow at any station, then the continuity equation gives

$$Q_o A_o = Q_i A_i = \int Q_s A_s$$

where the subscripts s refers to the measuring station.

Thus

$$\mu = \frac{A_o}{A_i} = \frac{1}{A_i}\int \frac{Q_s}{Q_o} dA_s. \tag{B.1}$$

The energy equation can be written in the form (equation 9–7, p. 189, Ref. 3)

$$\frac{\gamma}{\gamma-1}\frac{H}{\rho_{\text{stag}}} = \frac{\gamma}{\gamma-1}\frac{p}{\rho}+\frac{V^2}{2}, \tag{B.2}$$

where ρ_{stag} is the density at the stagnation point

and

$$\frac{\rho_{\text{stag}}}{\rho} = \left(\frac{H}{p}\right)^{1/\gamma}$$

Then

$$\begin{aligned} Q^2 &= \rho^2 V^2, \\ &= \frac{2\gamma}{\gamma-1}\left[H\rho\left(\frac{H}{p}\right)^{-1/\gamma} - p\rho\right] \\ &= \frac{2\gamma}{\gamma-1} p\rho\left[\left(\frac{H}{p}\right)^{\gamma-1/\gamma} - p\rho\right]. \end{aligned} \tag{B.3}$$

Similarly

$$\begin{aligned} Q_0^2 &= \rho_0^2 V_0^2, \\ &= \frac{2\gamma}{\gamma-1} p_o \rho_o\left[\left(\frac{H_o}{p_o}\right)^{\gamma-1/\gamma} - 1\right]. \end{aligned} \tag{B.4}$$

Dividing equation (B.3) by (B.4) gives

$$\frac{Q^2}{Q_0^2} = \frac{p\rho}{p_o \rho_o}\left[\left(\frac{H}{p}\right)^{\gamma-1/\gamma} - 1\right] \Big/ \left[\left(\frac{H_o}{p_o}\right)^{\gamma-1/\gamma} - 1\right]$$

and since $\frac{\rho}{\rho_o} = \left(\frac{p}{p_o}\right)^{1/\gamma}$

$$\frac{Q^2}{Q_0^2} = \left(\frac{p}{p_o}\right)^{\gamma+1/\gamma}\left[\left(\frac{H}{p}\right)^{\gamma-1/\gamma} - 1\right] \Big/ \left[\left(\frac{H_o}{p_o}\right)^{\gamma-1/\gamma} - 1\right],$$

hence

$$\mu = \frac{A_o}{A_i} = \frac{1}{A_i}\int\left[\left(\frac{p}{p_o}\right)^{\gamma+1/\gamma}\left[\left(\frac{H}{p}\right)^{\gamma-1/\gamma} - 1\right] \Big/ \left[\left(\frac{H_o}{p_o}\right)^{\gamma-1/\gamma} - 1\right]\right]^{\frac{1}{2}} dAs\,. \tag{B.5}$$

For the experimental results, the integral in equation (B.5) is replaced by a summation over the 17 tubes.

The shape of the boundary layer was not measured accurately in the experiment. A calculation using a 1/7th power law profile showed that the maximum error caused by not representing the boundary layer accurately in the mass flow ratio calculation is approximately 1 per cent. Instrumentation error increases this figure by a further 0·5 per cent thus the values of the mass flow ratios quoted throughout this Report have a maximum error of 1·5 per cent.

TABLE 1

Cowl No. 1 Ordinates

Outer surface				Inner surface			
x/c	r/d_i	x/c	r/d_i	x/c	r/d_i	x/c	r/d_i
0	0·5000	0·1597	0·5654	0	0·5000	0·1211	0·4480
0·0025	0·5113	0·1681	0·5667	0·0025	0·4887	0·1250	0·4483
0·0059	0·5166	0·1849	0·5693	0·0059	0·4832	0·1667	0·4513
0·0092	0·5201	0·2107	0·5716	0·0092	0·4791	0·2083	0·4544
0·0126	0·5227	0·2185	0·5737	0·0126	0·4757	0·2500	0·4575
0·0160	0·5249	0·2353	0·5756	0·0160	0·4728	0·2917	0·4605
0·0202	0·5273	0·2521	0·5773	0·0202	0·4696	0·3333	0·4636
0·0269	0·5307	0·2589	0·5789	0·0235	0·4674	0·3750	0·4666
0·0302	0·5322	0·2856	0·5803	0·0269	0·4653	0·4167	0·4697
0·0336	0·5336	0·3025	0·5816	0·0302	0·4634	0·4583	0·4727
0·0370	0·5350	0·3193	0·5827	0·0836	0·4617	0·5000	0·4758
0·0403	0·5363	0·3361	0·5837	0·0370	0·4602	0·5416	0·4789
0·0454	0·5381	0·3697	0·5853	0·0403	0·4587	0·5833	0·4819
0·0521	0·5404	0·4033	0·5865	0·0454	0·4568	0·6250	0·4850
0·0588	0·5426	0·4370	0·5874	0·0521	0·4546	0·6666	0·4880
0·0655	0·5446	0·4708	0·5879	0·0588	0·4527	0·7083	0·4911
0·0723	0·5466	0·5042	0·5882	0·0655	0·4512	0·7500	0·4941
0·0790	0·5484	0·5294	0·5882	0·0723	0·4499	0·7916	0·4972
0·0840	0·5497	0·5416	0·5881	0·0790	0·4489	0·8333	0·5003
0·0924	0·5518	0·5833	0·5864	0·0840	0·4483	0·8750	0·5033
0·1108	0·5538	0·6250	0·5827	0·0874	0·4480	0·9166	0·5064
0·1092	0·5557	0·6666	0·5774	0·0908	0·4477	0·9583	0·5094
0·1176	0·5575	0·7083	0·5708	0·0941	0·4475	1·0000	0·5125
0·1260	0·5593	0·7500	0·5633	0·0975	0·4474		
0·1345	0·5609	0·7916	0·5552	0·1008	0·4473		
0·1429	0·5625	0·8333	0·5469	0·1042	0·4472		
0·1513	0·5640	1·0000	0·5133	0·1056	0·4472		

TABLE 2

Cowl No. 2 Ordinates

Outer surface				Inner surface			
x/c	r/d_i	x/c	r/d_i	x/c	r/d_i	x/c	r/d_i
0	0·5000	0·48	0·5698	0	0·5000	0·48	0·4570
0·02	0·5267	0·50	0·5682	0·02	0·4797	0·50	0·4577
0·04	0·5363	0·52	0·5664	0·04	0·4720	0·52	0·4584
0·06	0·5429	0·54	0·5643	0·06	0·4671	0·54	0·4591
0·08	0·5479	0·56	0·5620	0·08	0·4636	0·56	0·4597
0·10	0·5520	0·58	0·5595	0·10	0·4609	0·58	0·4604
0·12	0·5554	0·60	0·5567	0·12	0·4588	0·60	0·4611
0·14	0·5584	0·62	0·5536	0·14	0·4572	0·62	0·4617
0·16	0·5612	0·65	0·5486	0·16	0·4560	0·65	0·4626
0·18	0·5638	0·67	0·5449	0·18	0·4552	0·67	0·4632
0·20	0·5661	0·69	0·5411	0·20	0·4546	0·69	0·4638
0·22	0·5681	0·72	0·5351	0·22	0·4543	0·72	0·4645
0·24	0·5698	0·75	0·5288	0·24	0·4541	0·75	0·4653
0·26	0·5711	0·78	0·5223	0·26	0·4540	0·78	0·4659
0·28	0·5722	0·81	0·5156	0·28	0·4541	0·81	0·4666
0·30	0·5731	0·84	0·5086	0·30	0·4542	0·84	0·4672
0·32	0·5737	0·87	0·5014	0·32	0·4542	0·87	0·4677
0·34	0·5742	0·89	0·4965	0·34	0·4543	0·89	0·4678
0·36	0·5744	0·92	0·4888	0·36	0·4544	0·92	0·4677
0·38	0·5743	0·95	0·4807	0·38	0·4546	0·95	0·4660
0·40	0·5740	0·97	0·4748	0·40	0·4549	0·97	0·4651
0·42	0·5733	0·98	0·4717	0·42	0·4553	0·98	0·4647
0·44	0·5724	0·99	0·4685	0·44	0·4558	0·99	0·4644
0·46	0·5712	1·00	0·4650	0·46	0·4564	1·00	0·4642

TABLE 3

Cowl No. 3 Ordinates

Outer Surface				Inner Surface			
x/c	r/d_i	x/c	r/d_i	x/c	r/d_i	x/c	r/d_i
0	5·000	0·50	0·5587	0	0·5000	0·50	0·4587
0·02	0·5240	0·52	0·5568	0·02	0·4757	0·52	0·4592
0·04	0·5327	0·55	0·5535	0·04	0·4663	0·55	0·4599
0·06	0·5389	0·57	0·5512	0·06	0·4596	0·57	0·4603
0·08	0·5436	0·59	0·5486	0·08	0·4543	0·59	0·4608
0·10	0·5471	0·62	0·5444	0·10	0·4501	0·62	0·4616
0·12	0·5500	0·65	0·5399	0·12	0·4472	0·65	0·4623
0·14	0·5525	0·67	0·5367	0·14	0·4458	0·67	0·4628
0·16	0·5547	0·70	0·5317	0·16	0·4461	0·70	0·4635
0·18	0·5568	0·73	0·5265	0·18	0·4475	0·73	0·4642
0·20	0·5586	0·76	0·5210	0·20	0·4493	0·76	0·4649
0·22	0·5603	0·79	0·5151	0·22	0·4510	0·80	0·4659
0·24	0·5618	0·80	0·5131	0·24	0·4523	0·83	0·4666
0·26	0·5630	straight		0·26	0·4530	0·86	0·4673
0·28	0·5640	line to		0·28	0·4535	0·90	0·4681
0·30	0·5648	1·00	0·4704	0·30	0·4539	0·93	0·4687
0·32	0·5654			0·32	0·4543	0·95	0·4690
0·34	0·5657			0·34	0·4548	0·97	0·4693
0·36	0·5658			0·36	0·4553	0·99	0·4696
0·38	0·5656			0·38	0·4558	1·0	0·4696
0·40	0·5651			0·40	0·4563		
0·42	0·5643			0·42	0·4568		
0·44	0·5633			0·44	0·4573		
0·46	0·5620			0·46	0·4578		
0·48	0·5604			0·48	0·4582		

TABLE 4

Principal Parameters for Cowls Nos. 1 -3

Cowl	t/c	d_i/d_m	l/d_m	Trailing-edge slope	Leading edge radius/c
1	0·14	0·850	0·450	11·38°	0·02639
2	0·12	0·871	0·322	18·15°	0·02385
3	0·12	0·884	0·314	12·03°	0·01802

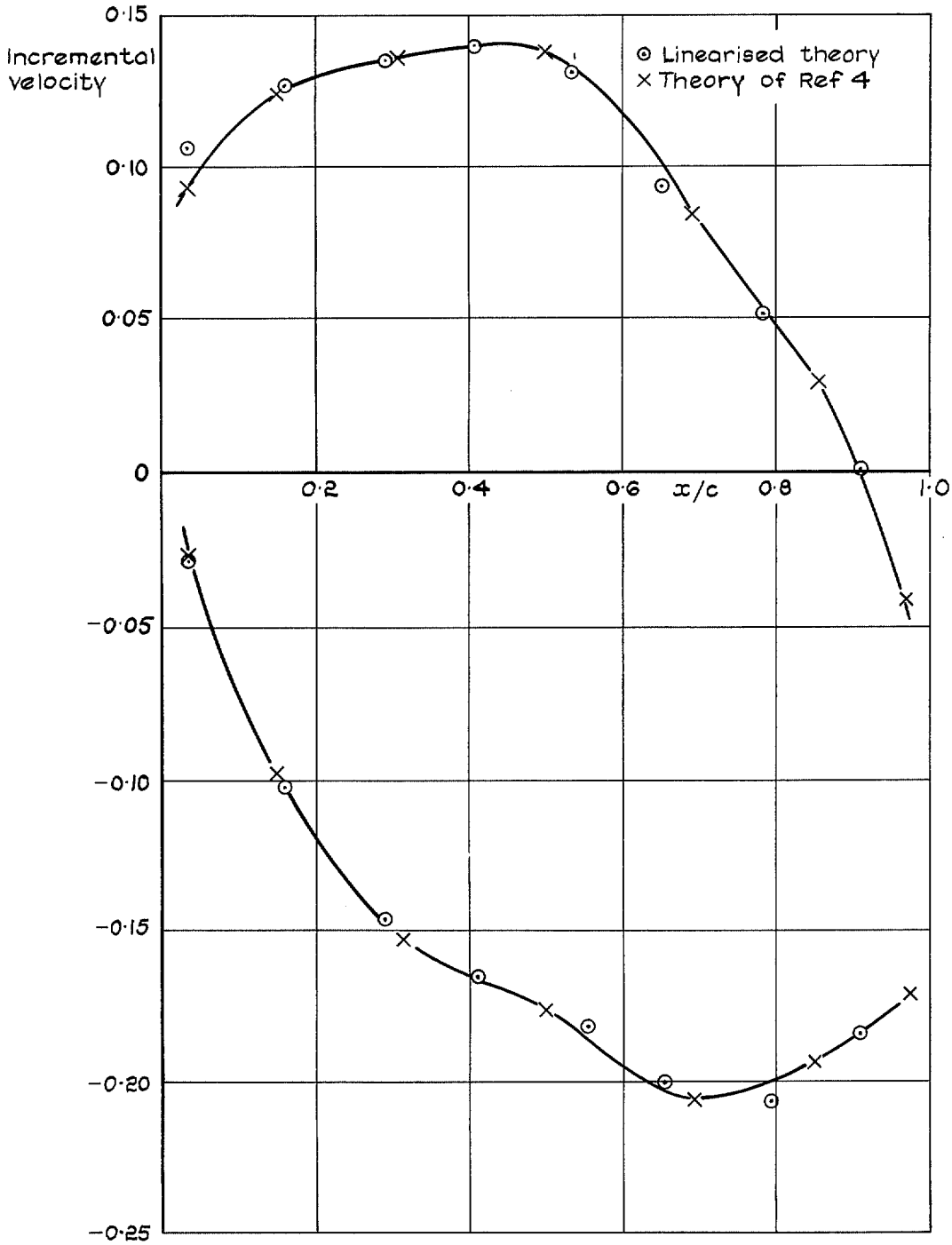

FIG. 1. Comparison of incremental velocities predicted by the method of Ref. 4 and linearised theory.

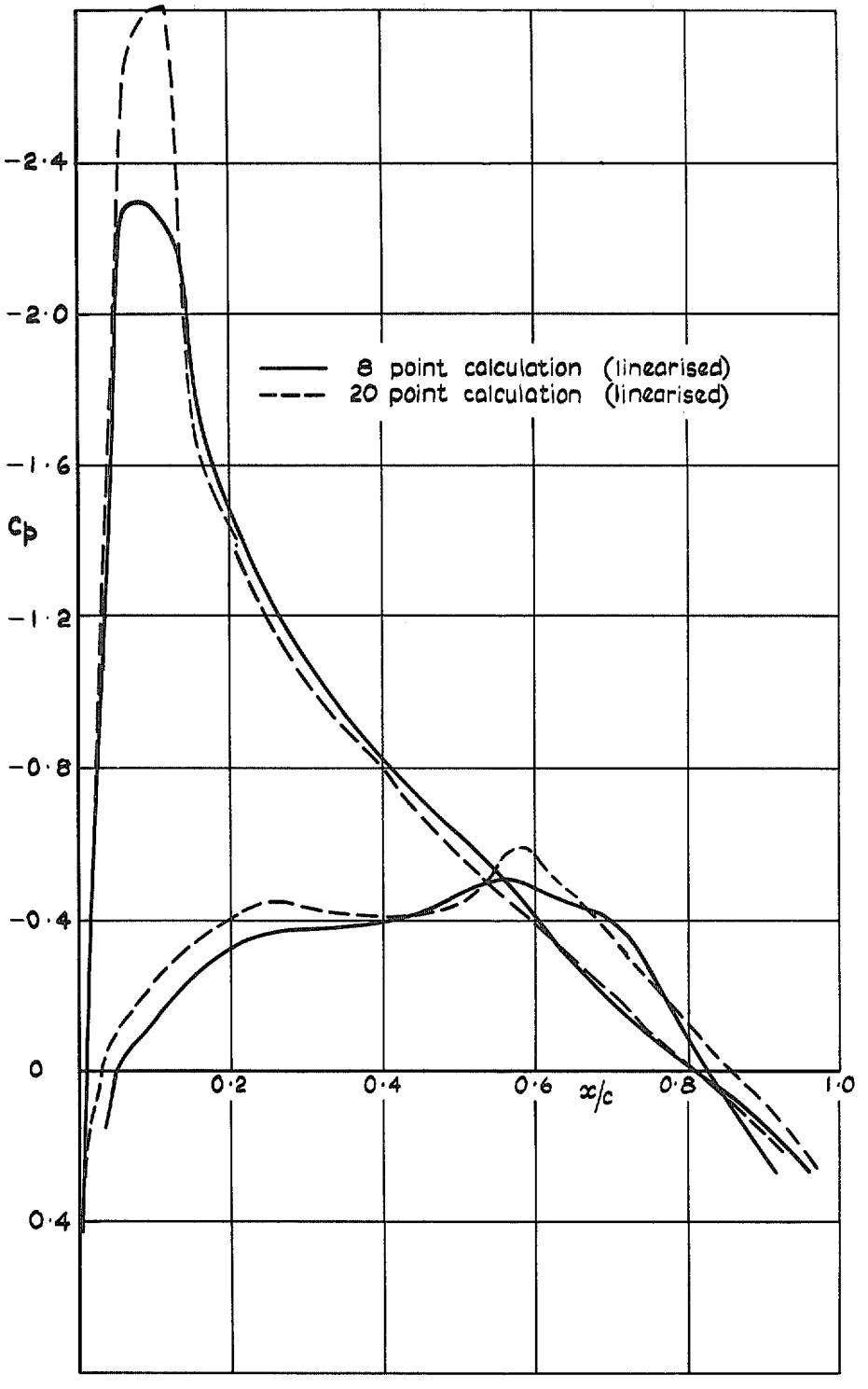

FIG. 2. Theoretical pressure distribution cowl No. 1. $M = 0{\cdot}80$: $VR = 0{\cdot}90$.

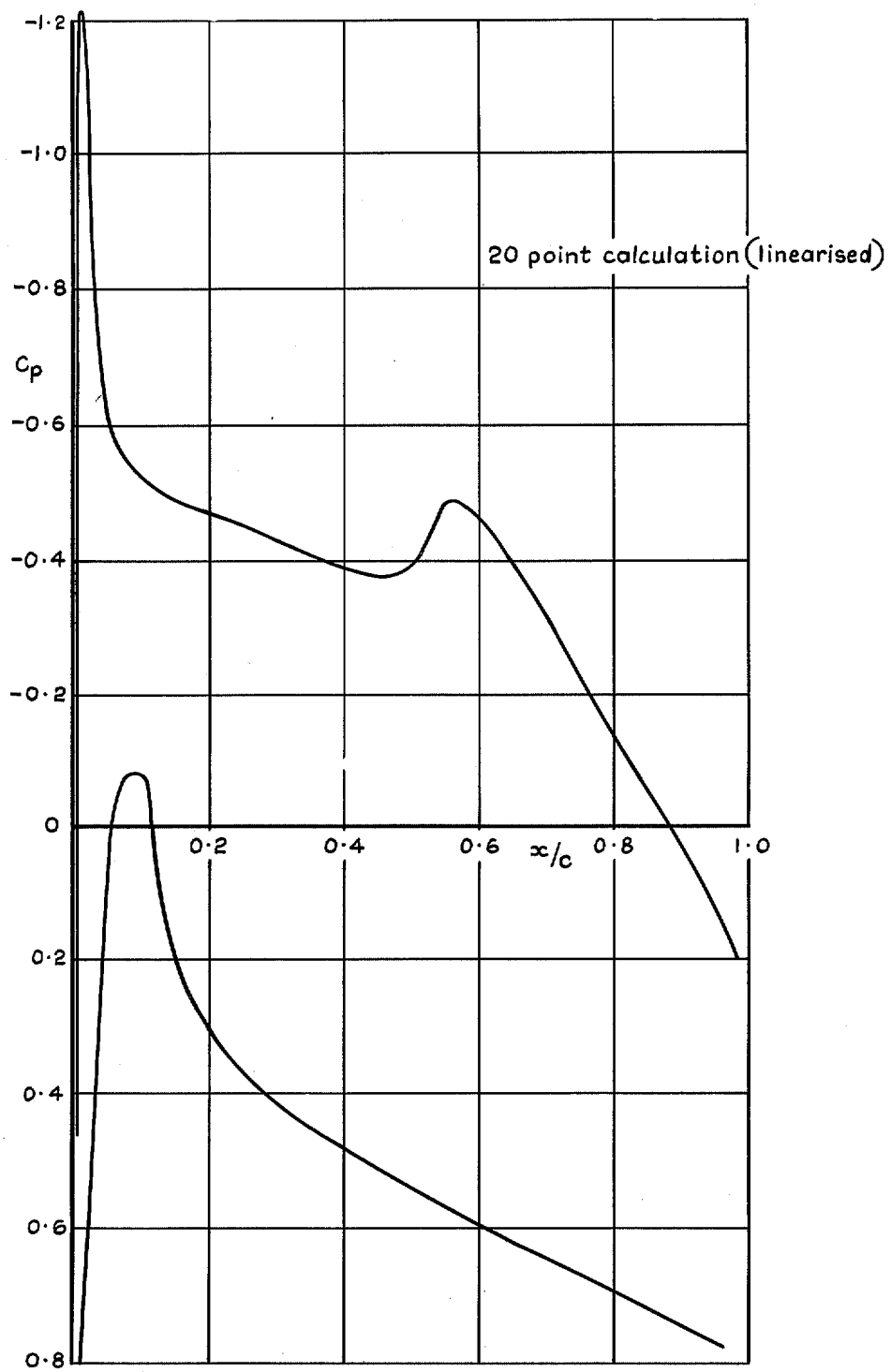

FIG. 3. Theoretical pressure distribution cowl 1: $M = 0{\cdot}5$: $VR = 0{\cdot}5$.

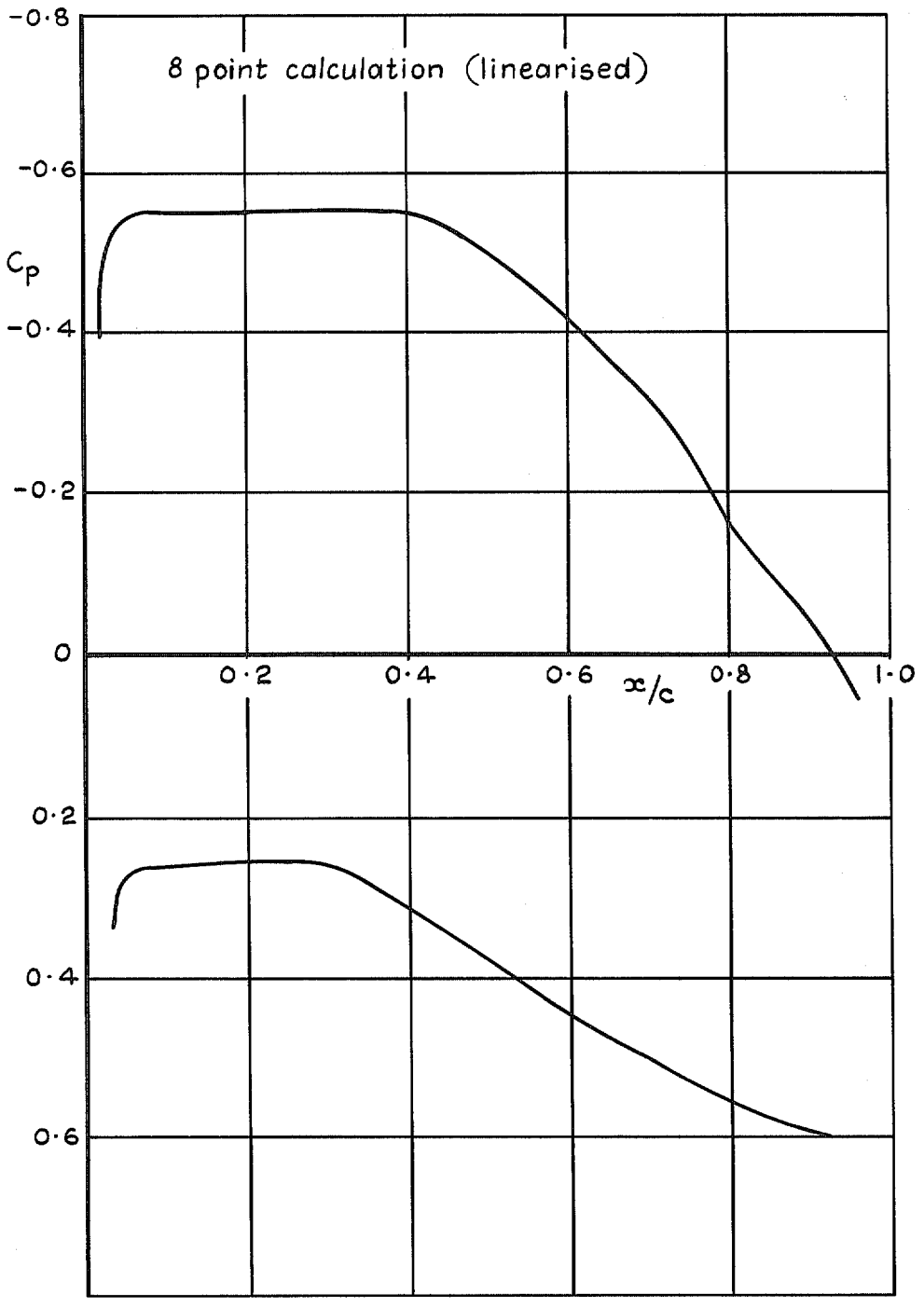

FIG. 4. Theoretical pressure distribution cowl 2: $M = 0{\cdot}75$: $VR = 0{\cdot}73$.

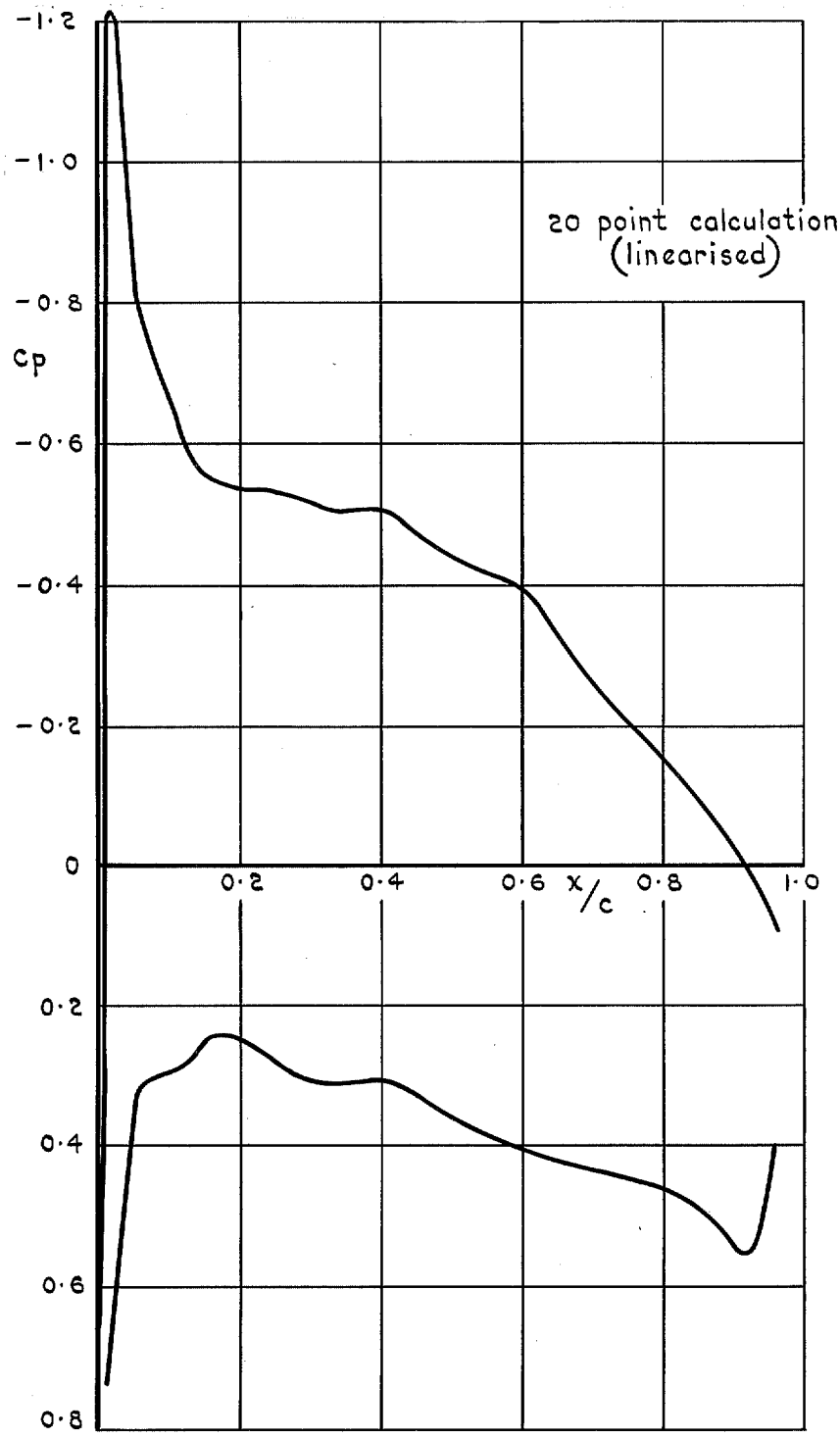

FIG. 5. Theoretical pressure distribution cowl 2: $M = 0{\cdot}5$: $VR = 0{\cdot}49$

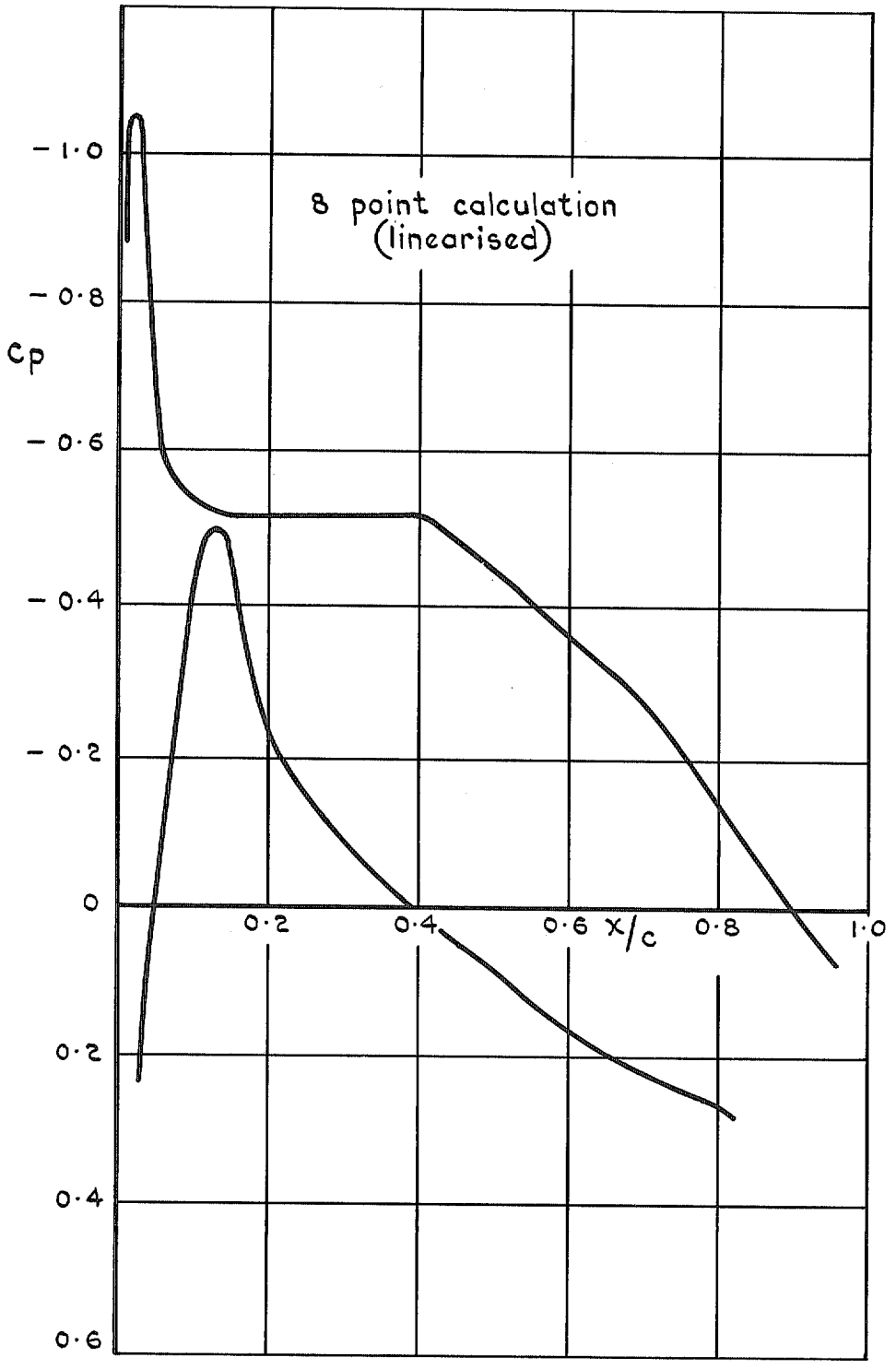

FIG. 6. Theoretical pressure distribution cowl 3: $M = 0{\cdot}78$: VR 0·74.

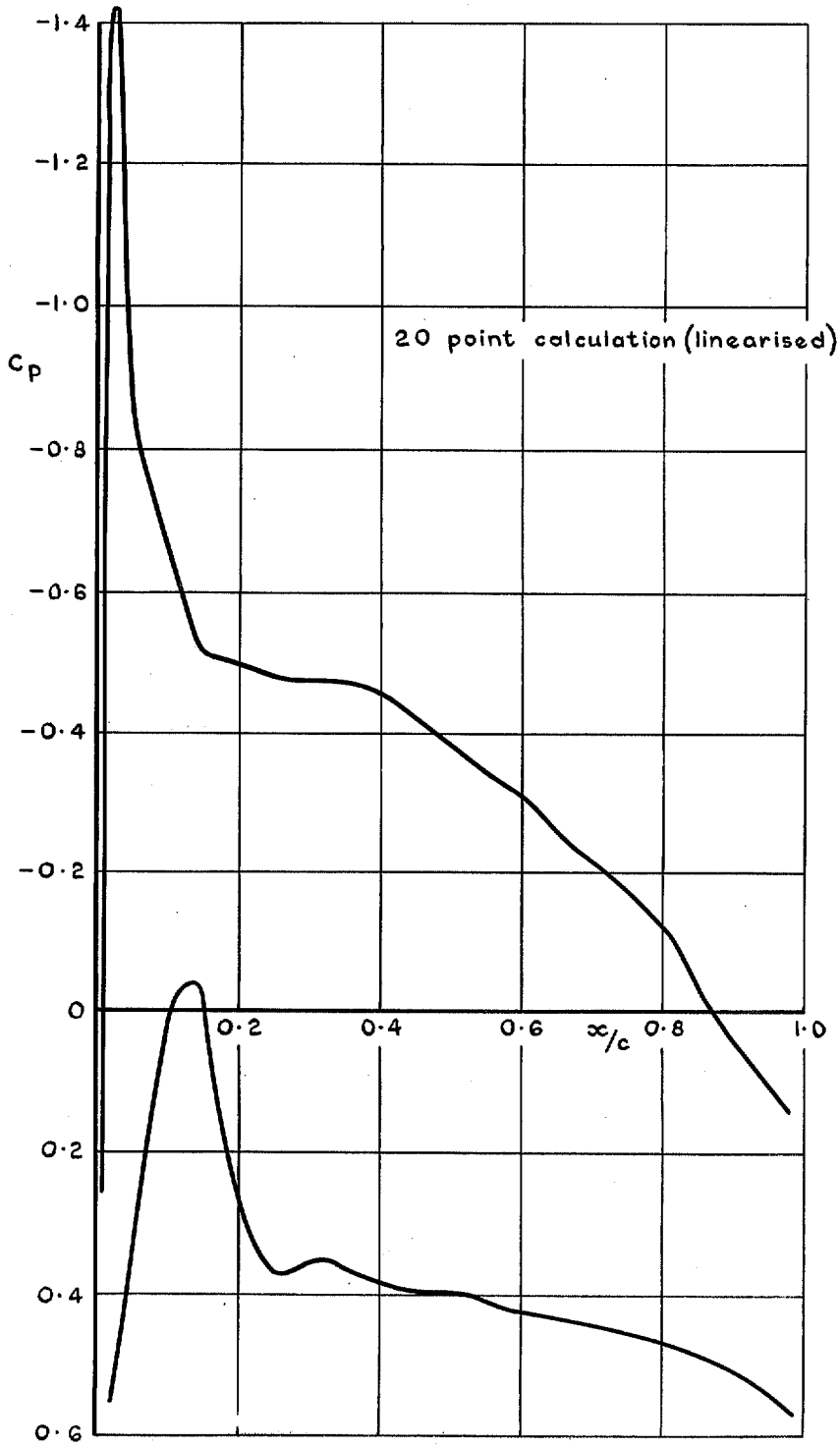

FIG. 7. Theoretical pressure distribution cowl 3: $M = 0{\cdot}5$: $VR = 0{\cdot}5$.

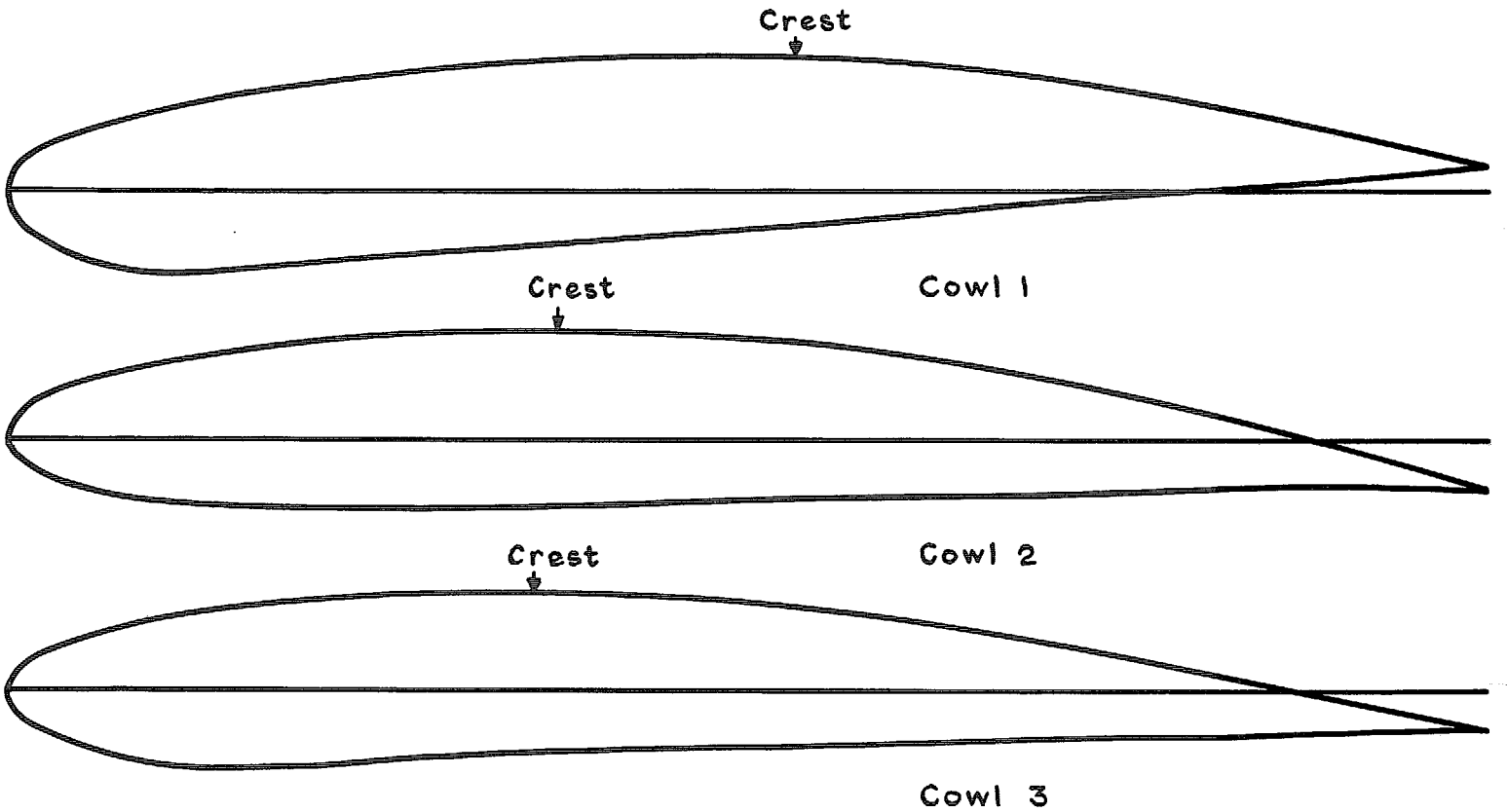

FIG. 8. Cowl profiles.

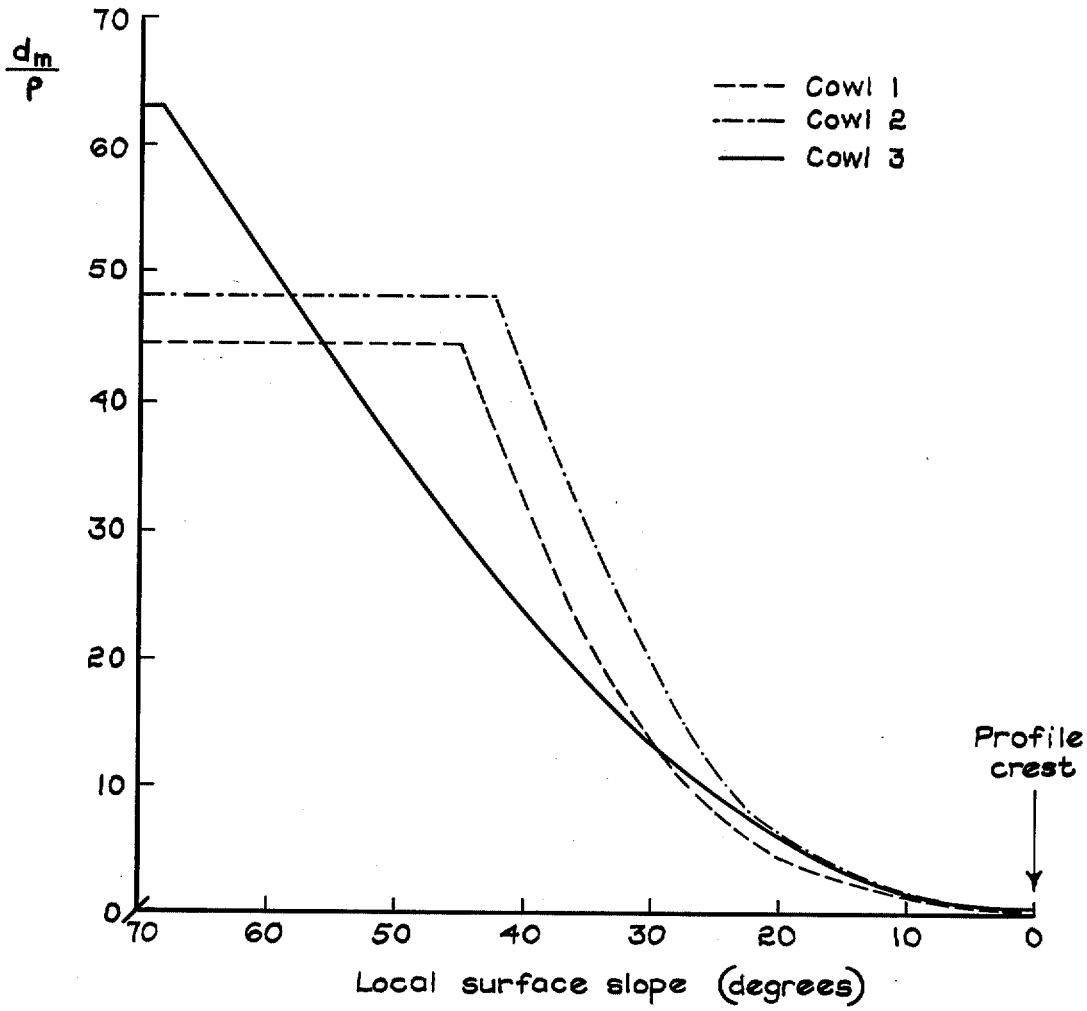

Where d_m = maximum cowl diameter
ρ = local radius of curvature

FIG. 9. Slope and curvature distribution.

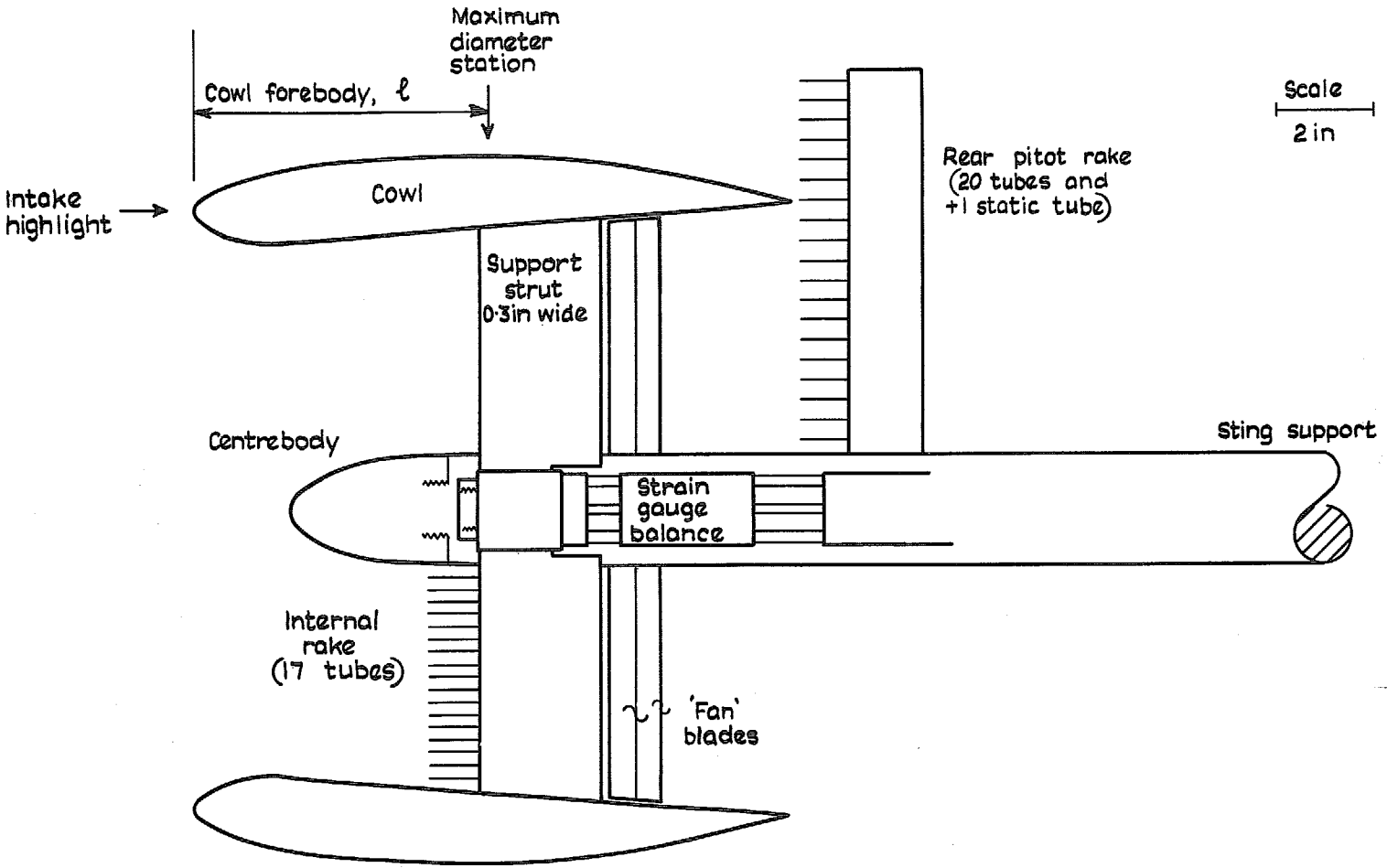

FIG. 10. Diagram of cowl rig.

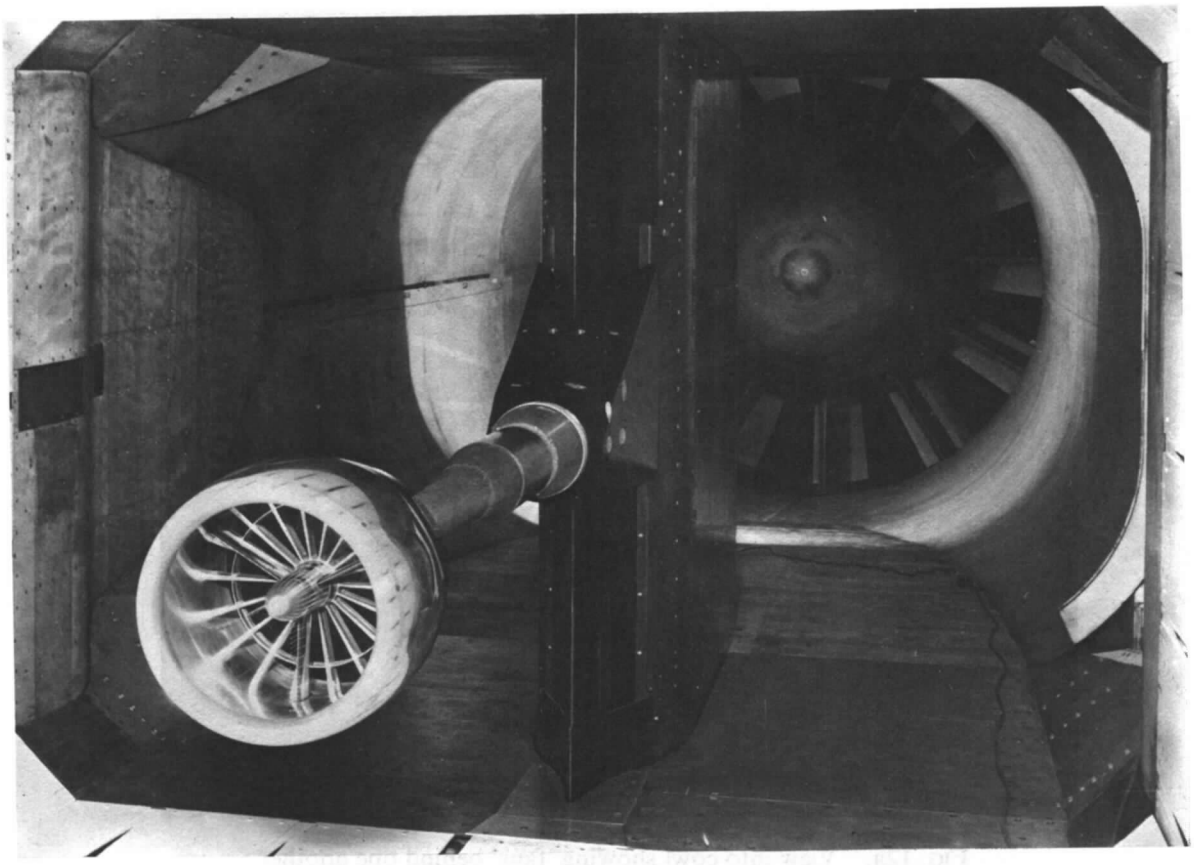

FIG. 11a. Cowl rig in 8ft × 6ft tunnel.

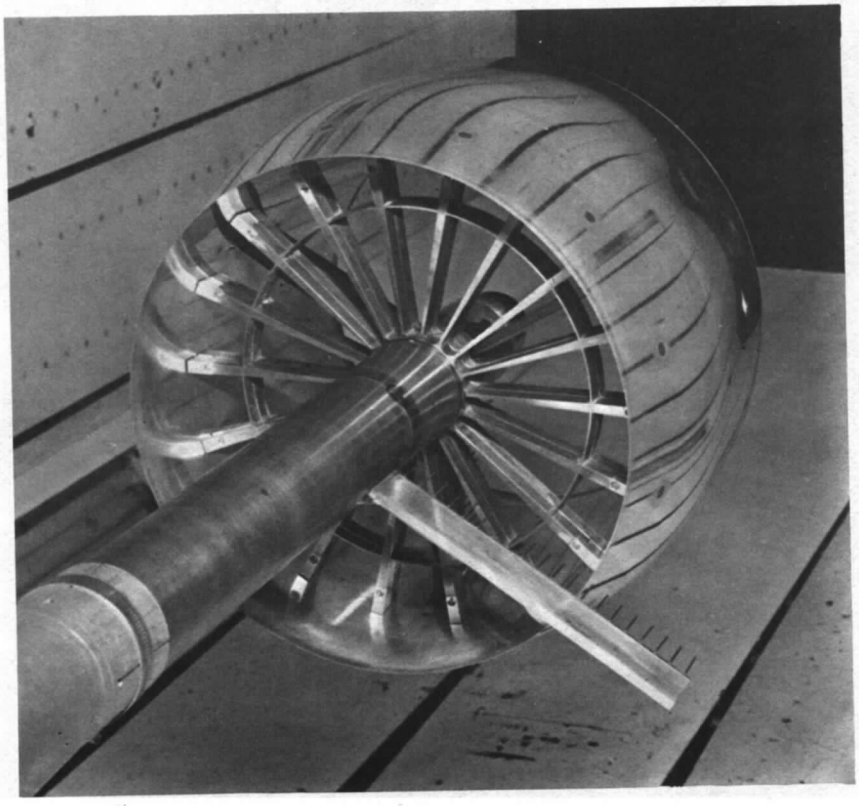

FIG. 11b. Rear view of cowl rig showing 'fans' and pitot rake.

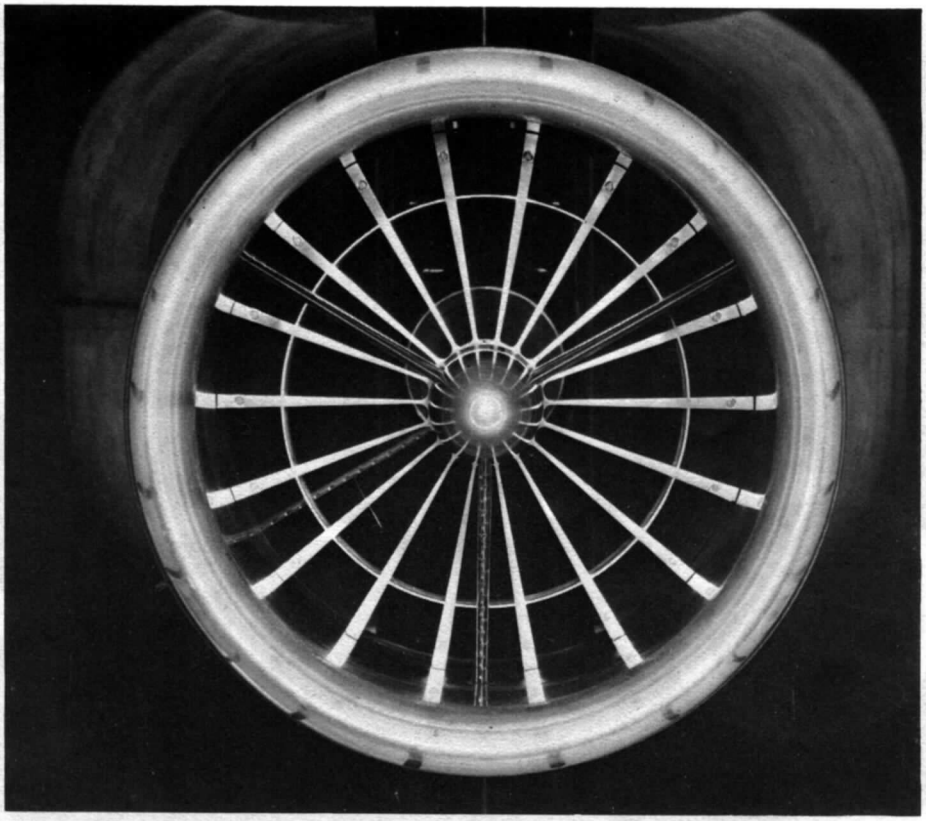

FIG. 12a. View into cowl showing 'fans' behind one another.

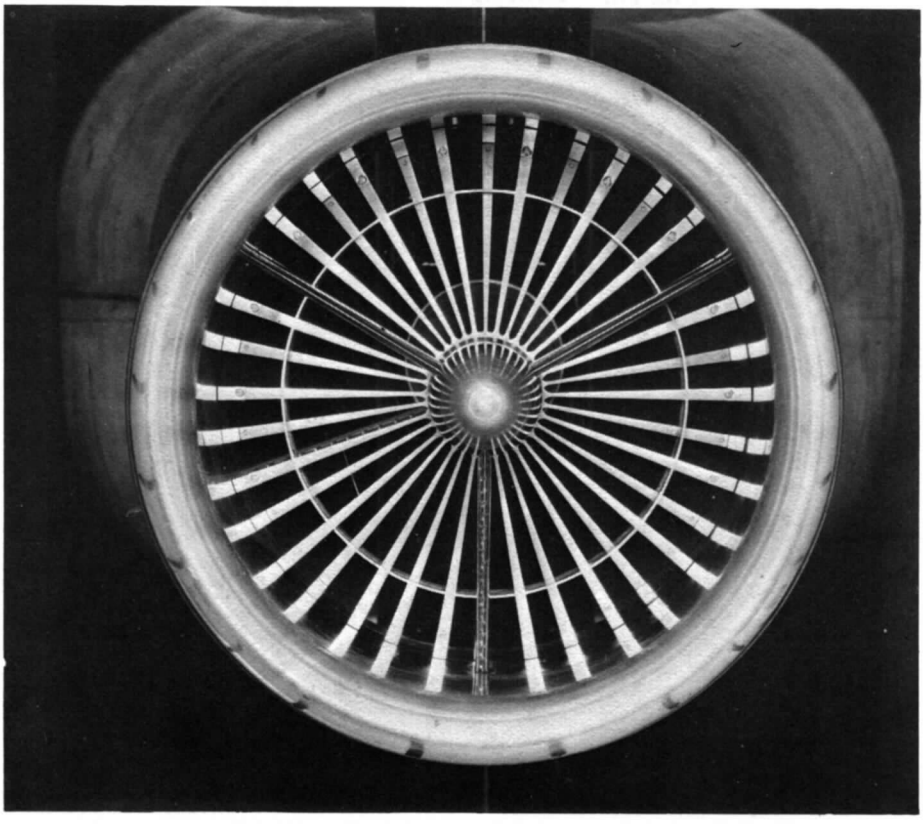

FIG. 12b. View into cowl showing rear 'fan' displaced by 10°.

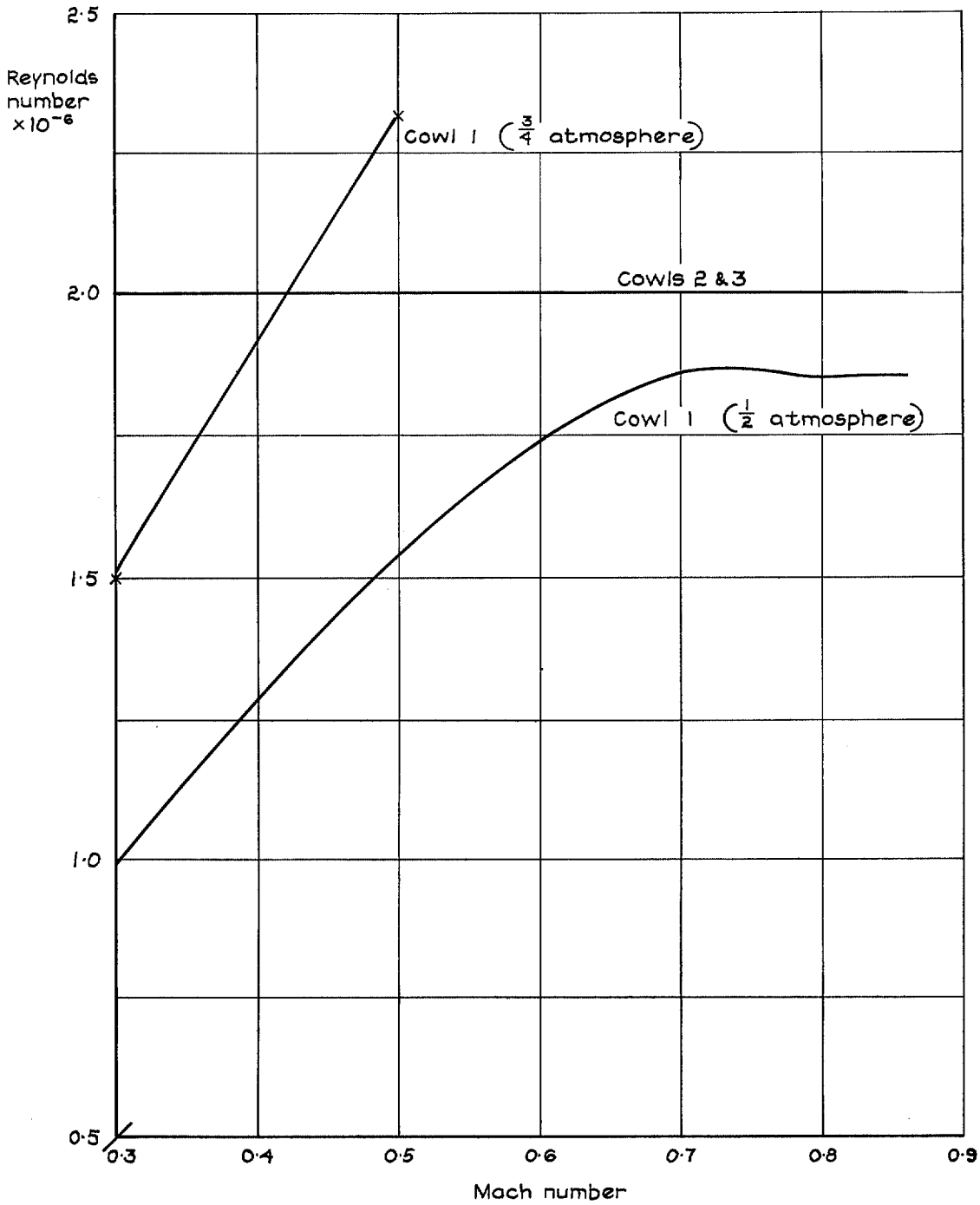

FIG. 13. Variation of Reynolds number with Mach number.

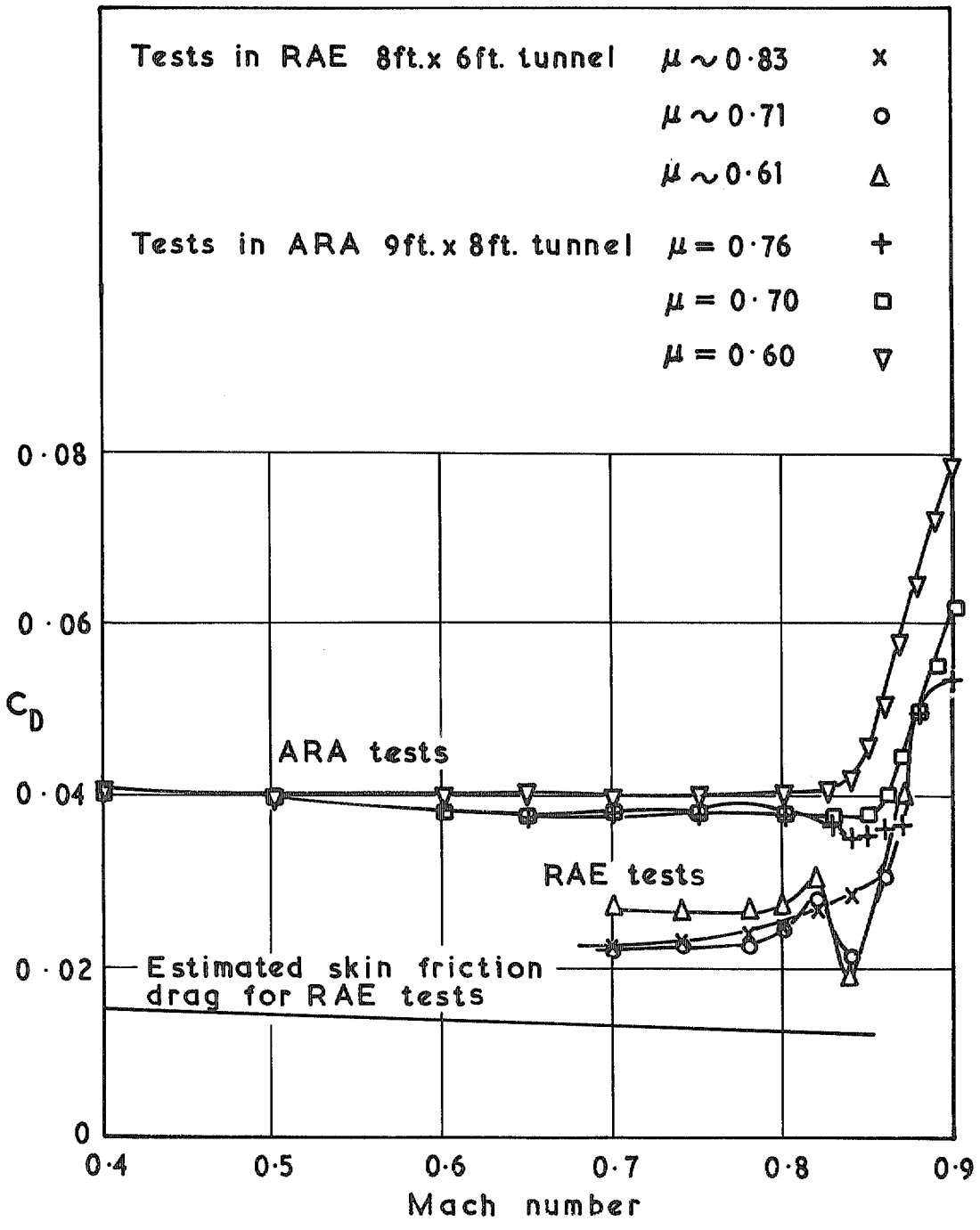

FIG. 14. Drag and Mach number: Cowl 1.

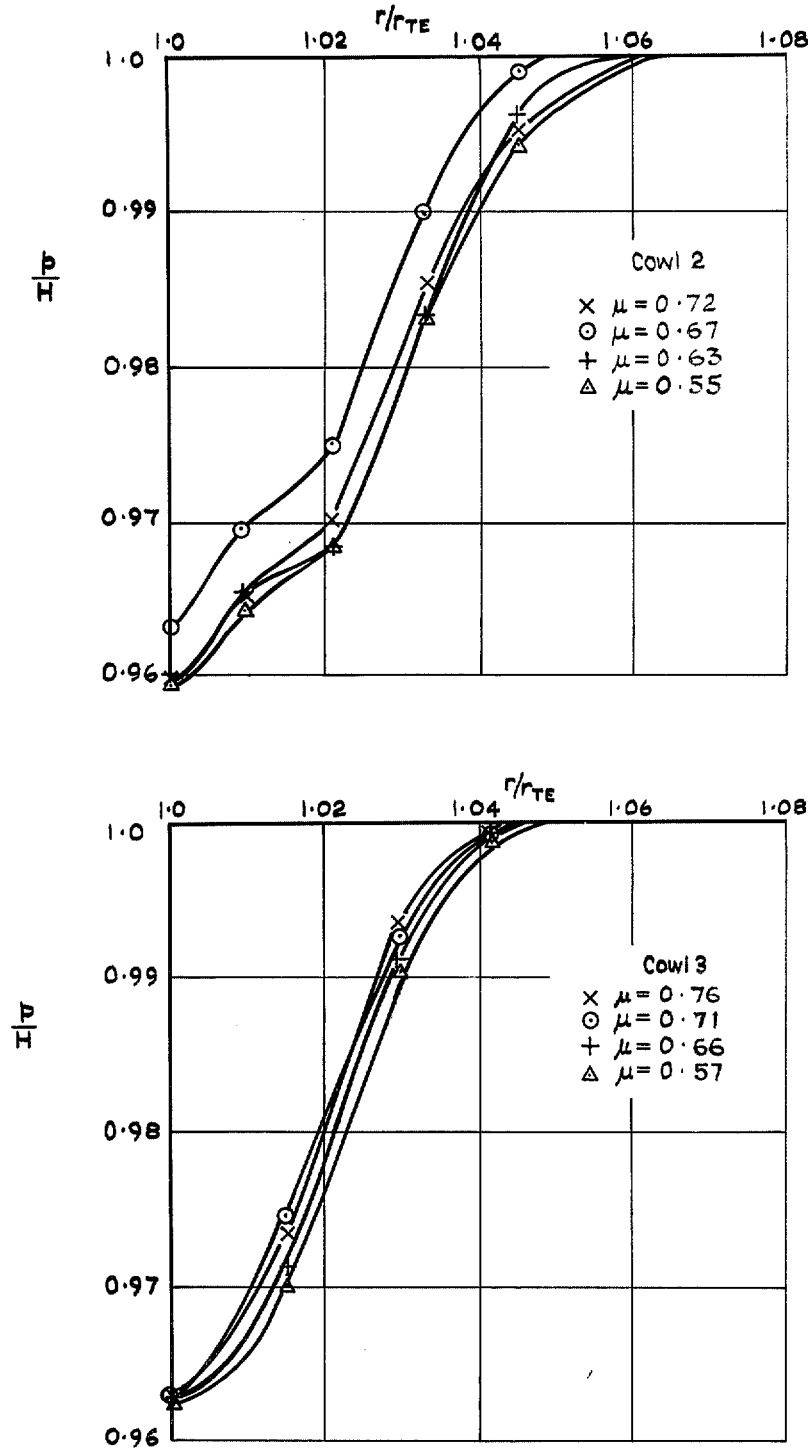

FIG. 15. Measured boundary layer profiles: $M = 0{\cdot}3$.

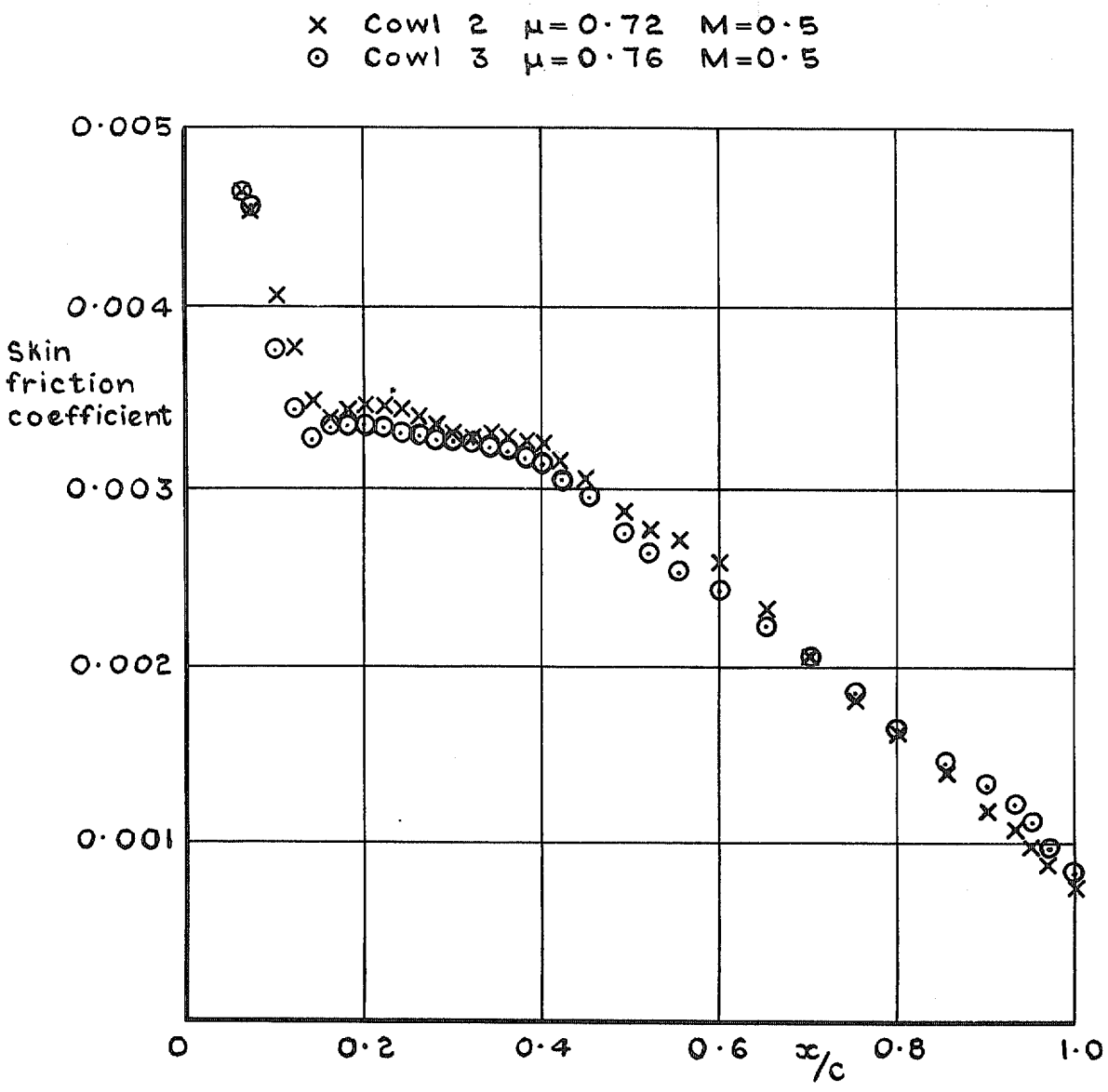

FIG. 16. Calculated skin friction coefficient: cowls 2 and 3.

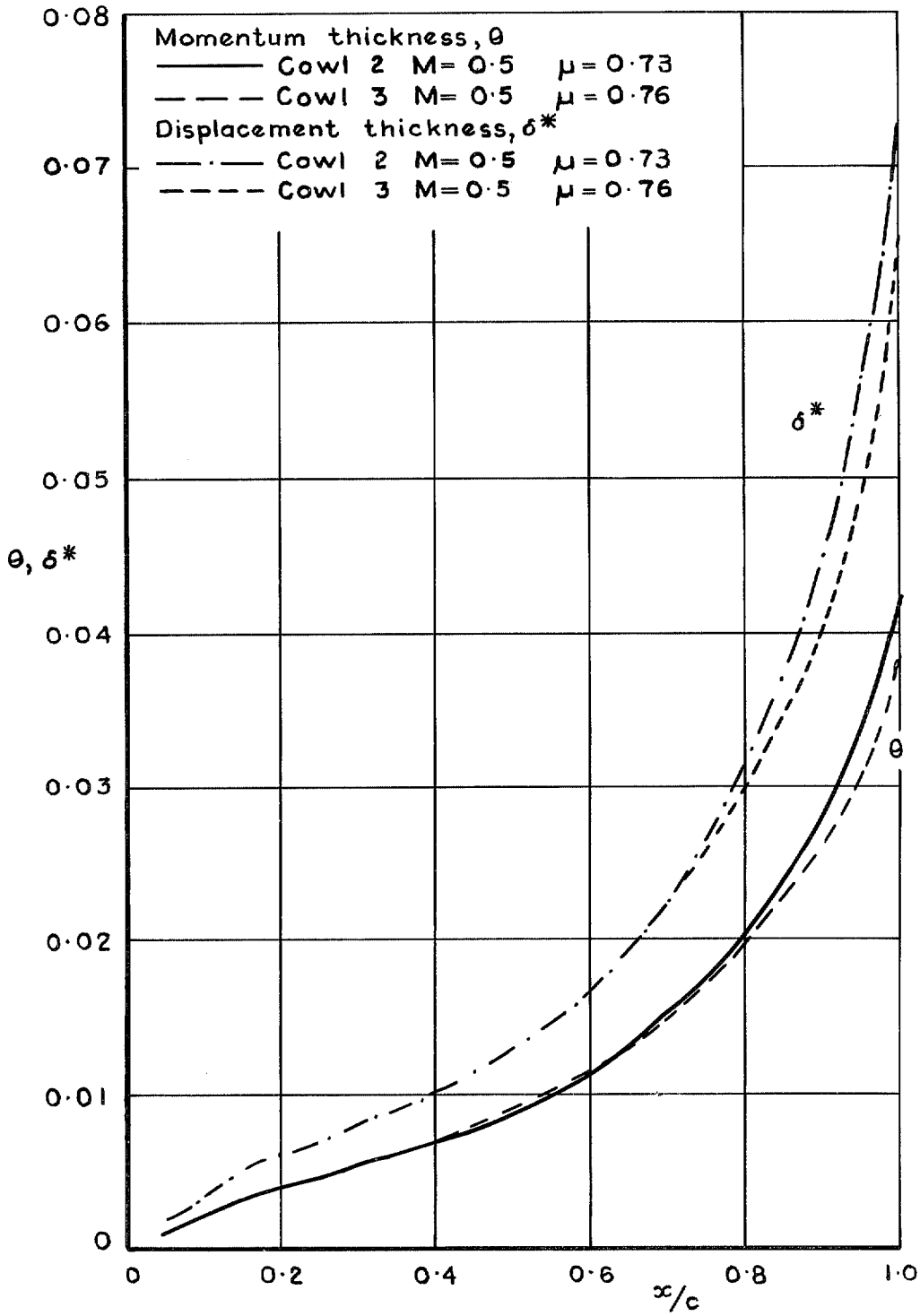

FIG. 17. Calculated momentum and displacement thickness: cowls 2 and 3.

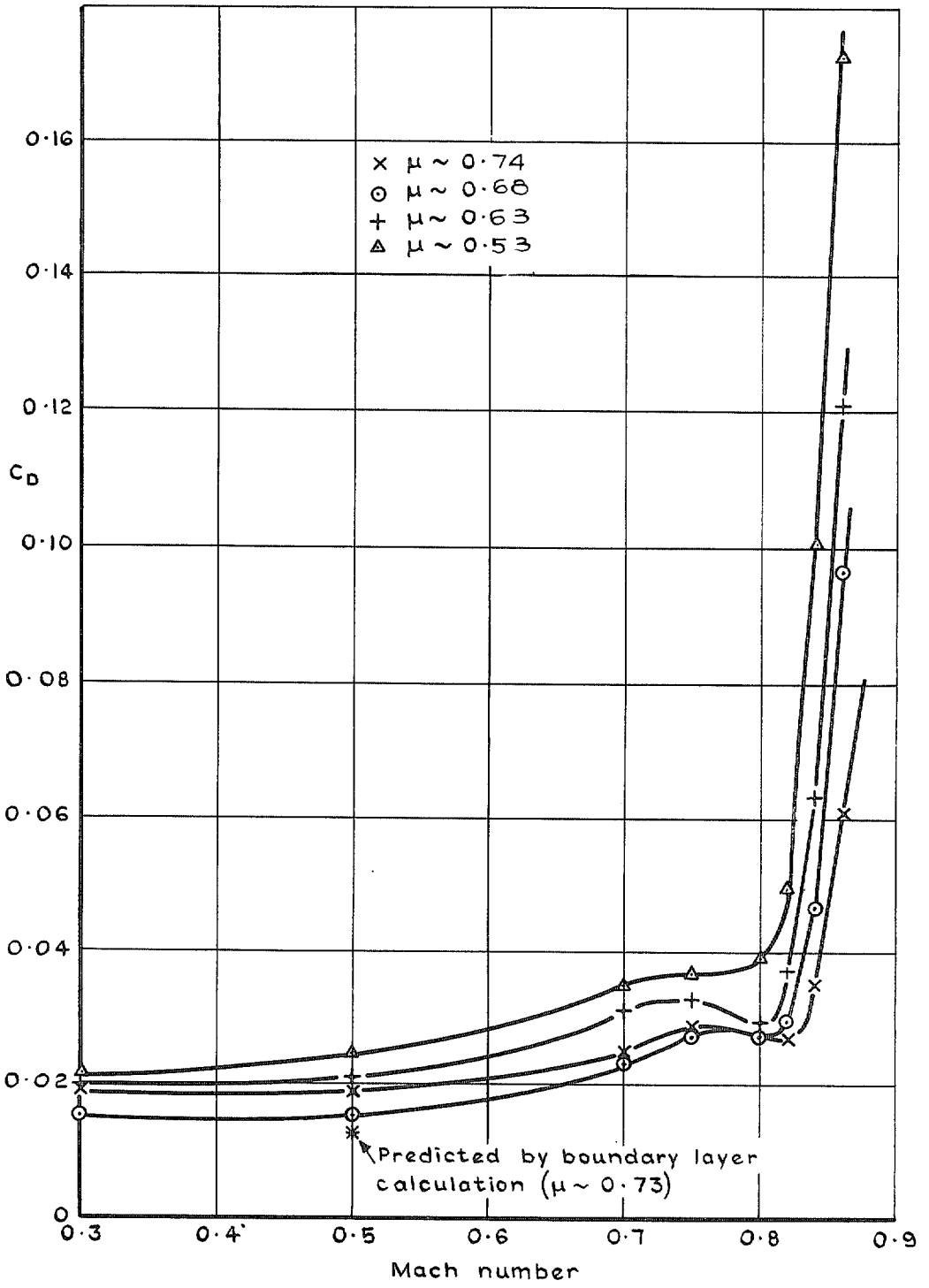

FIG. 18. Drag v Mach number: cowl 2.

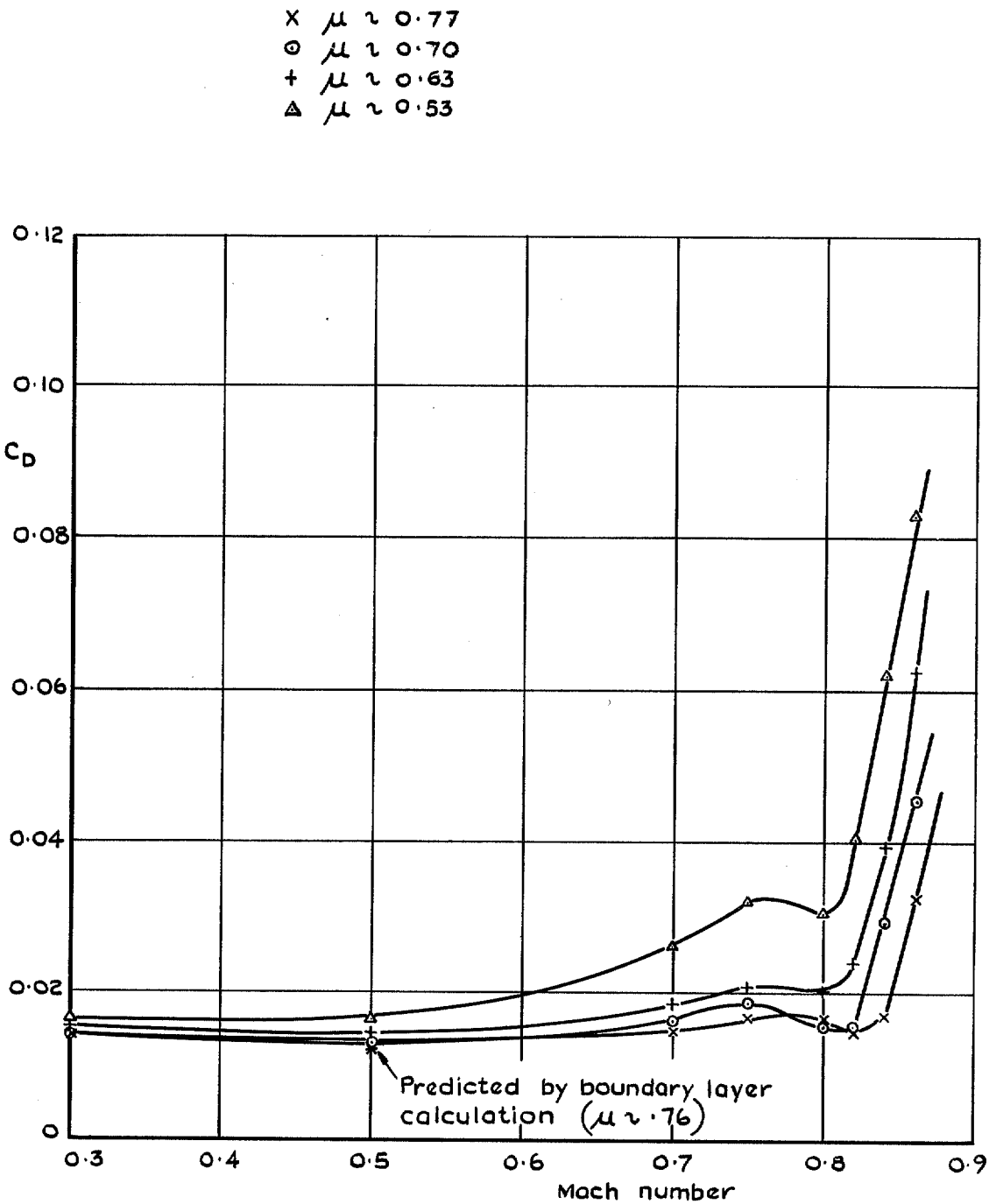

FIG. 19. Drag v Mach number: cowl 3.

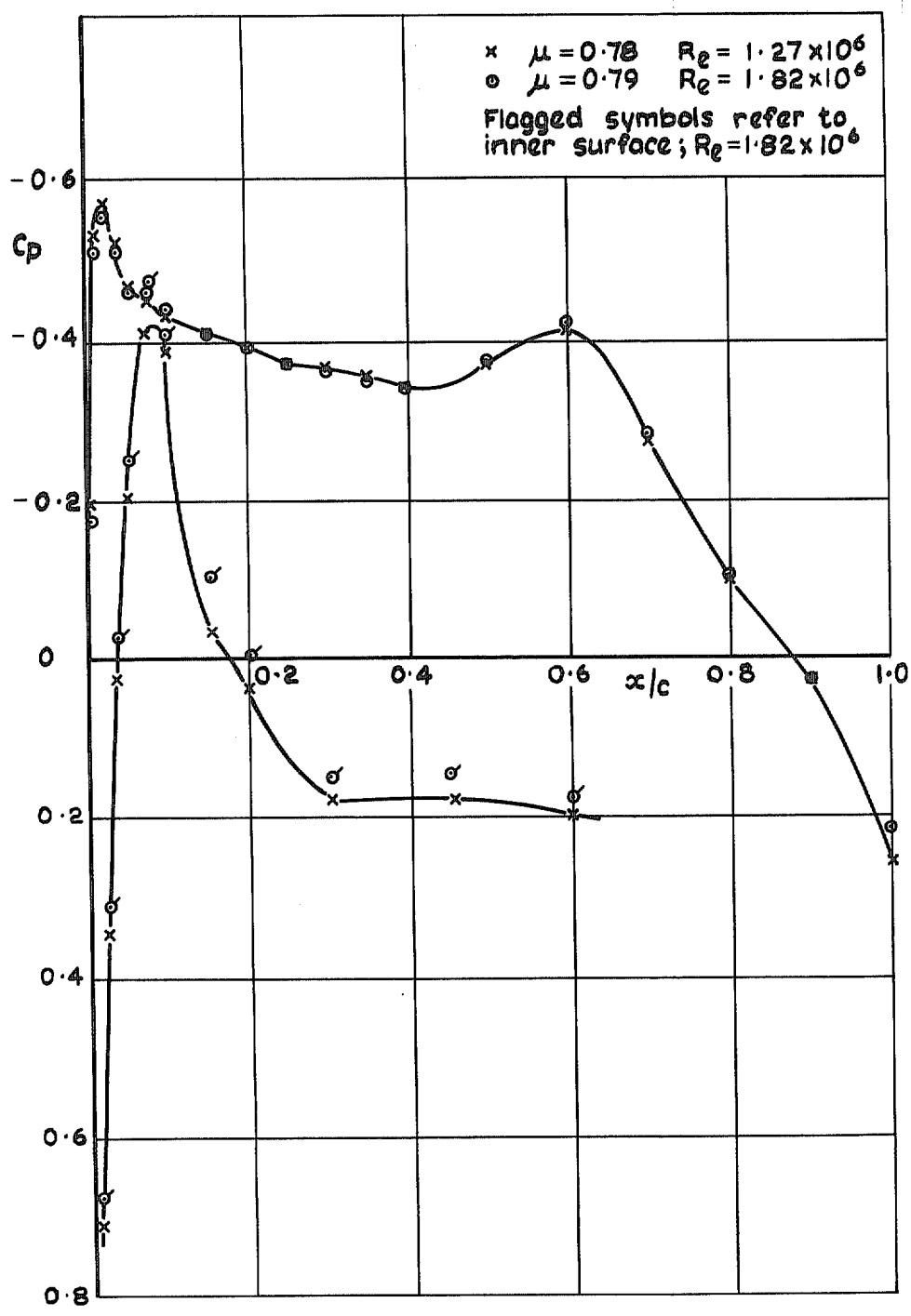

FIG. 20. Effect of Reynolds number on cowl 1 pressure distribution: $M = 0{\cdot}4$.

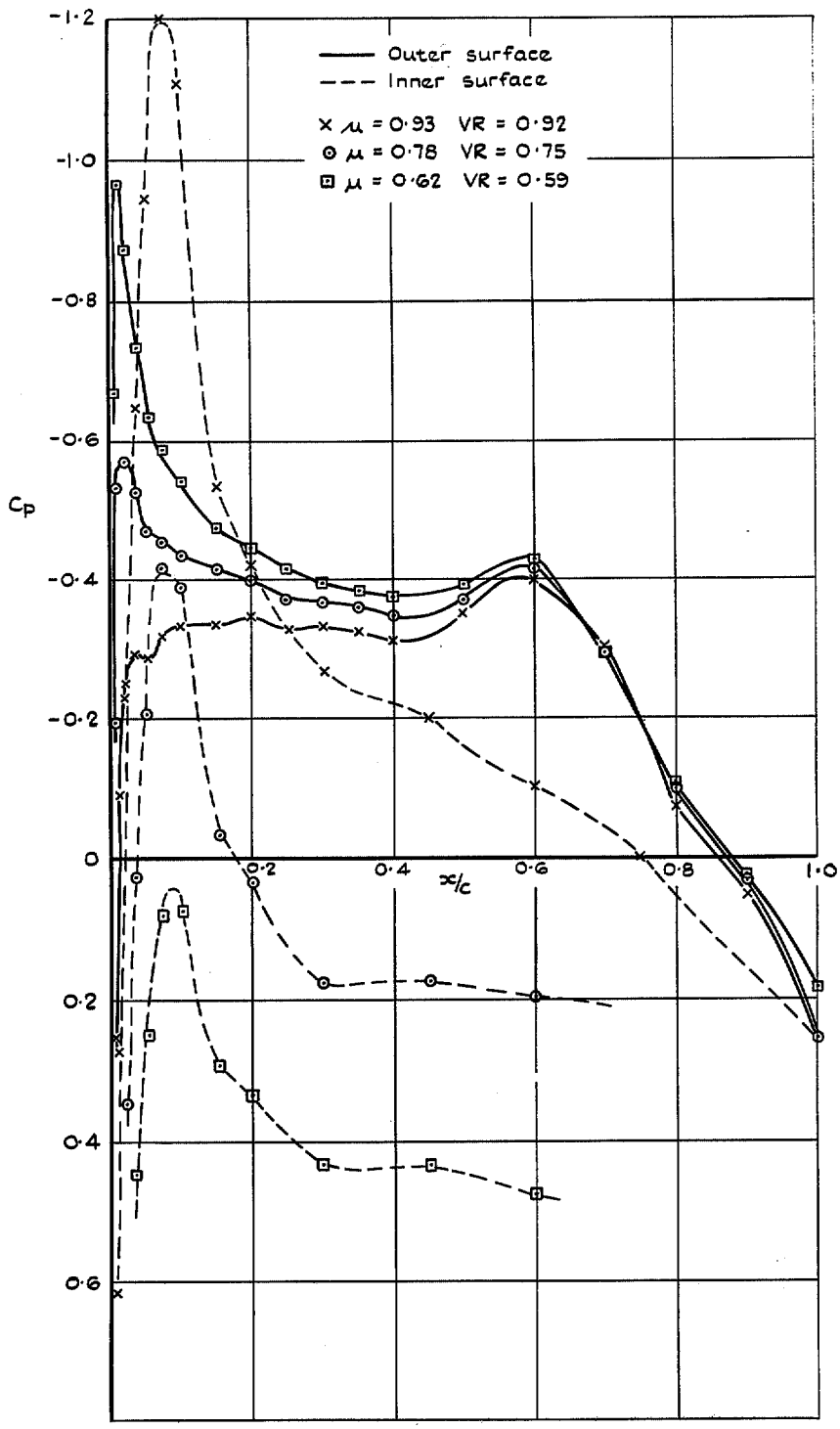

FIG. 21. Cowl 1 pressure distribution: $M = 0{\cdot}4$.

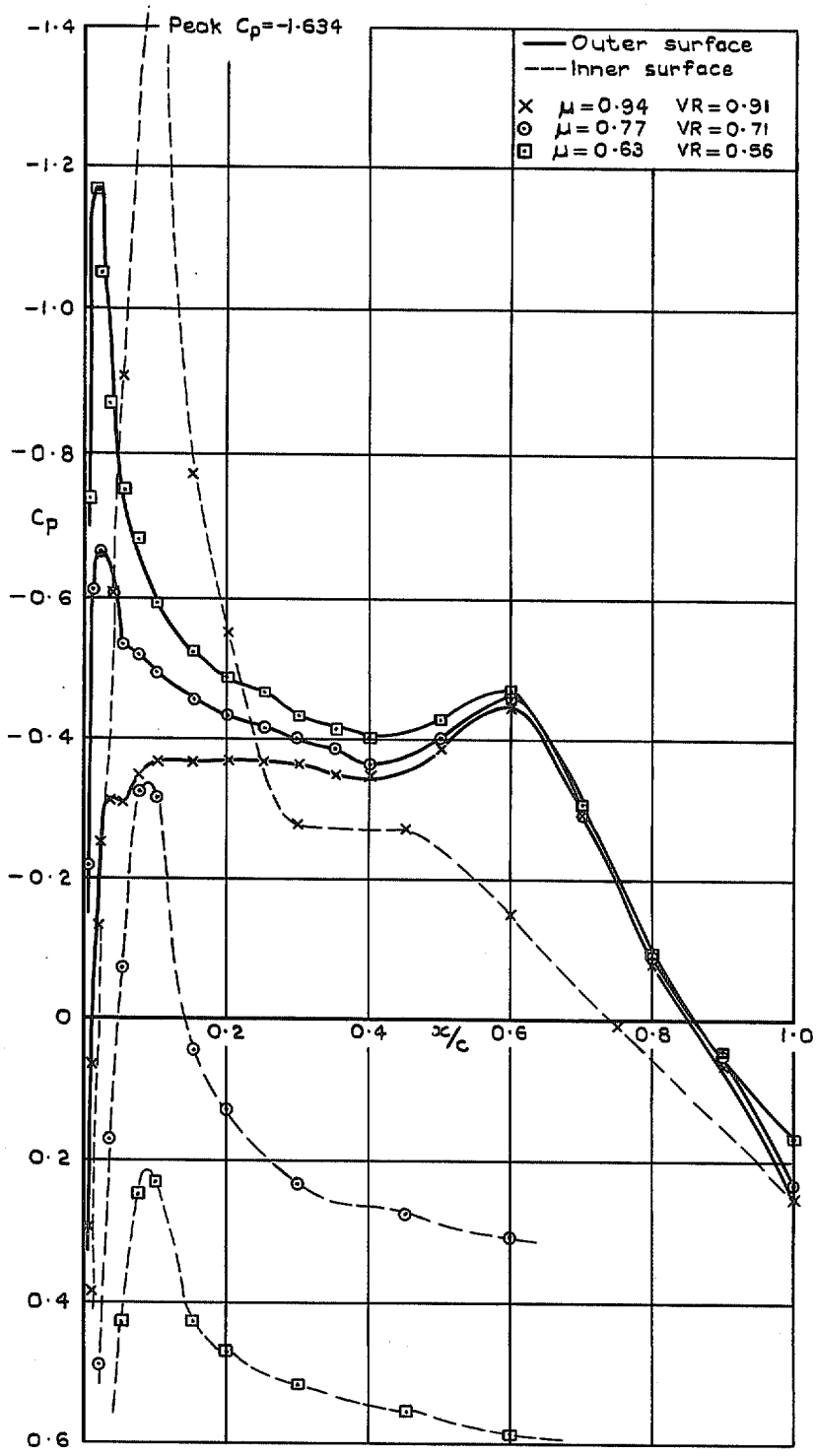

FIG. 22. Cowl 1 pressure distribution: $M = 0{\cdot}6$.

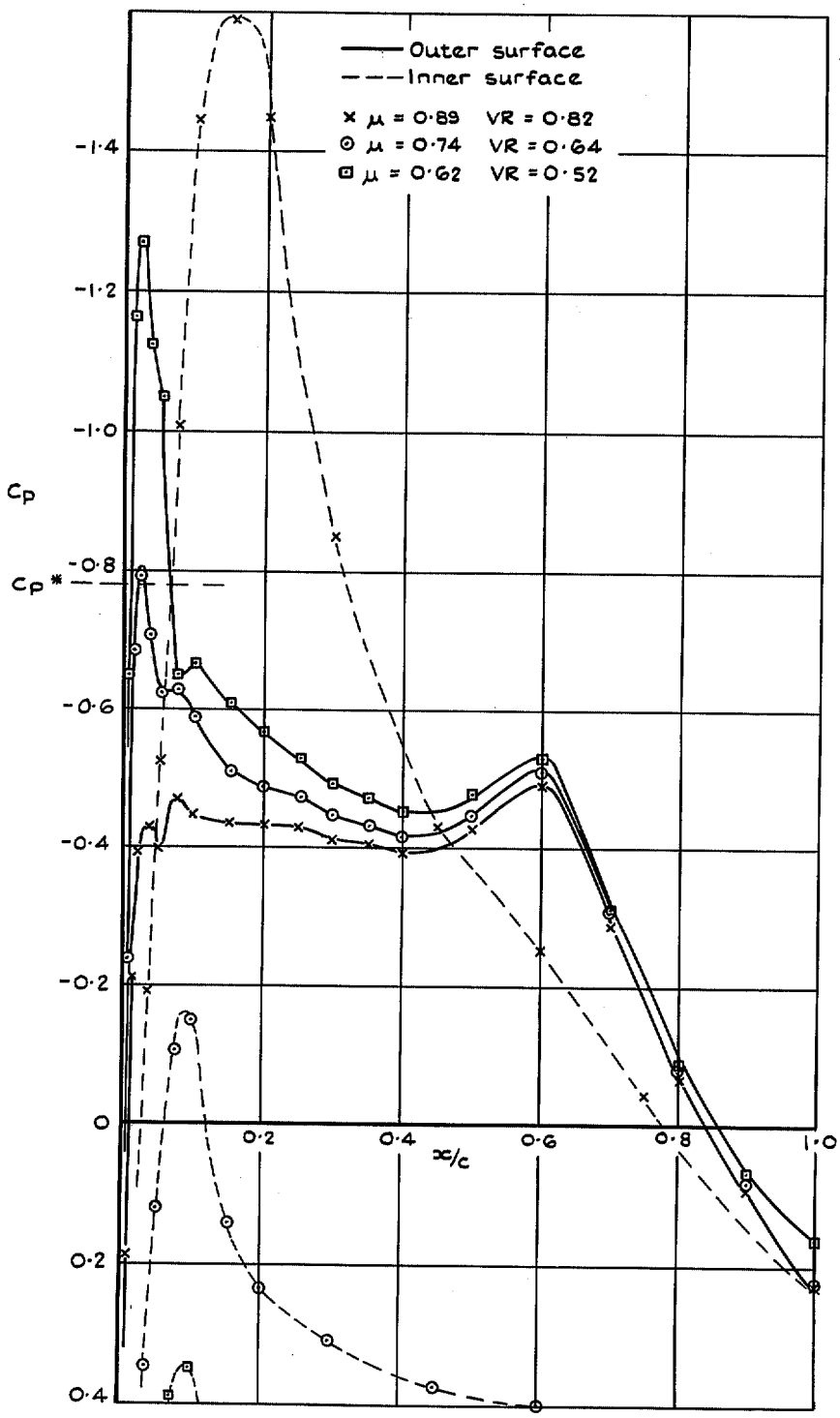

FIG. 23. Cowl 1 pressure distribution: $M = 0{\cdot}7$.

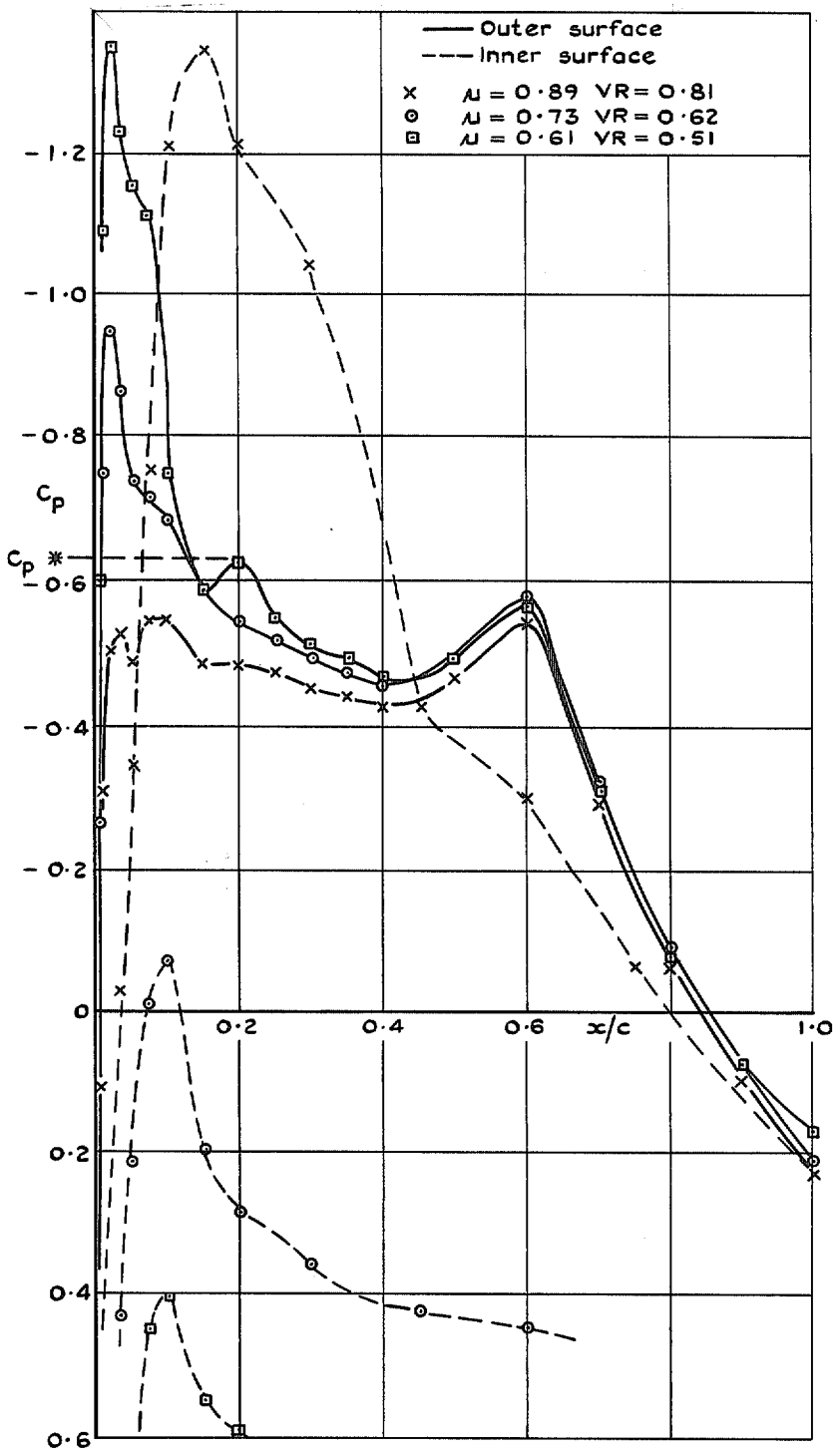

FIG. 24. Cowl 1 pressure distribution: $M = 0{\cdot}74$.

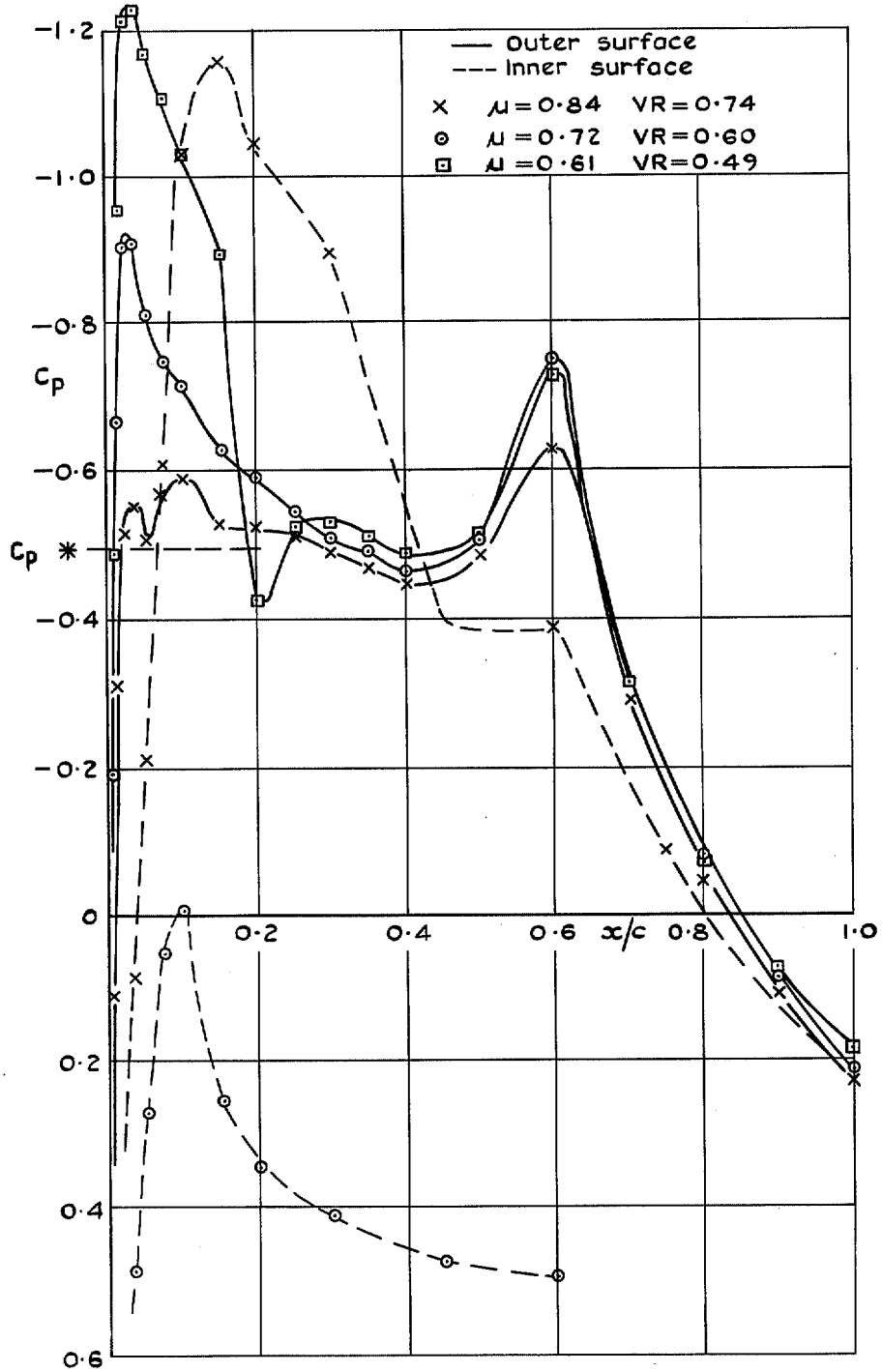

FIG. 25. Cowl 1 pressure distribution: $M = 0{\cdot}78$.

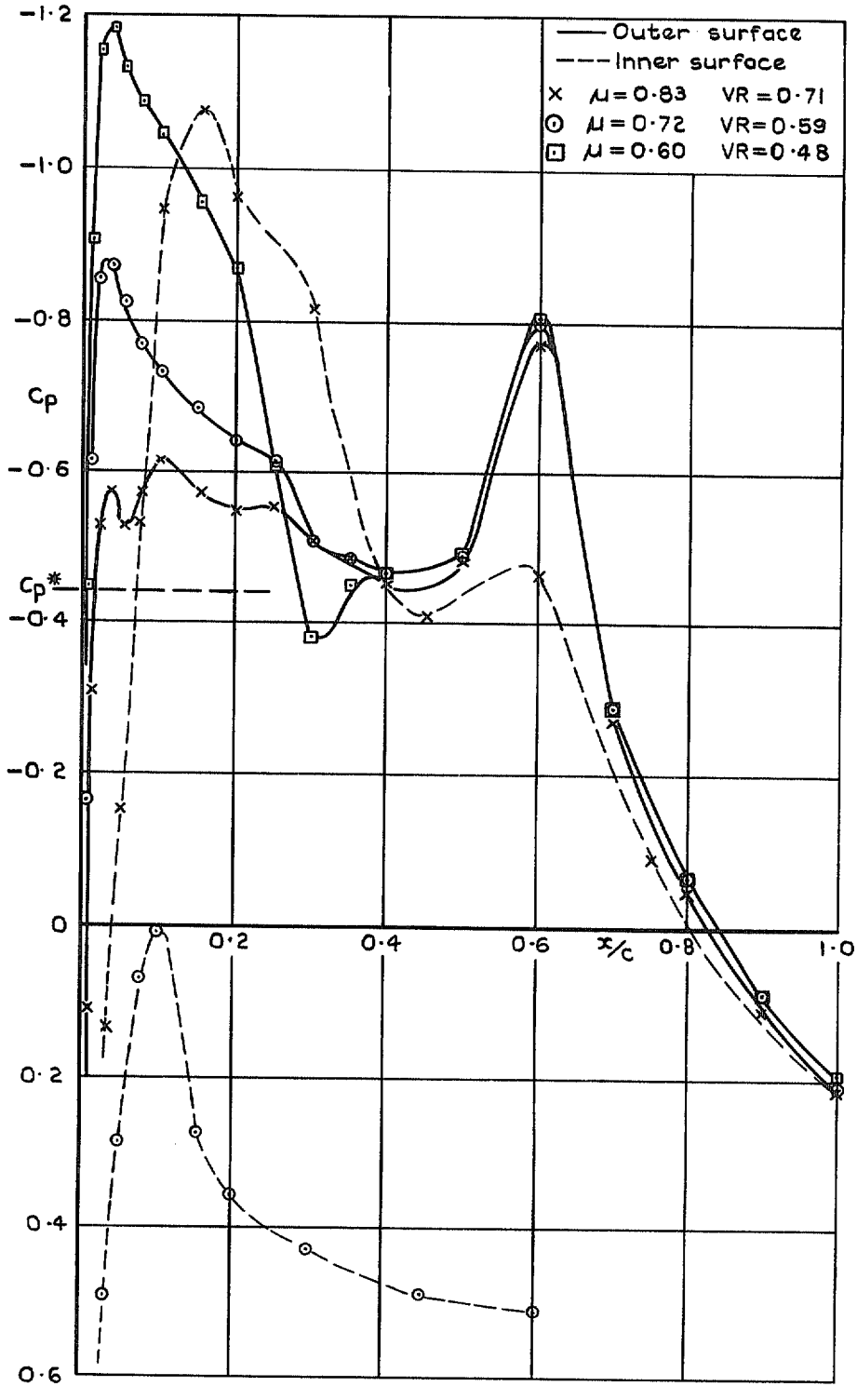

FIG. 26. Cowl 1 pressure distribution: $M = 0{\cdot}80$.

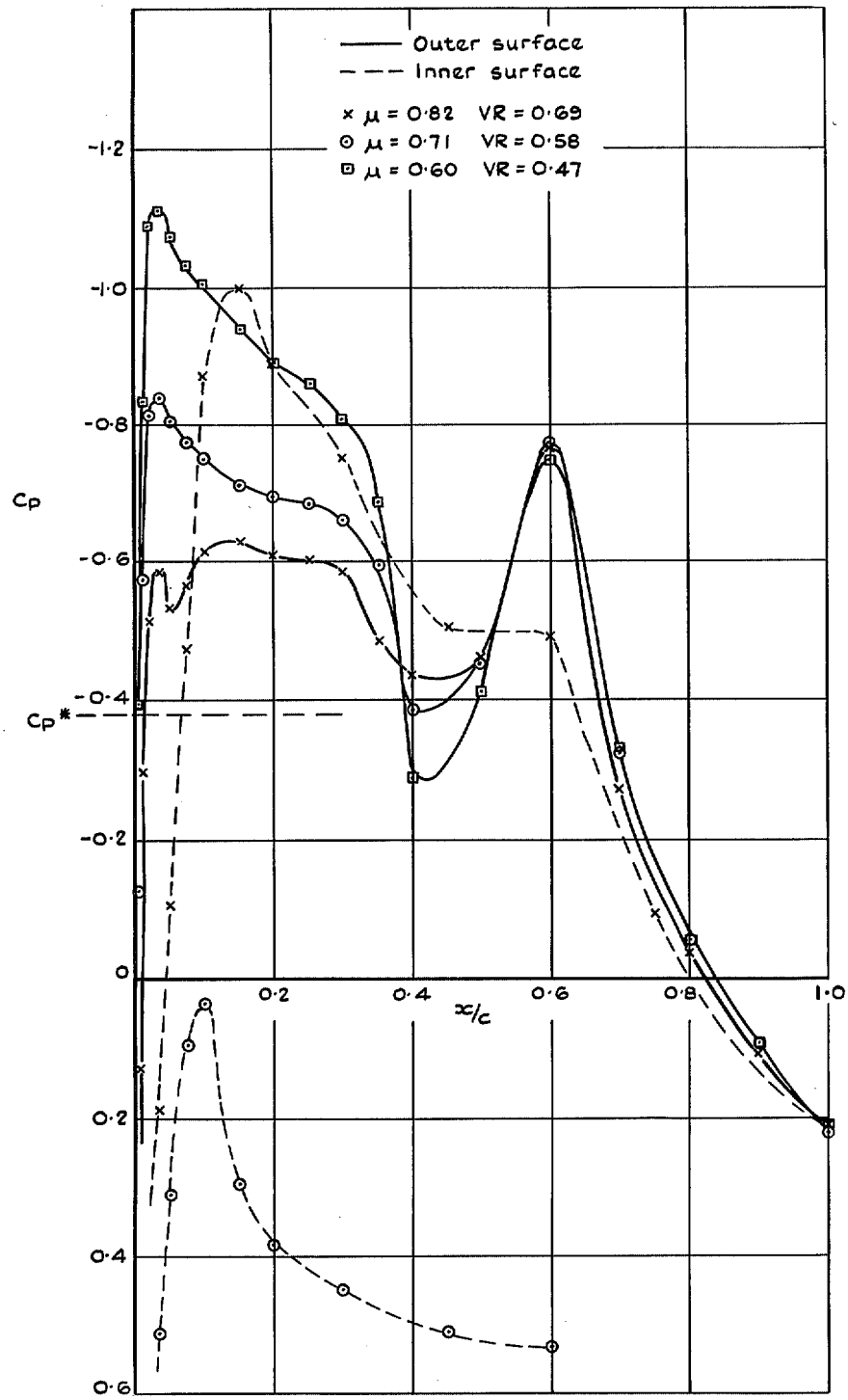

FIG. 27. Cowl 1 pressure distribution: $M = 0{\cdot}82$.

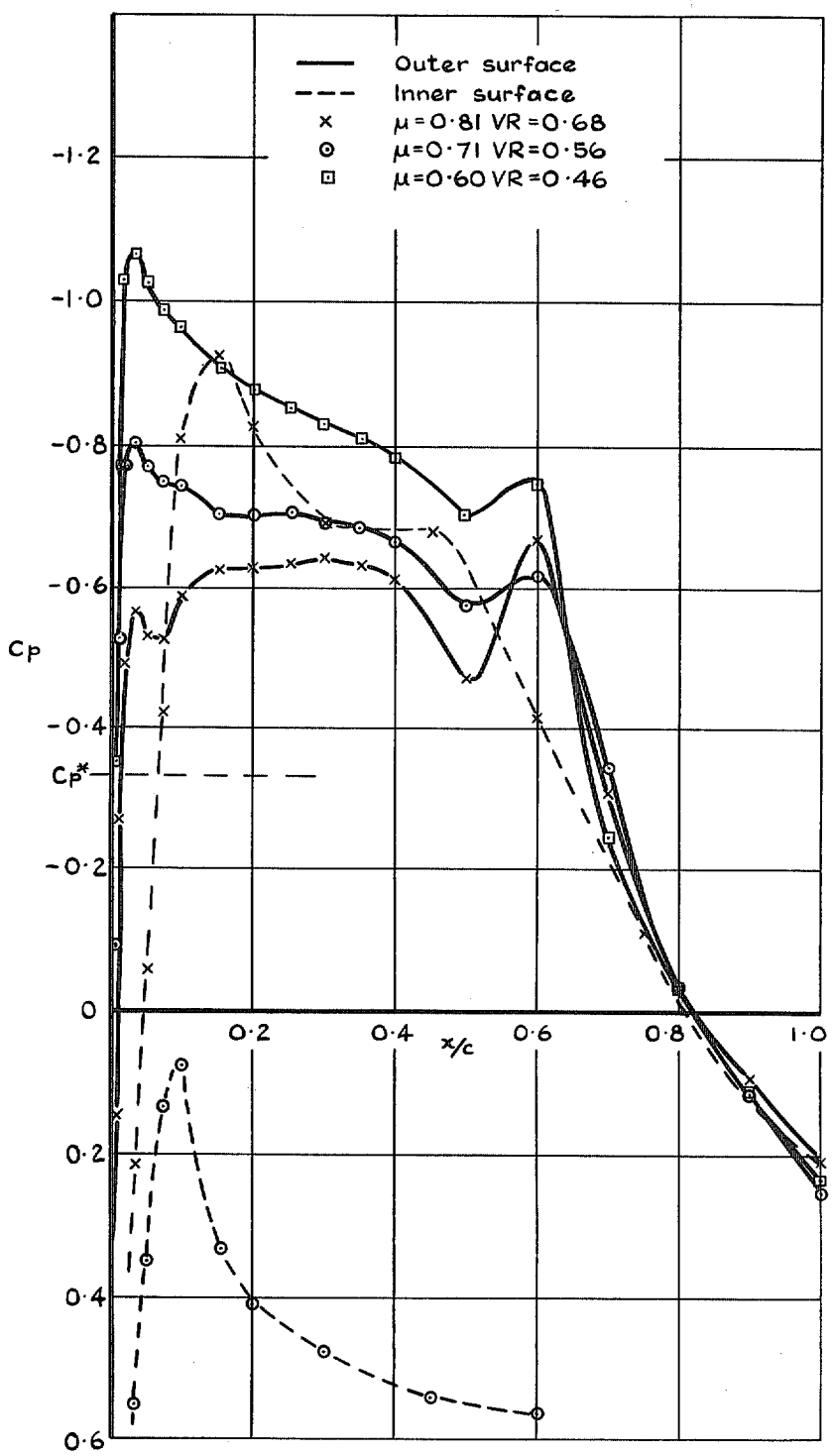

FIG. 28. Cowl 1 pressure distribution: $M = 0{\cdot}84$.

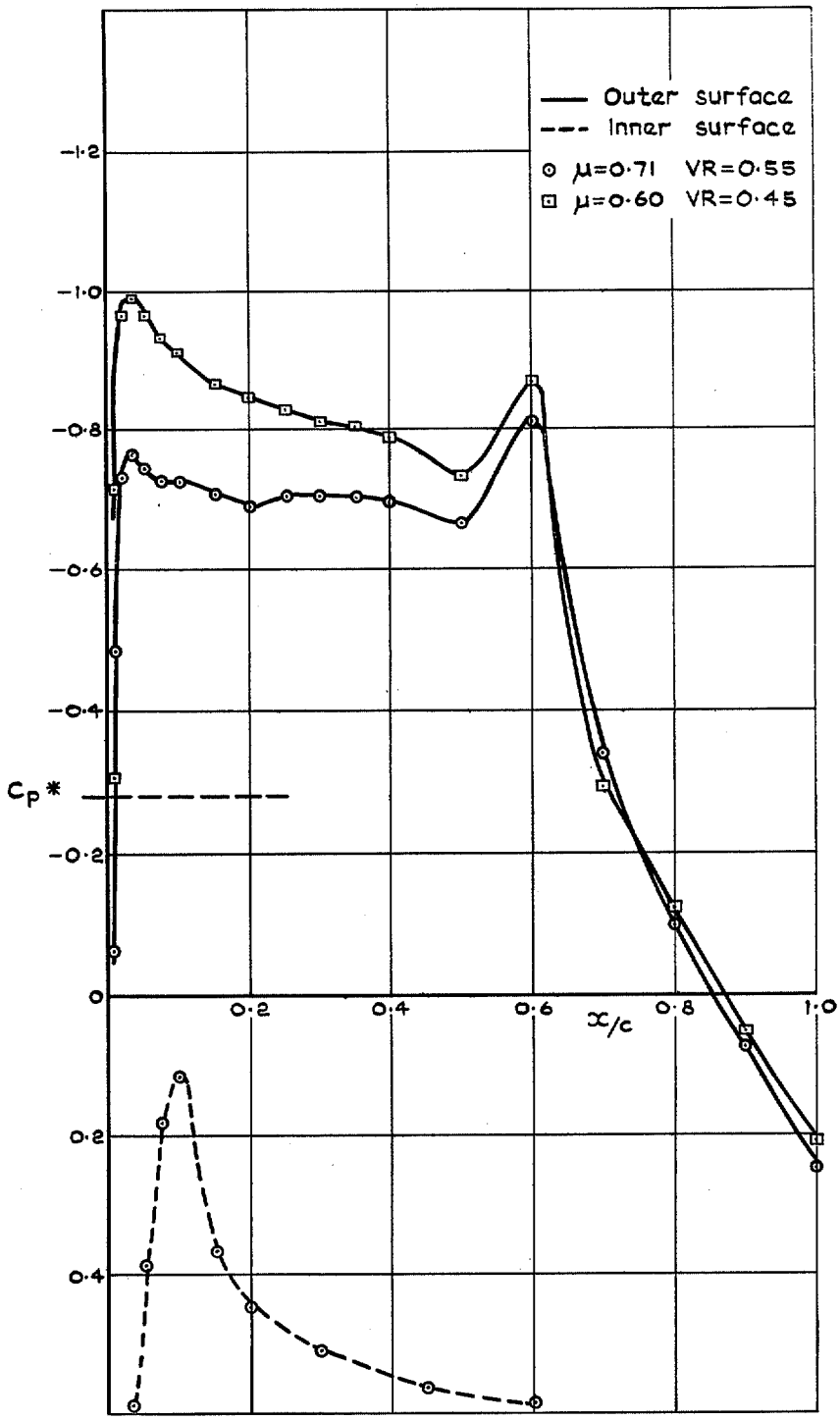

FIG. 29. Cowl 1 pressure distribution: $M = 0{\cdot}86$.

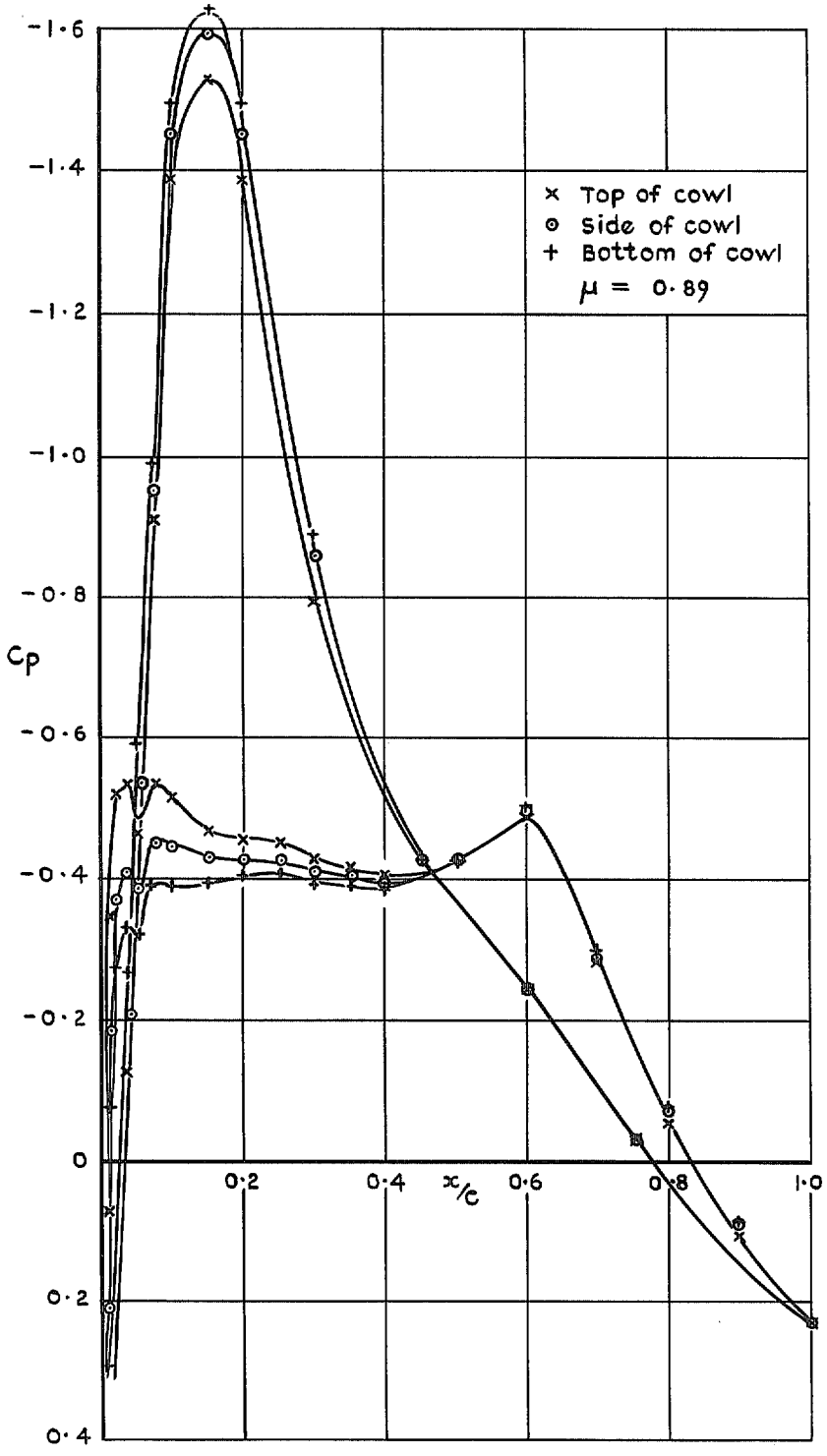

FIG. 30. Cowl 1 pressure distribution: $M = 0{\cdot}7$: $\alpha = +1°$.

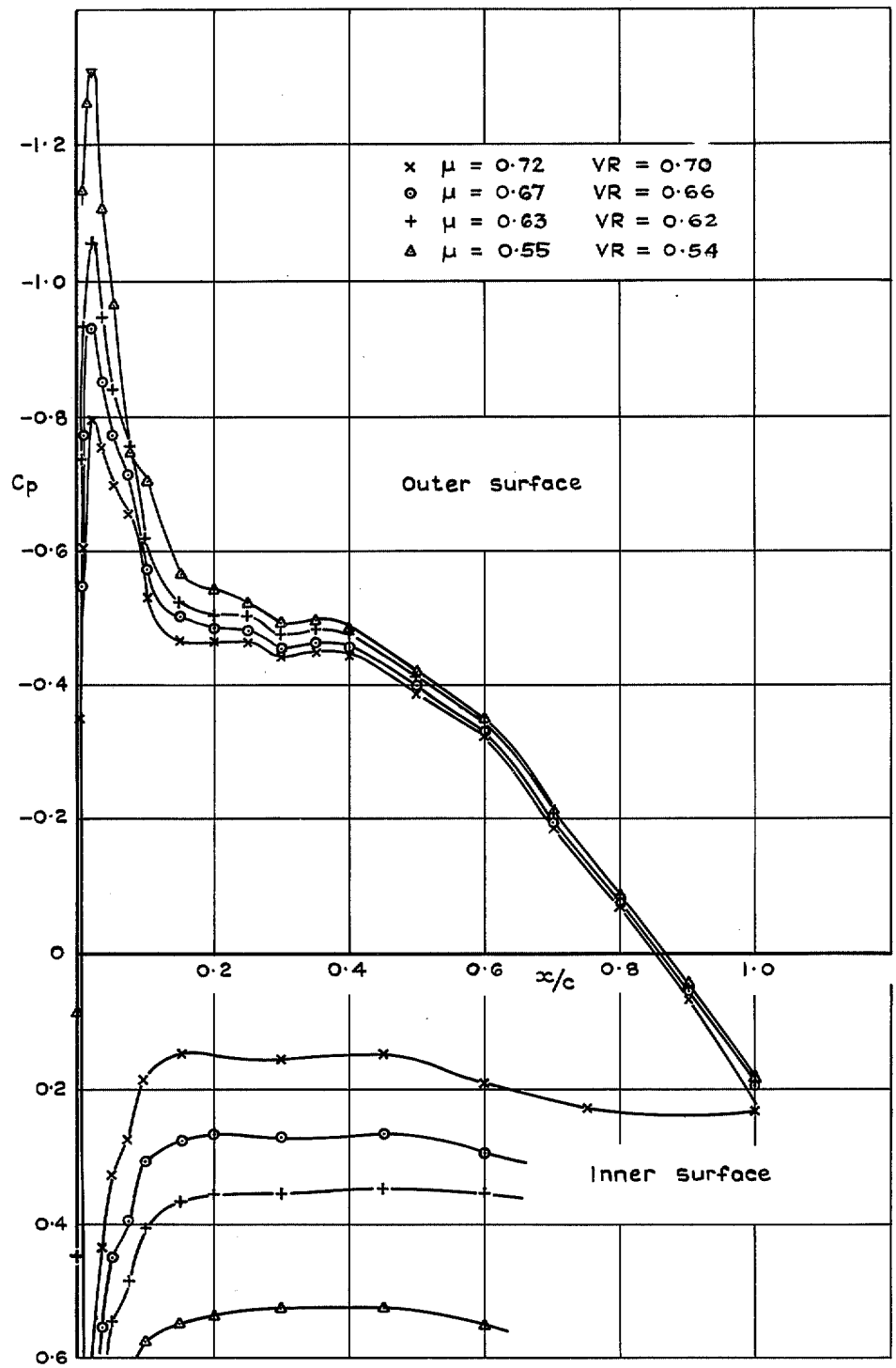

FIG. 31. Cowl 2 pressure distribution: $M = 0{\cdot}3$.

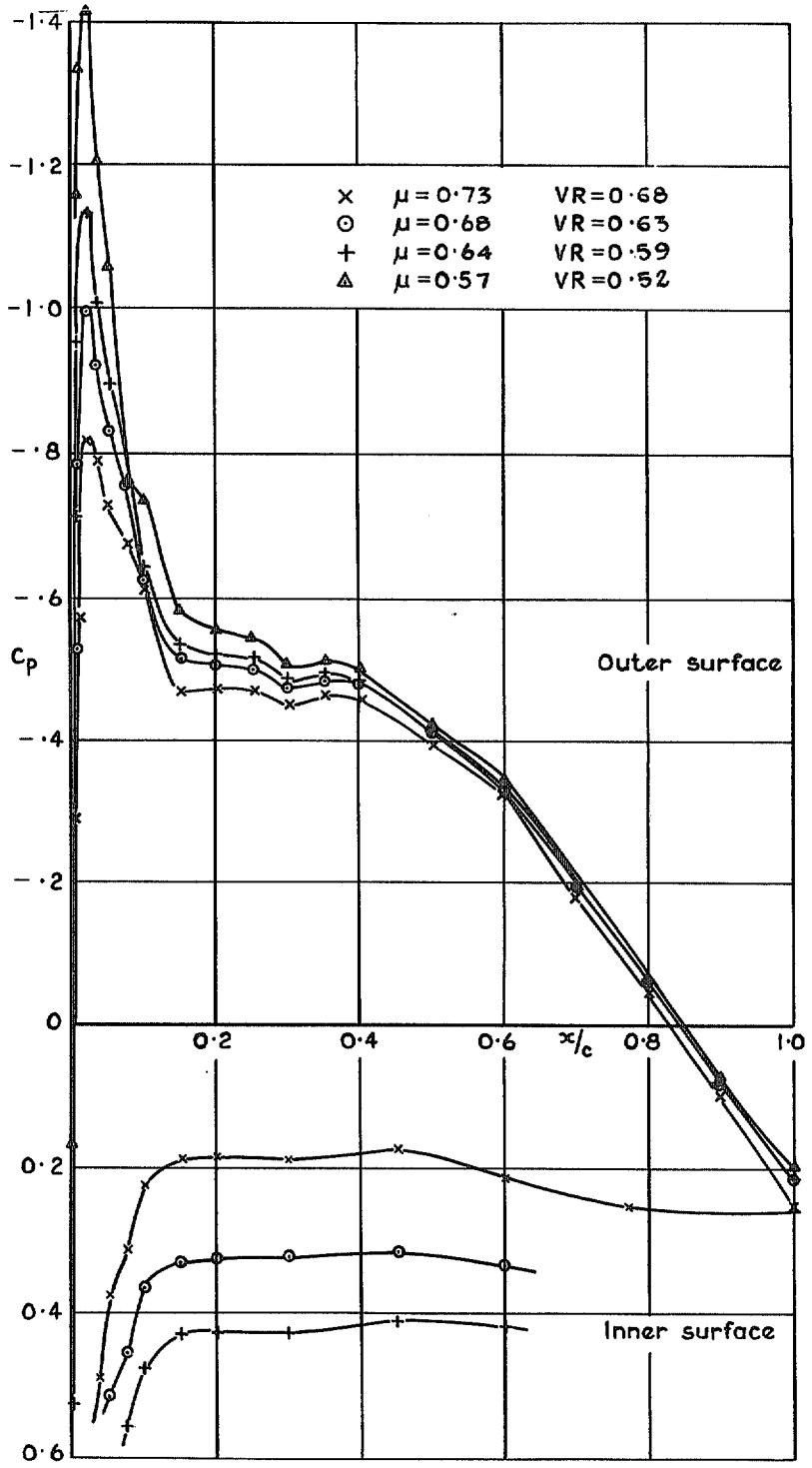

FIG. 32. Cowl 2 pressure distribution: $M = 0{\cdot}5$.

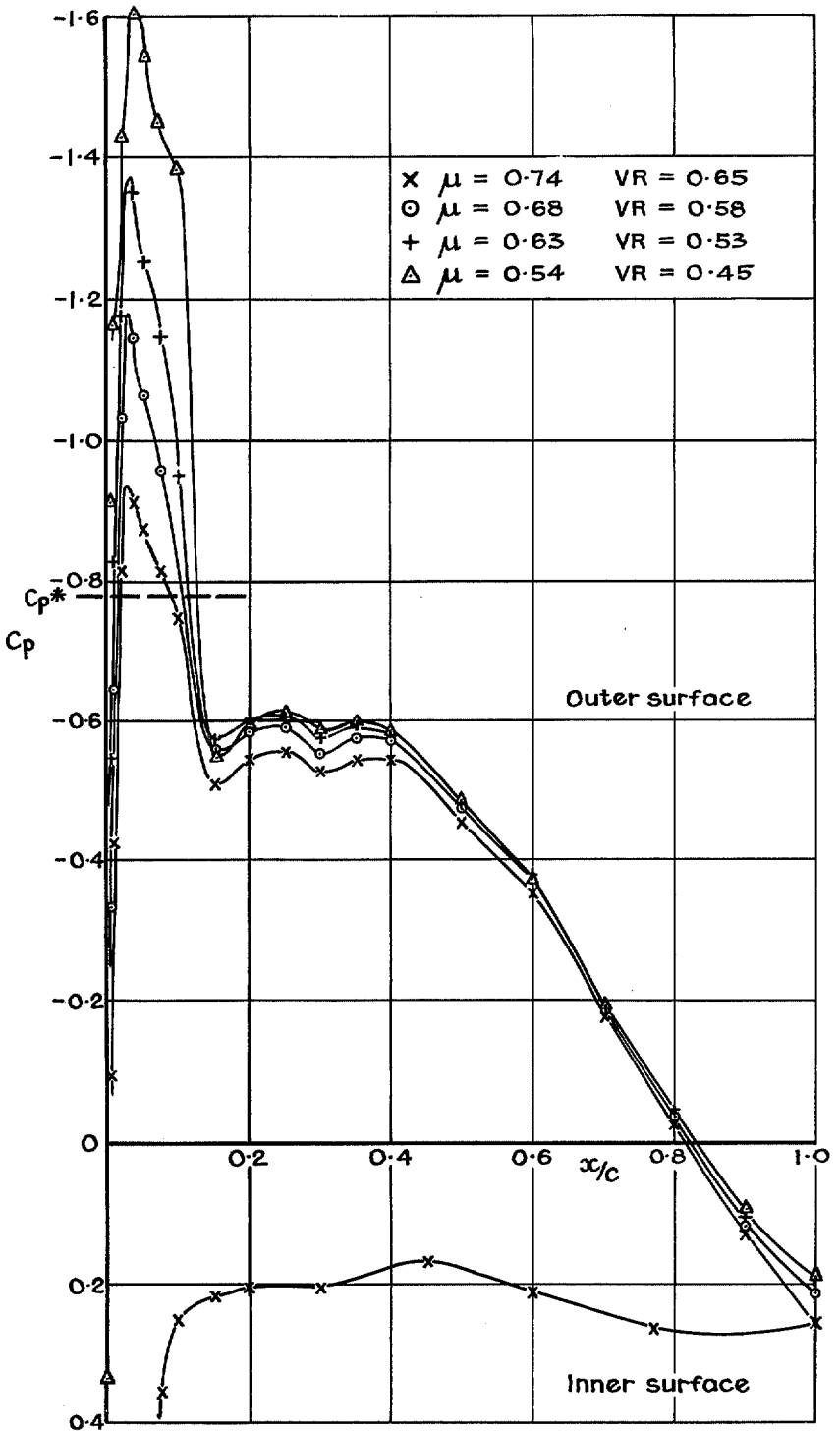

FIG. 33. Cowl 2 pressure distribution: $M = 0{\cdot}7$.

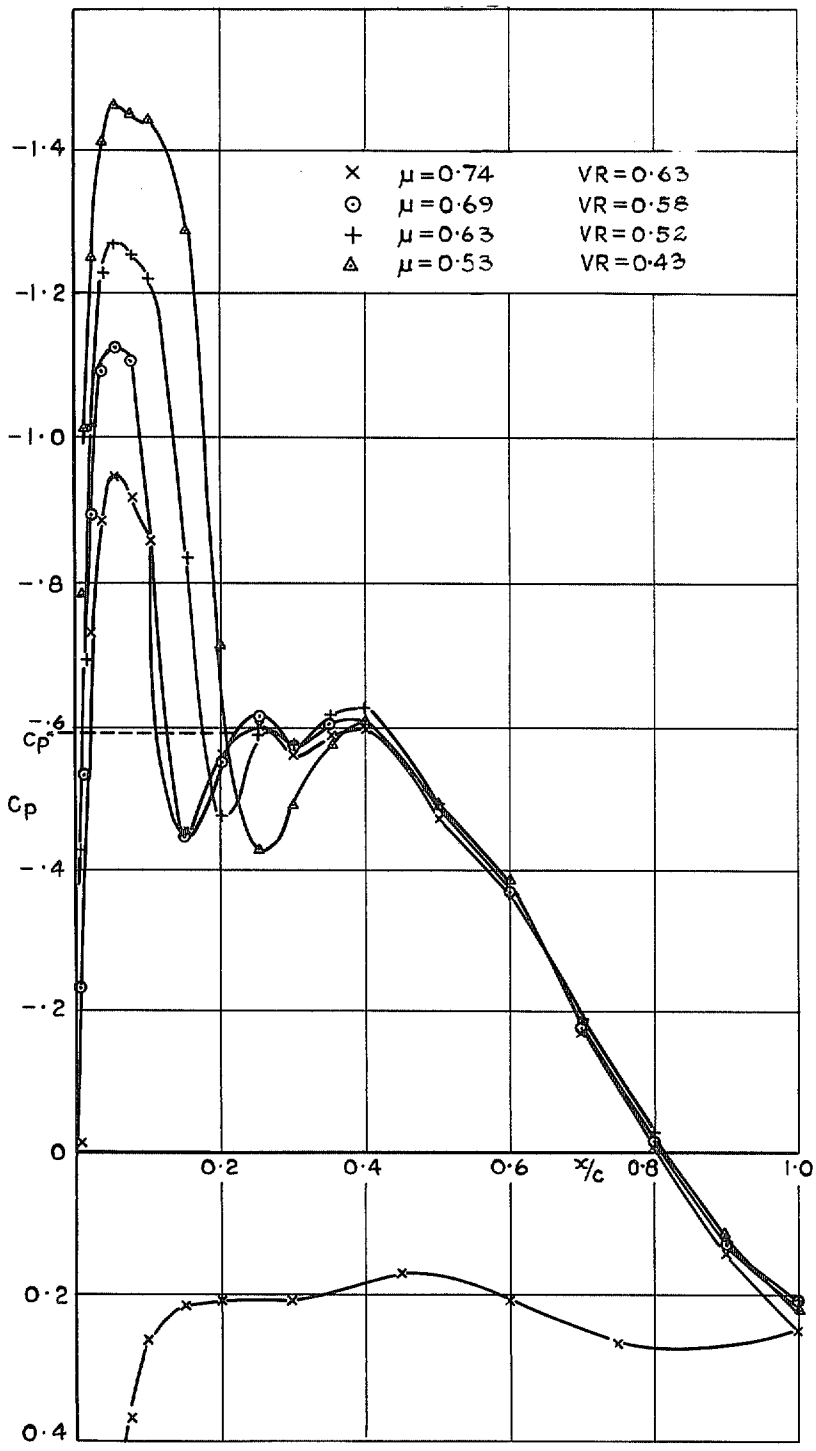

FIG. 34. Cowl 2 pressure distribution: $M = 0{\cdot}75$.

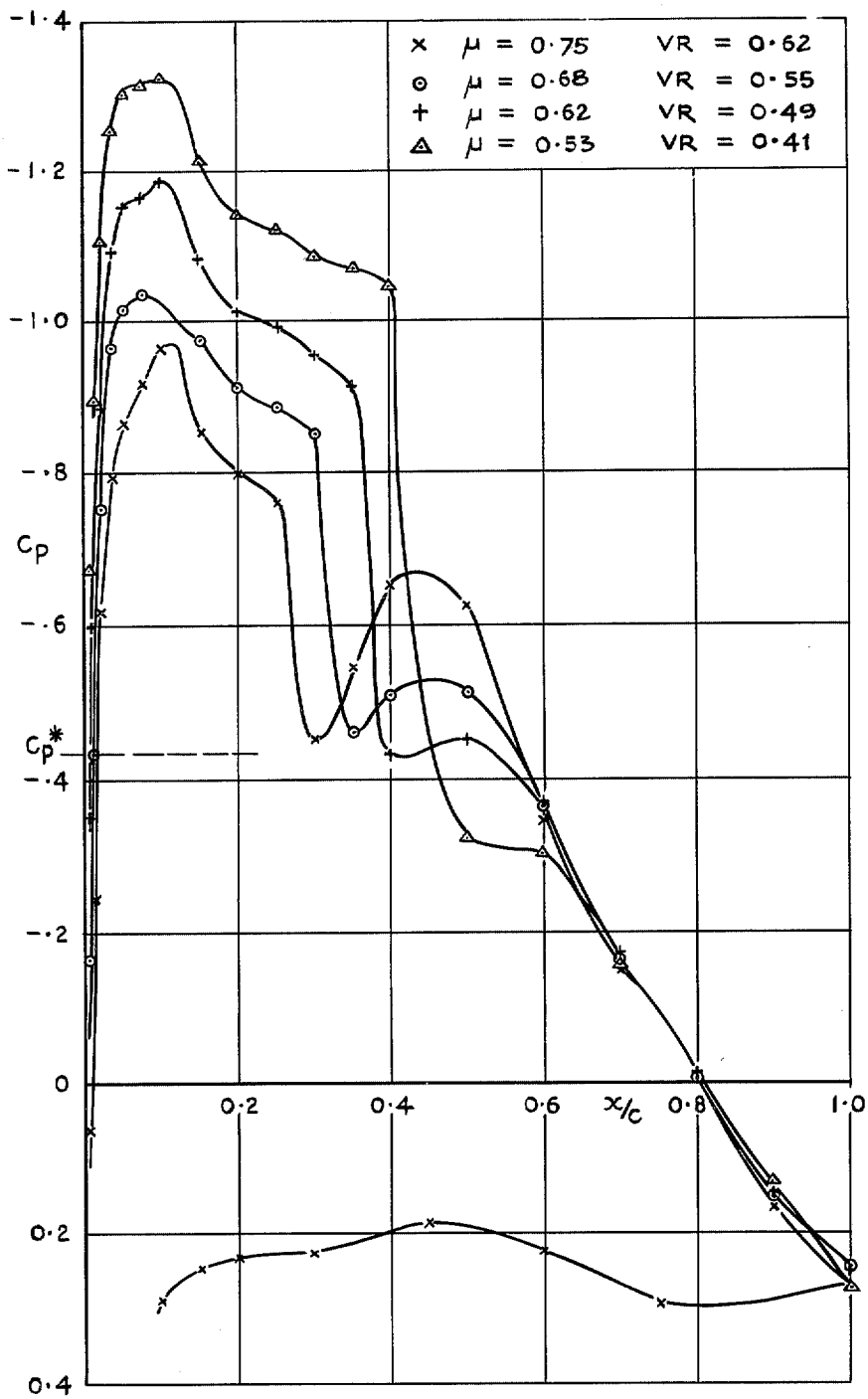

FIG. 35. Cowl 2 pressure distribution: $M = 0{\cdot}80$.

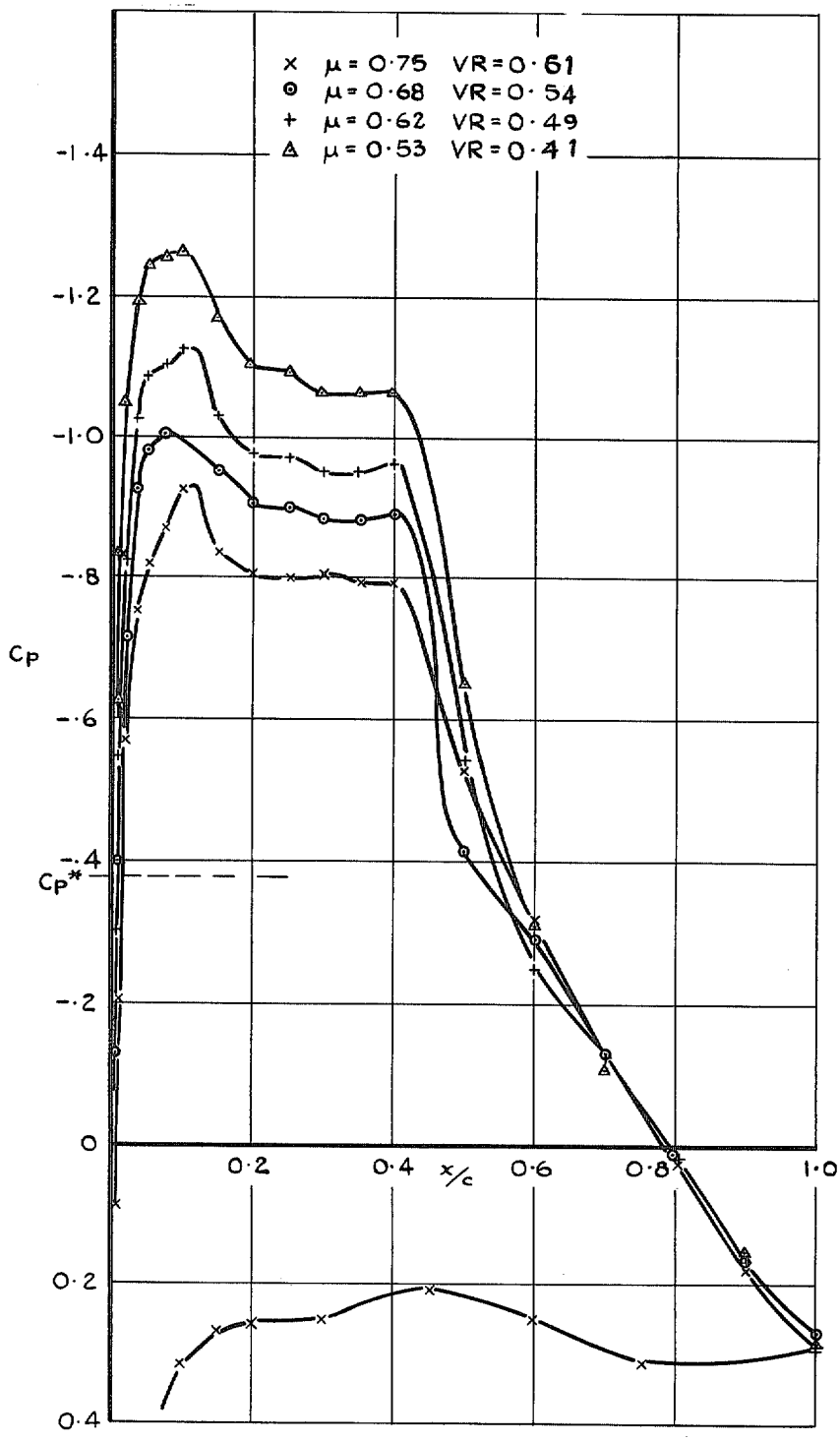

FIG. 36. Cowl 2 pressure distribution: $M = 0{\cdot}82$.

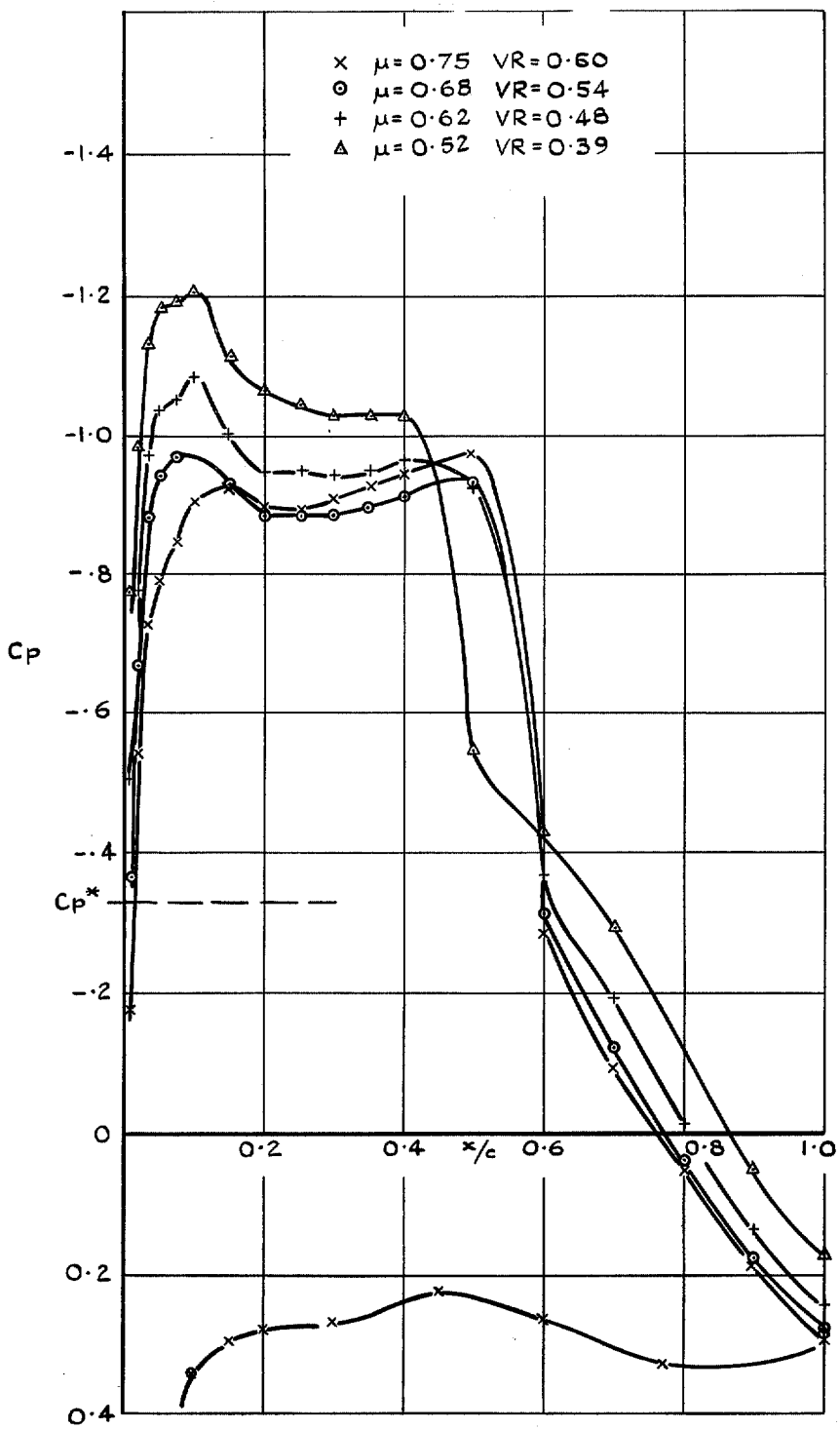

FIG. 37. Cowl 2 pressure distribution: $M = 0{\cdot}84$.

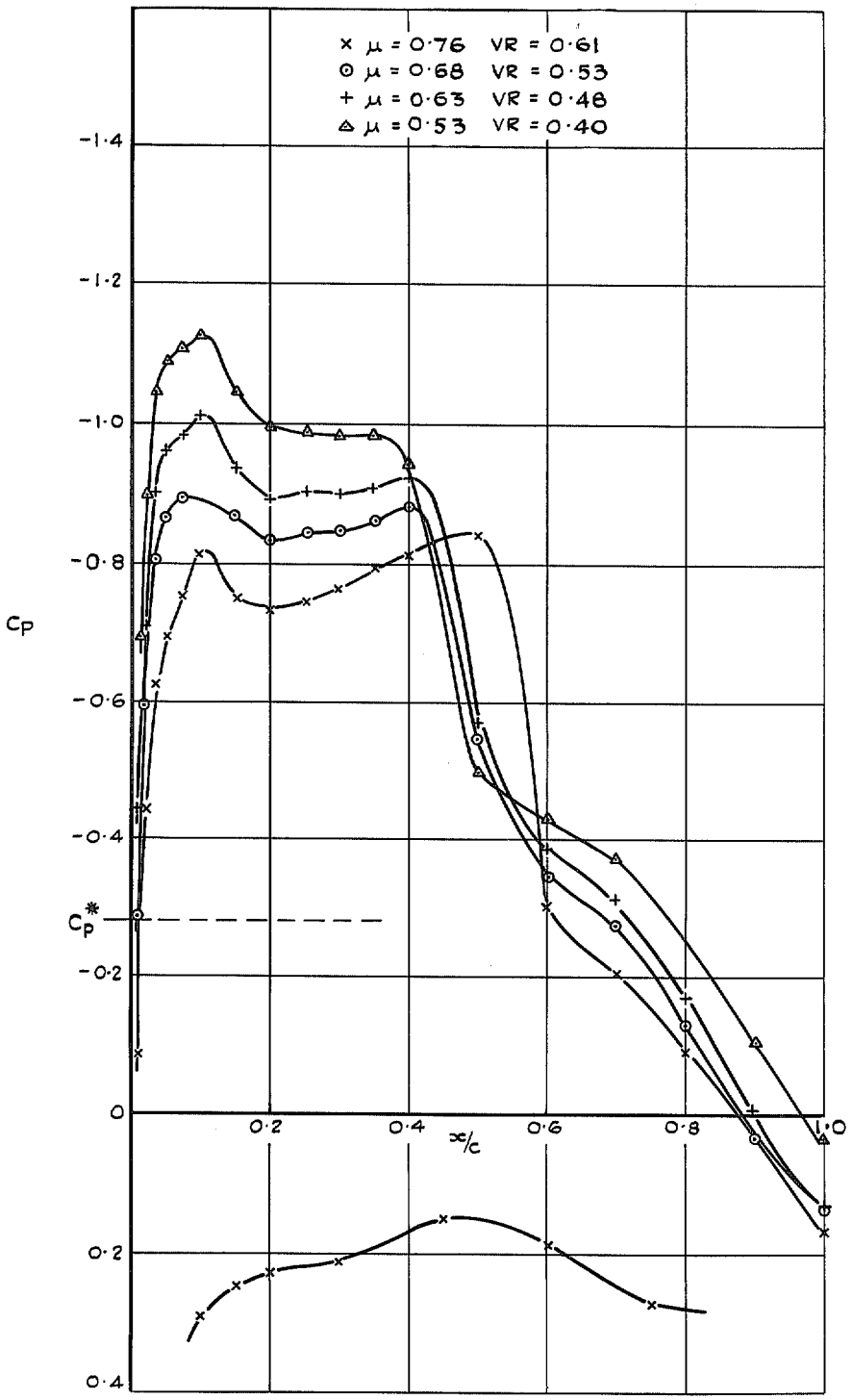

FIG. 38. Cowl 2 pressure distribution: $M = 0{\cdot}86$.

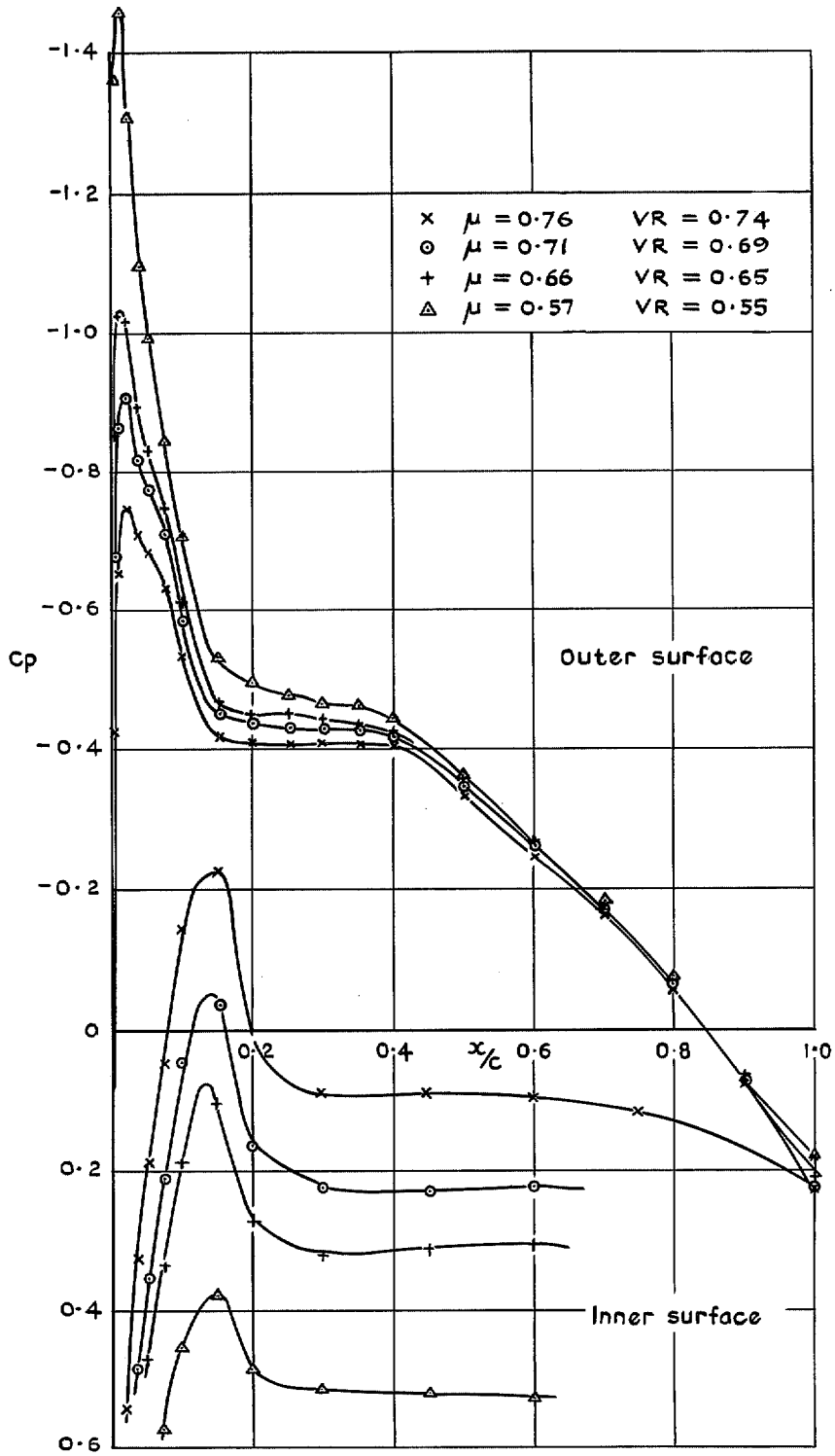

FIG. 39. Cowl 3 pressure distribution: $M = 0{\cdot}3$.

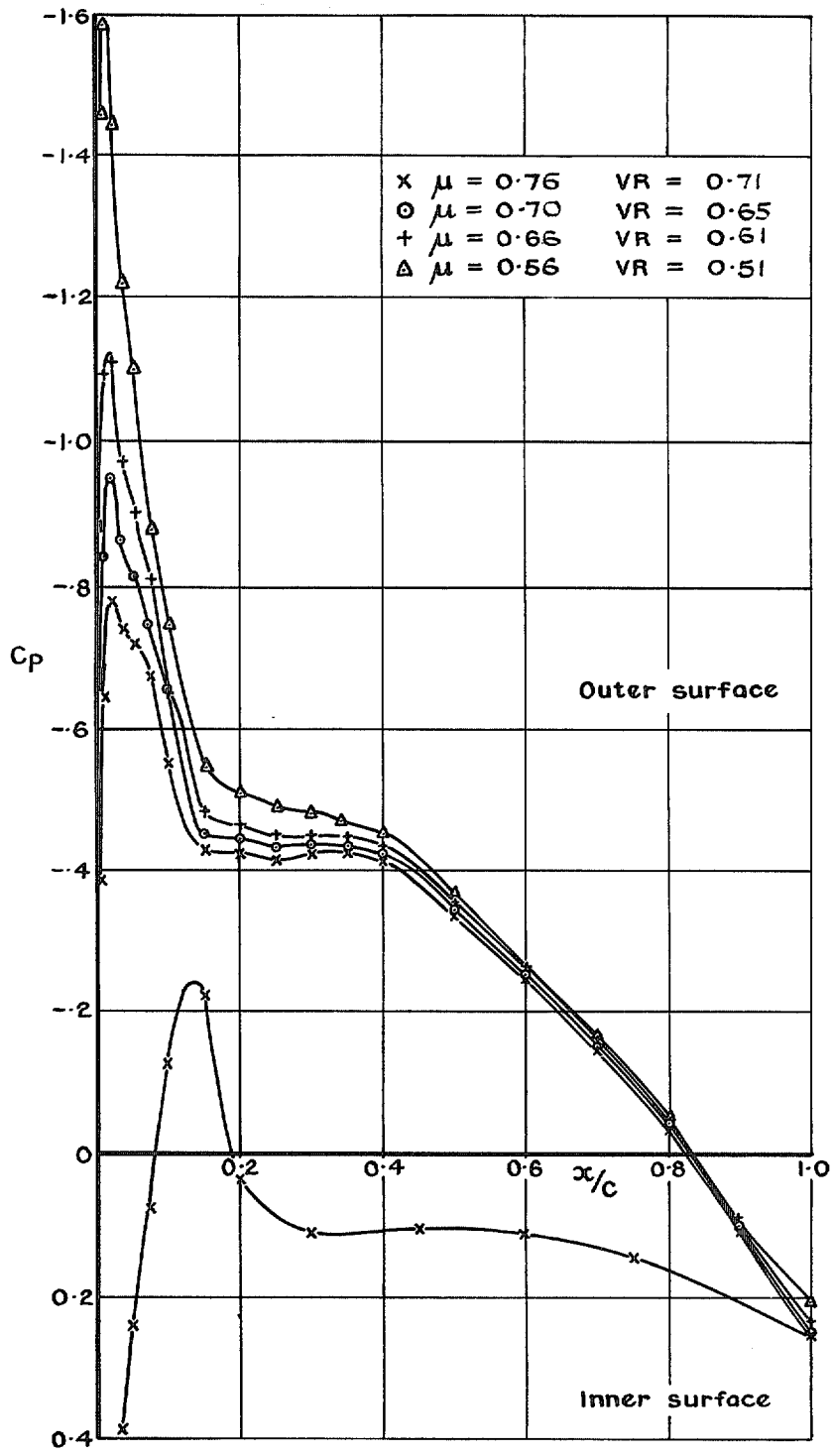

FIG. 40. Cowl 3 pressure distribution: $M = 0{\cdot}5$.

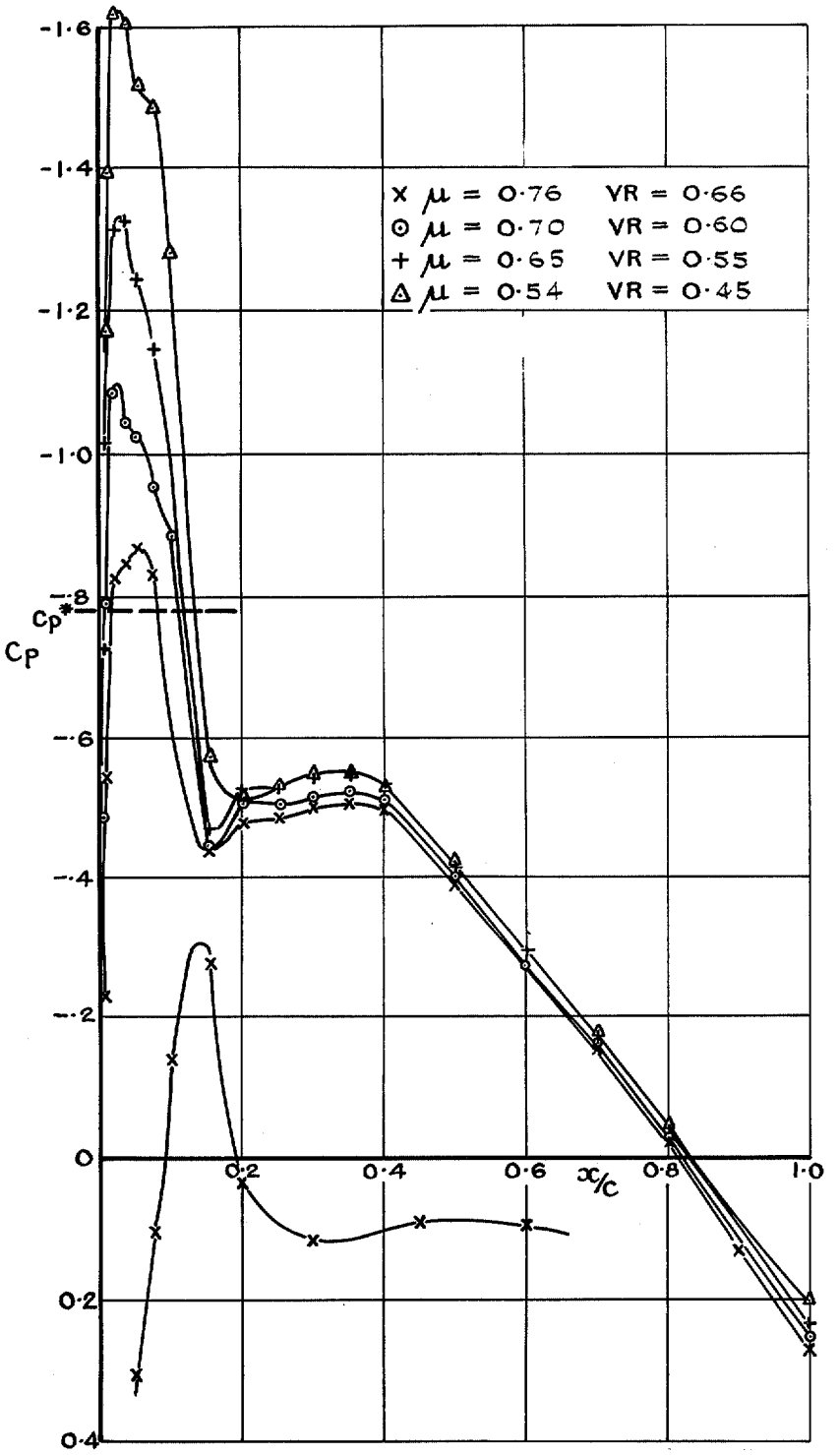

FIG. 41. Cowl 3 pressure distribution: $M = 0{\cdot}7$.

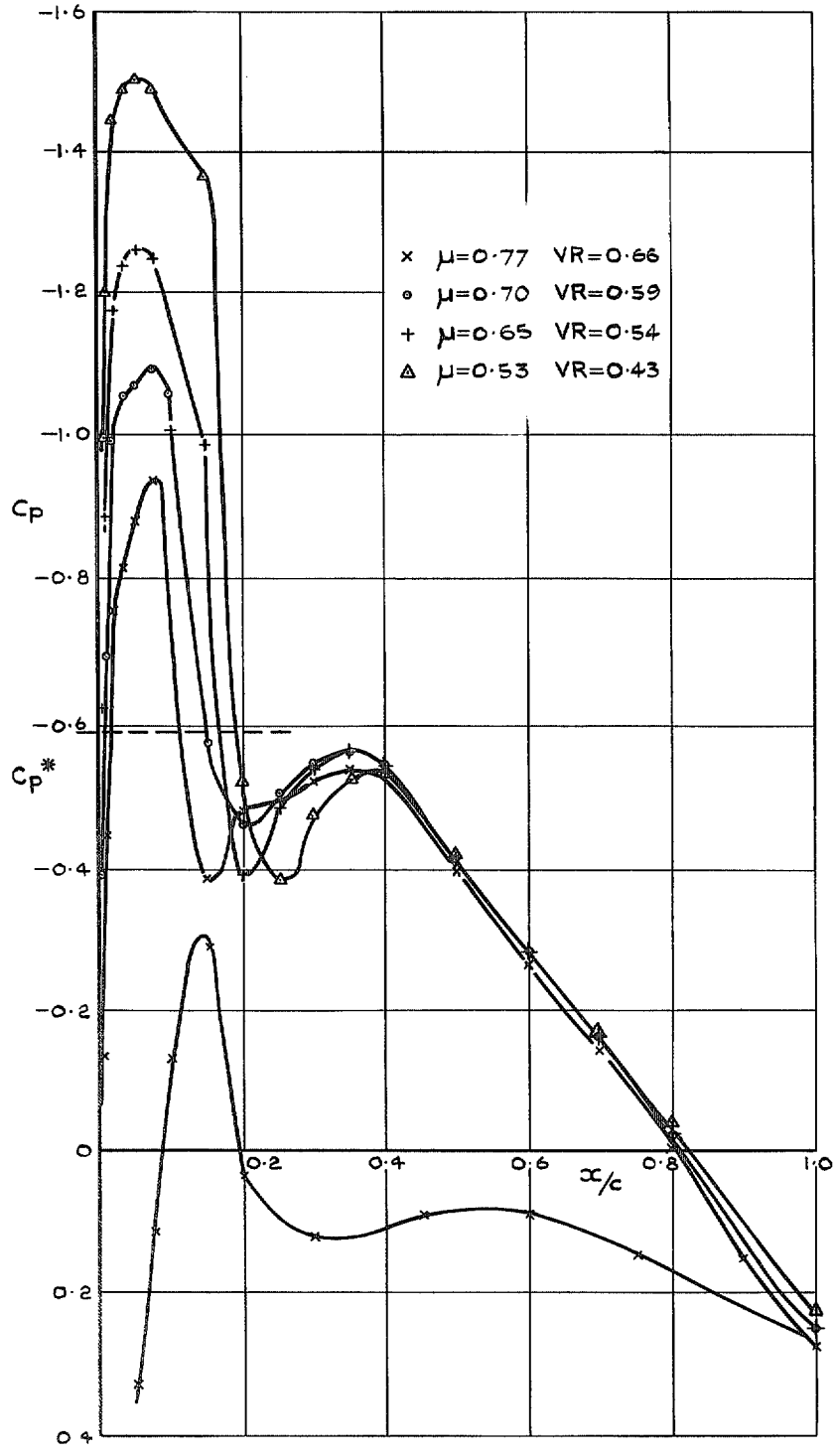

FIG. 42. Cowl 3 pressure distribution: $M = 0{\cdot}75$.

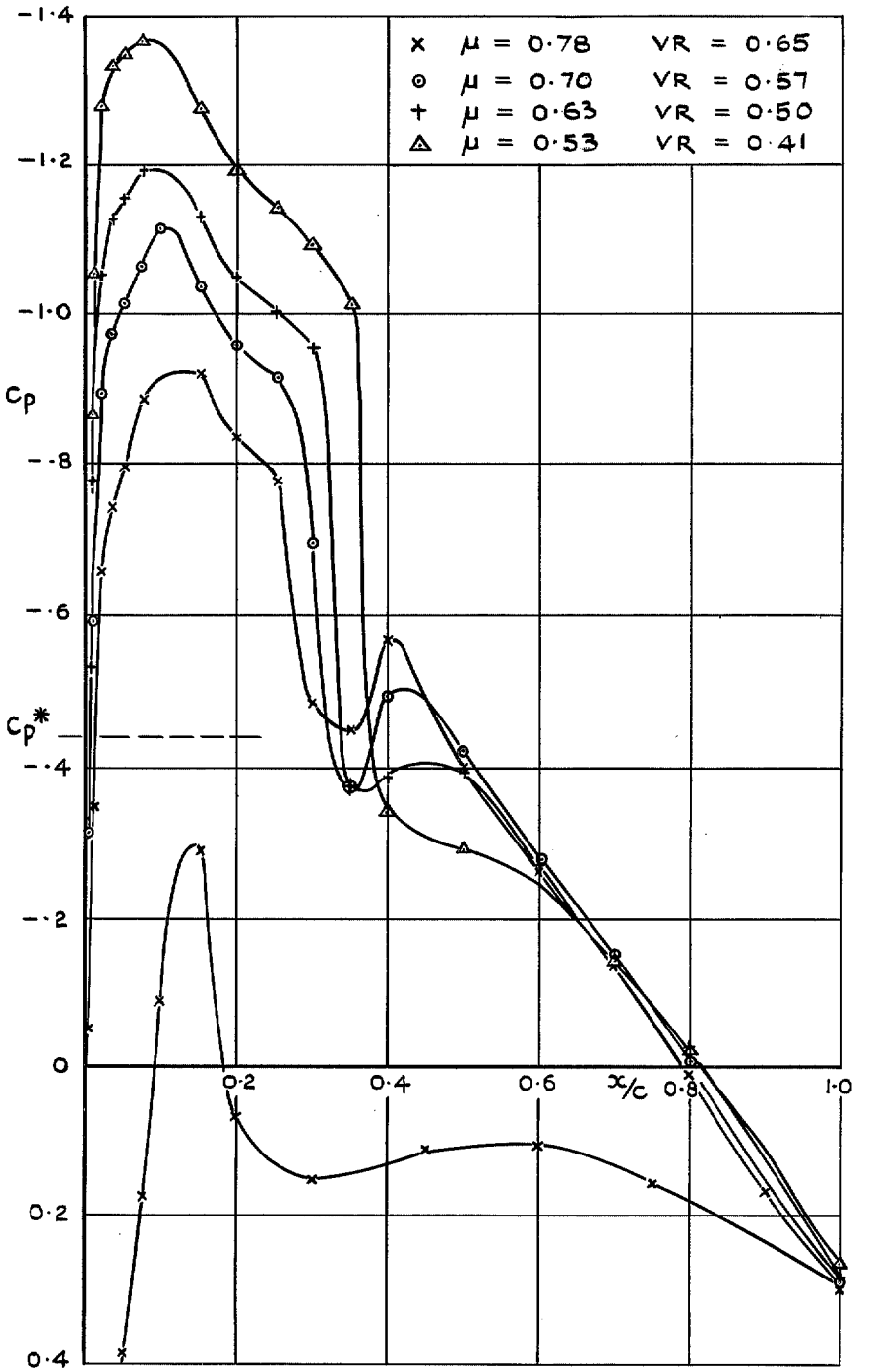

FIG. 43. Cowl 3 pressure distribution: $M = 0{\cdot}80$.

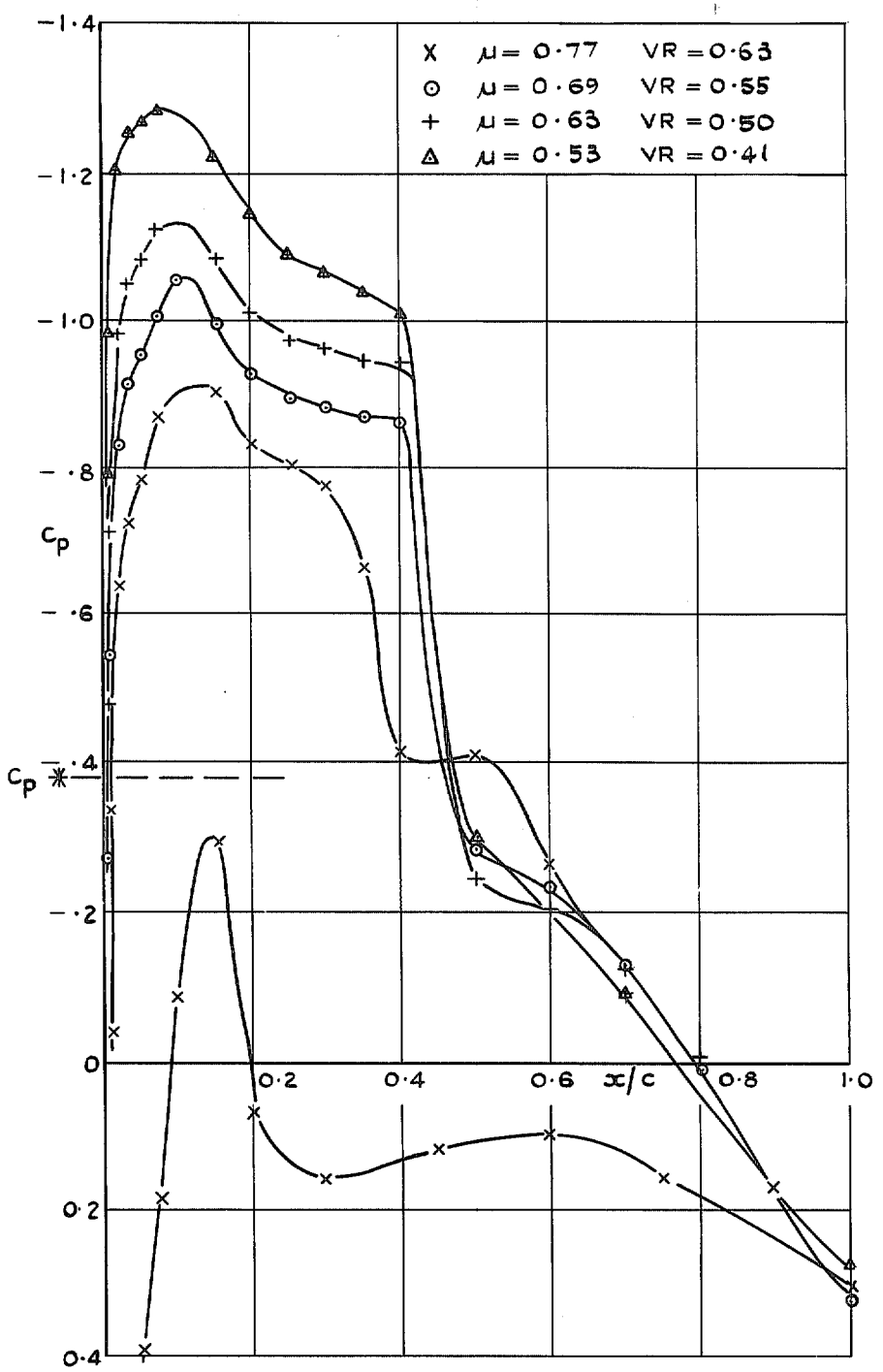

FIG. 44. Cowl 3 pressure distribution: $M = 0{\cdot}82$.

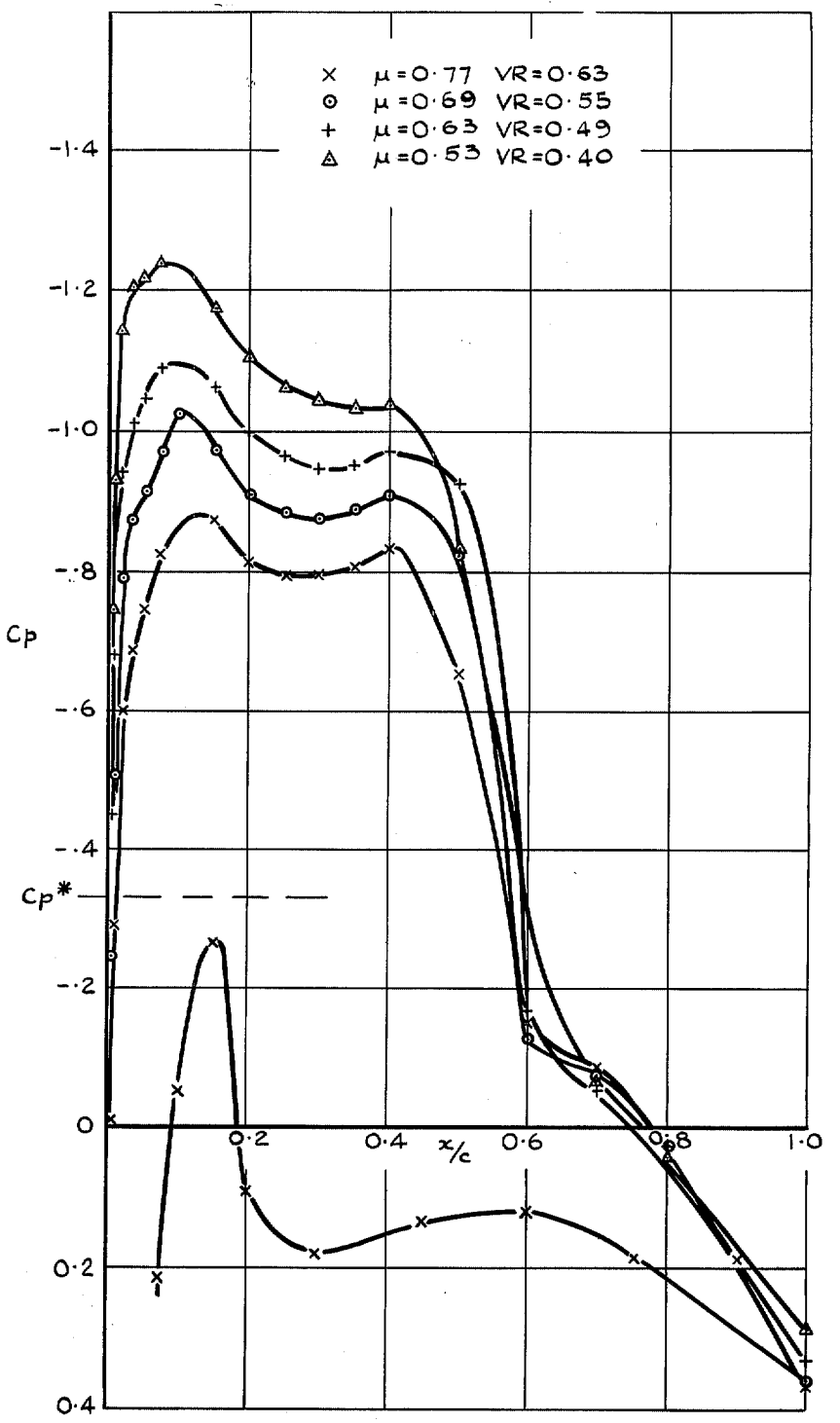

FIG. 45. Cowl 3 pressure distribution: $M = 0{\cdot}84$.

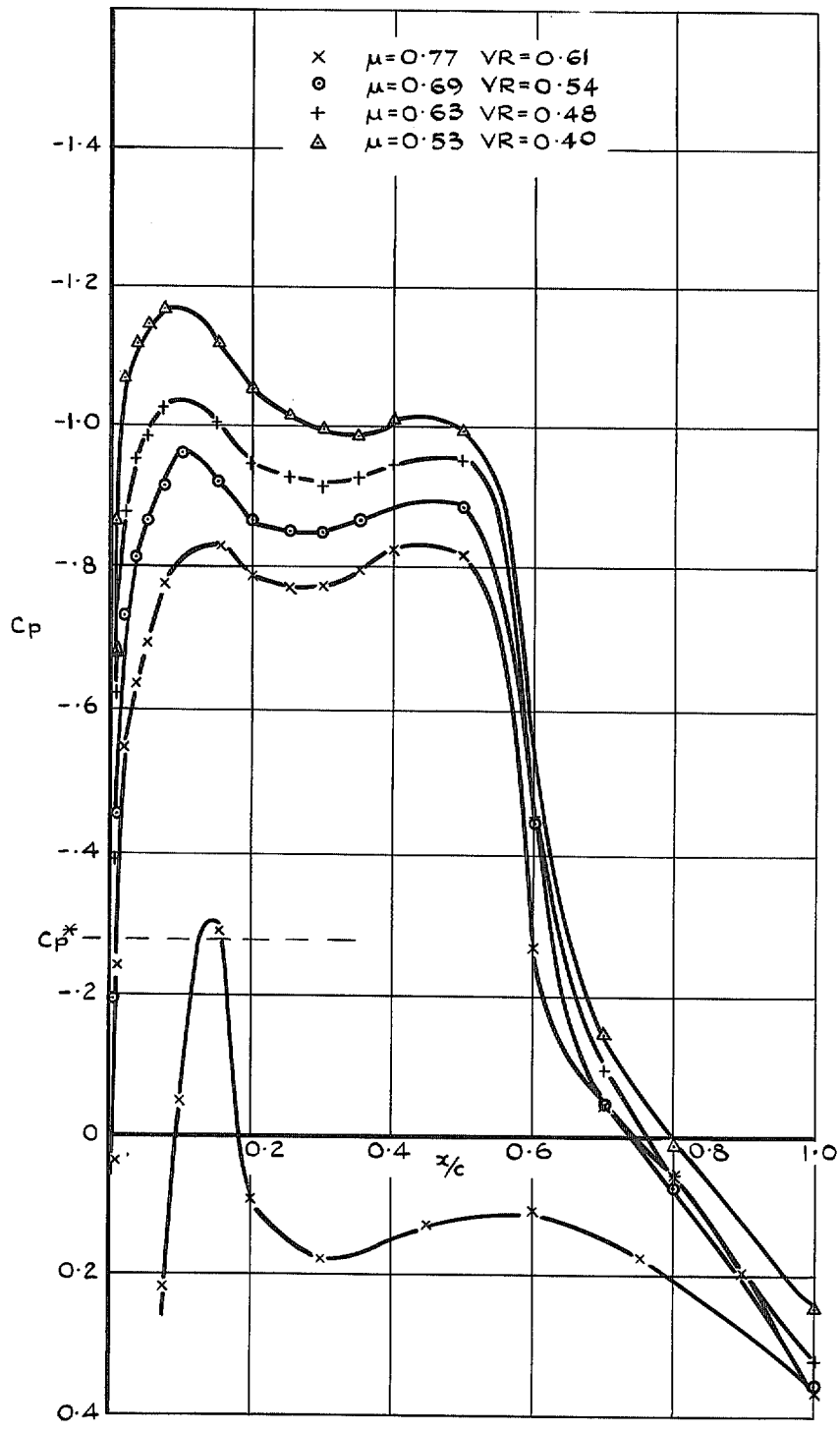

FIG. 46. Cowl 3 pressure distribution: $M = 0{\cdot}86$.

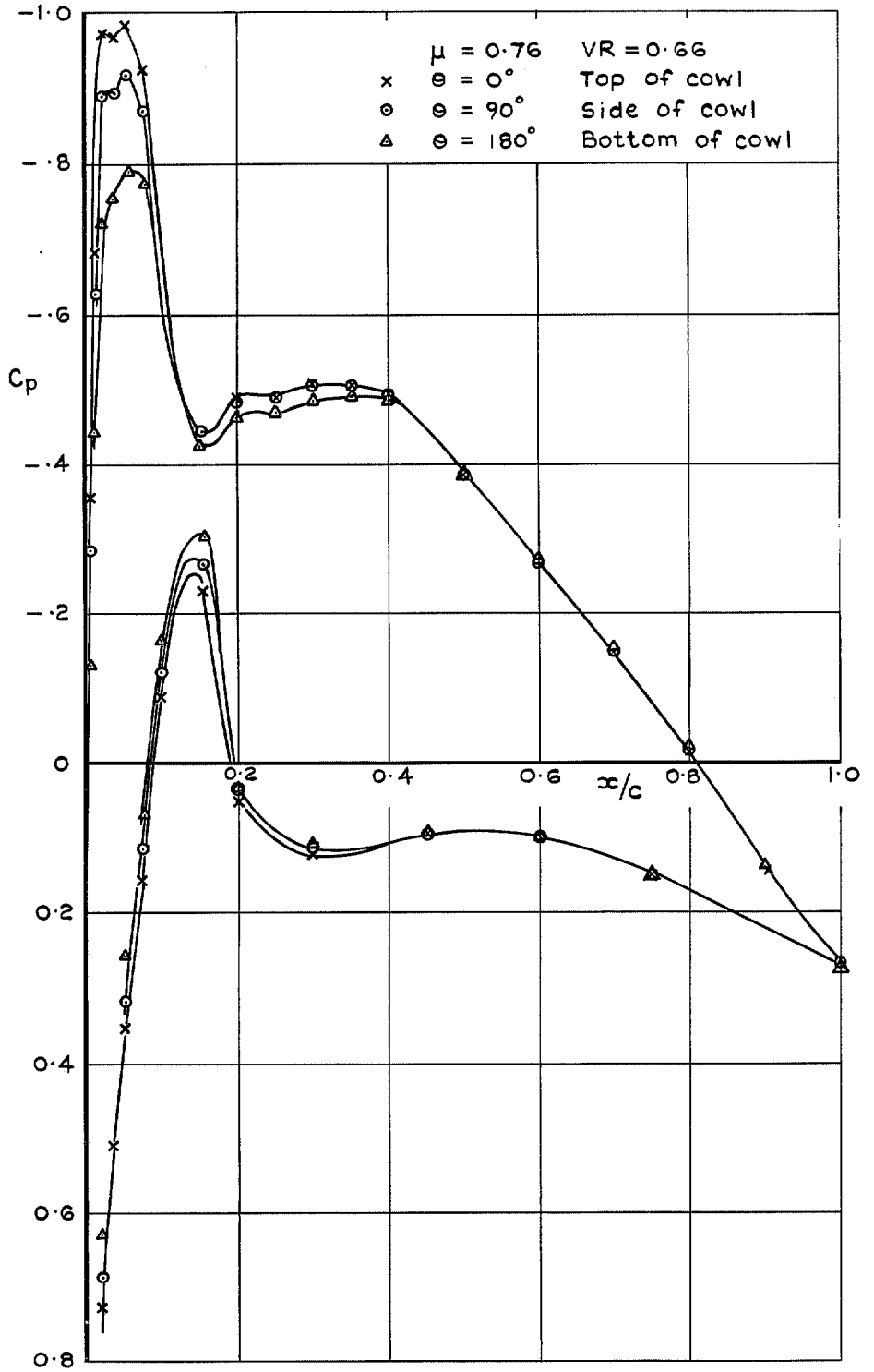

FIG. 47. Cowl 3 pressure distribution: $M = 0{\cdot}7$: $\alpha = +1°$.

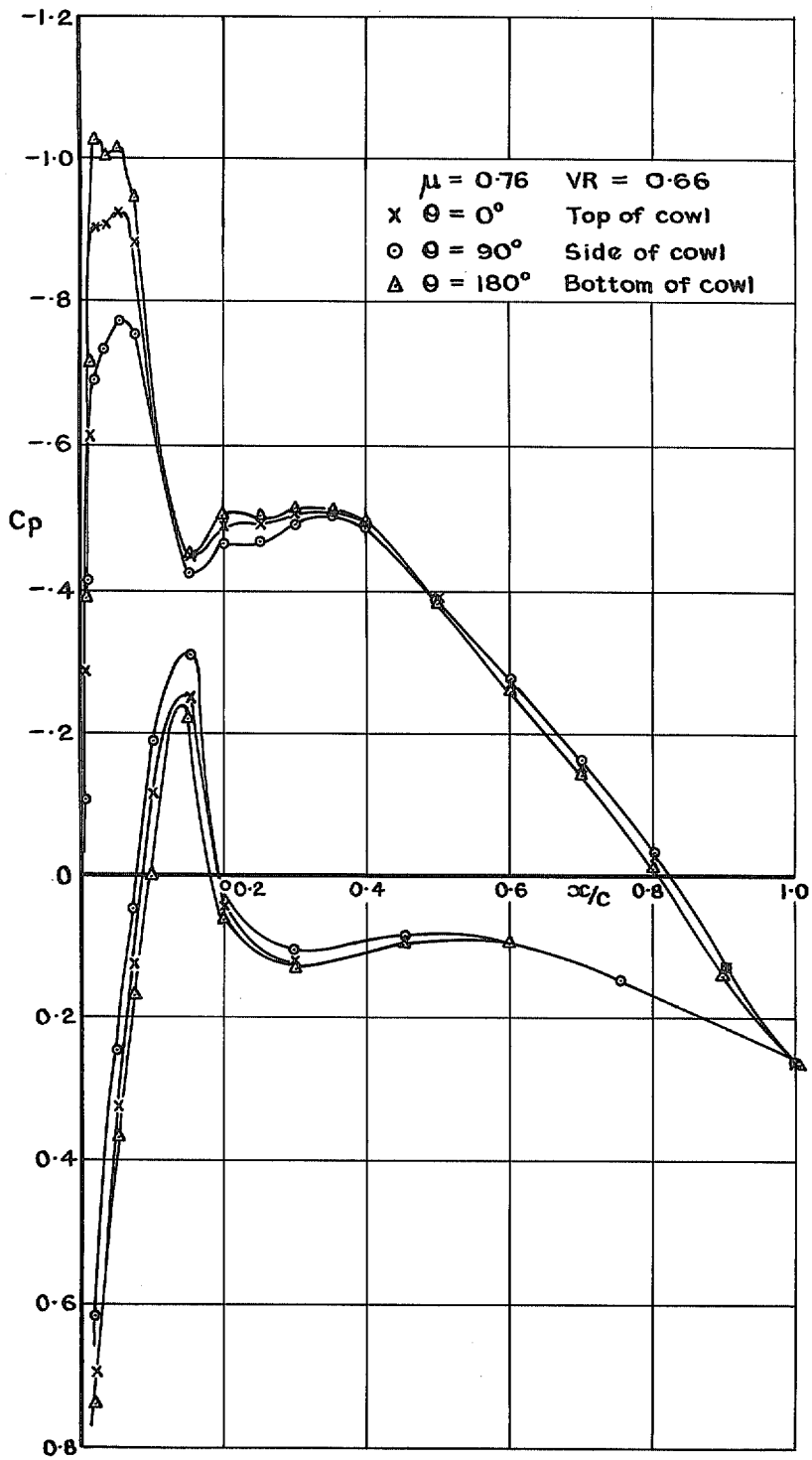

FIG. 48. Cowl 3: pressure distribution: $M = 0{\cdot}7$: $\alpha = -1°$.

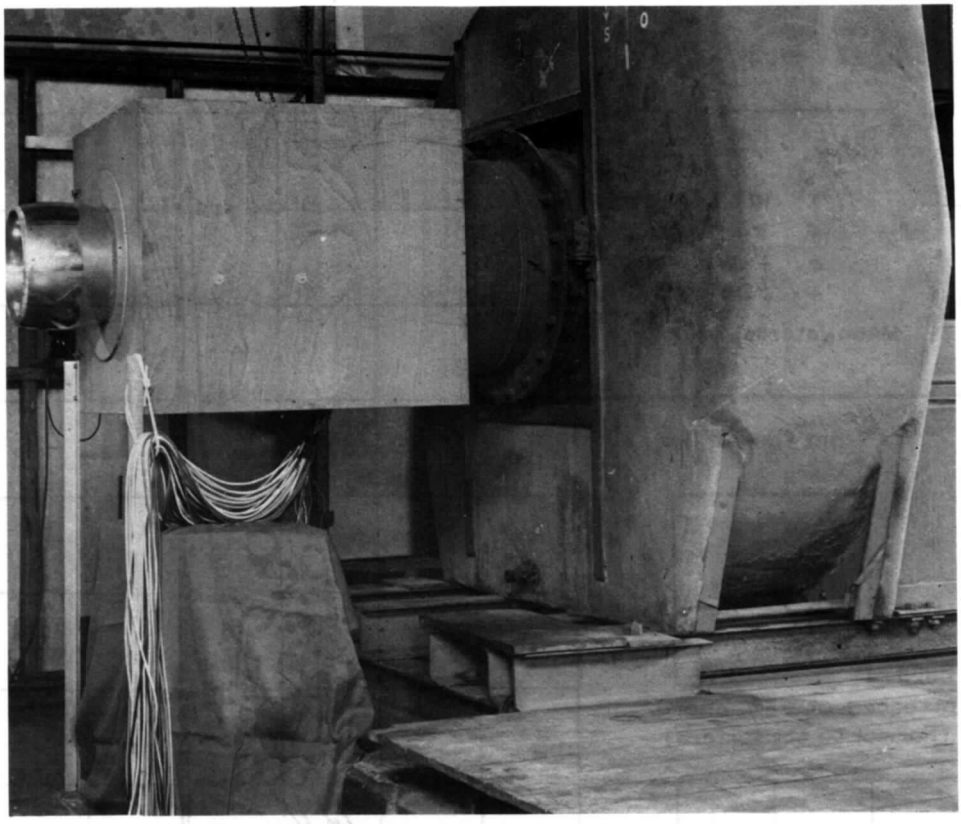

FIG. 49a. General view of static test rig.

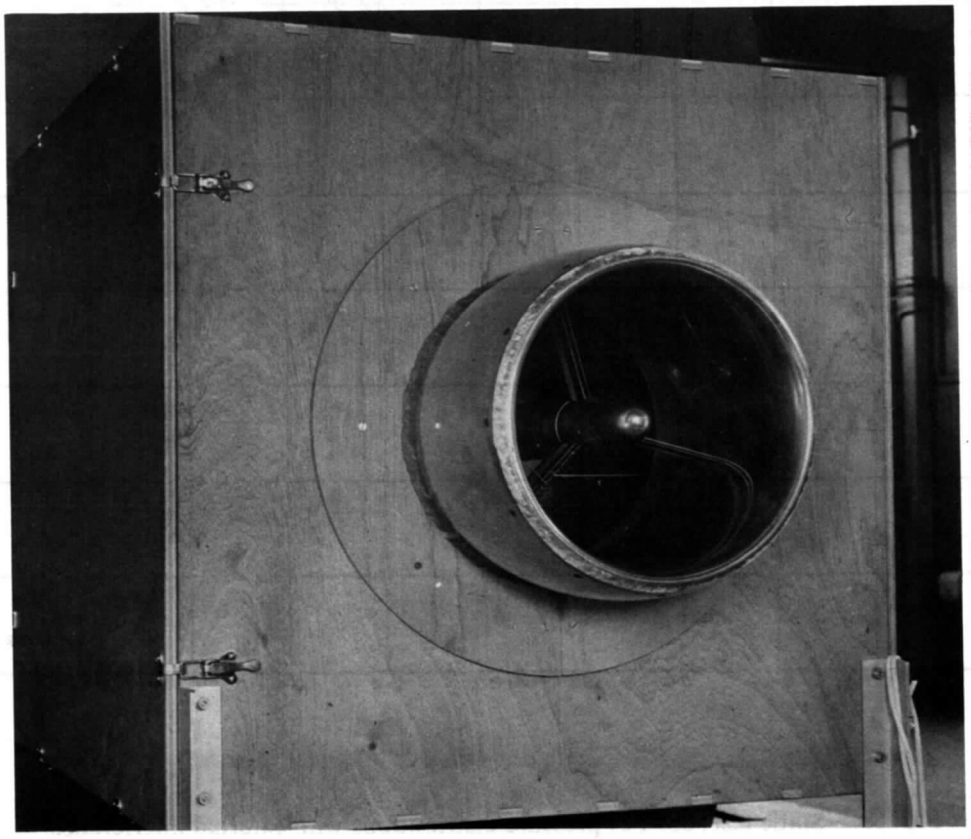

FIG. 49b. Cowl installed in static test rig.

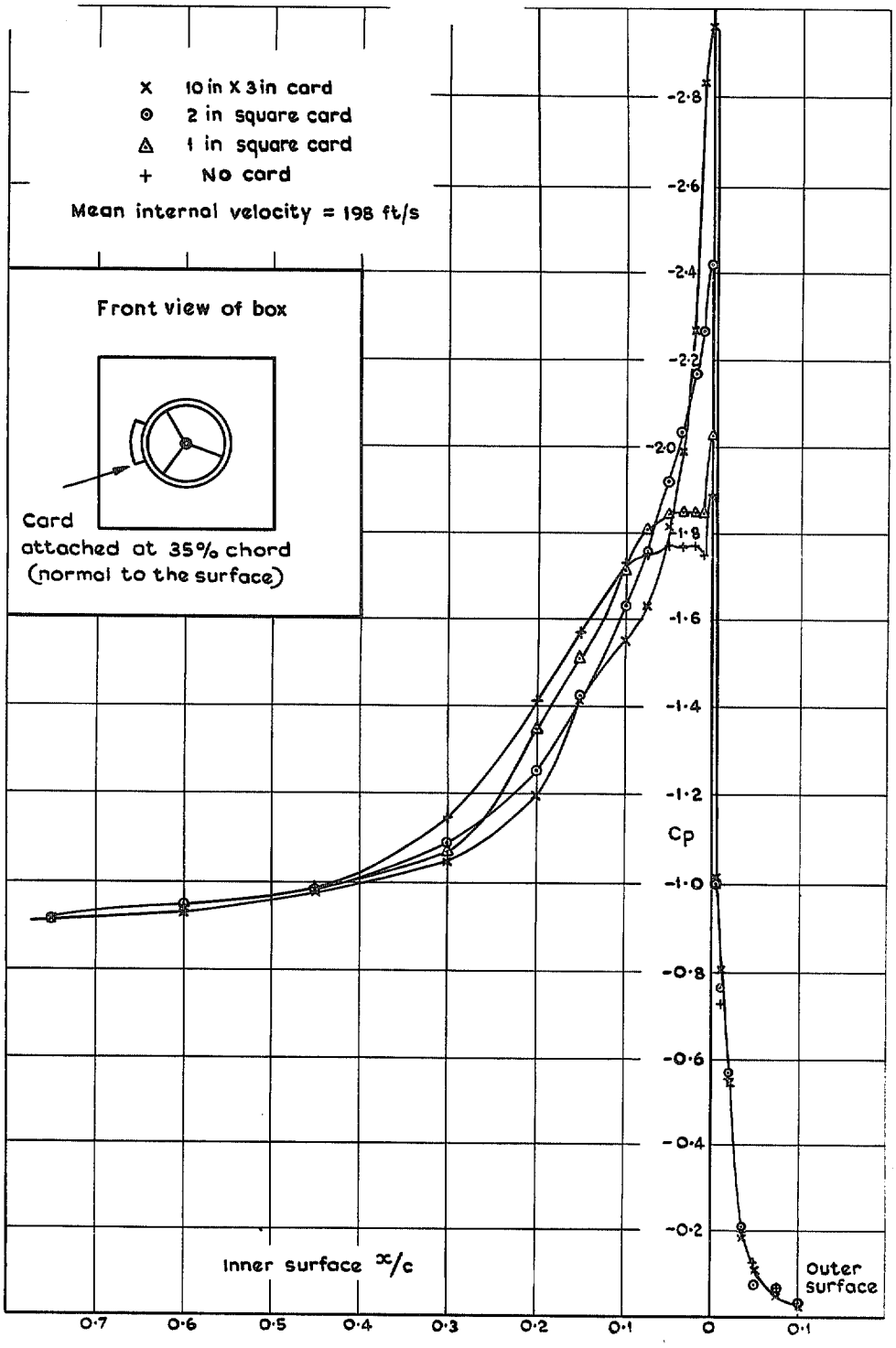

FIG. 50. Static test: cowl 3: pressure distributions with external interference.

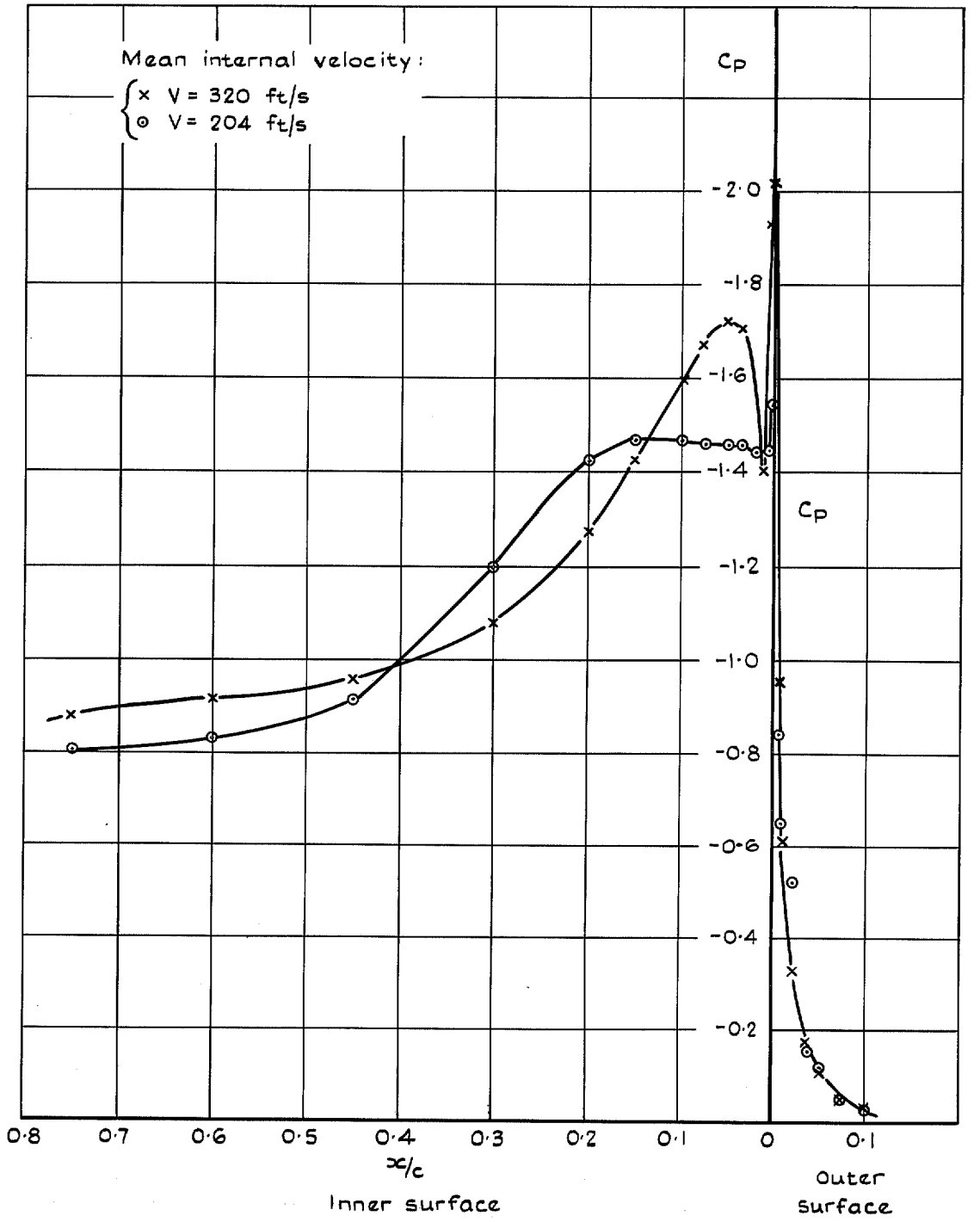

FIG. 51. Static test: cowl 2: surface pressure distribution.

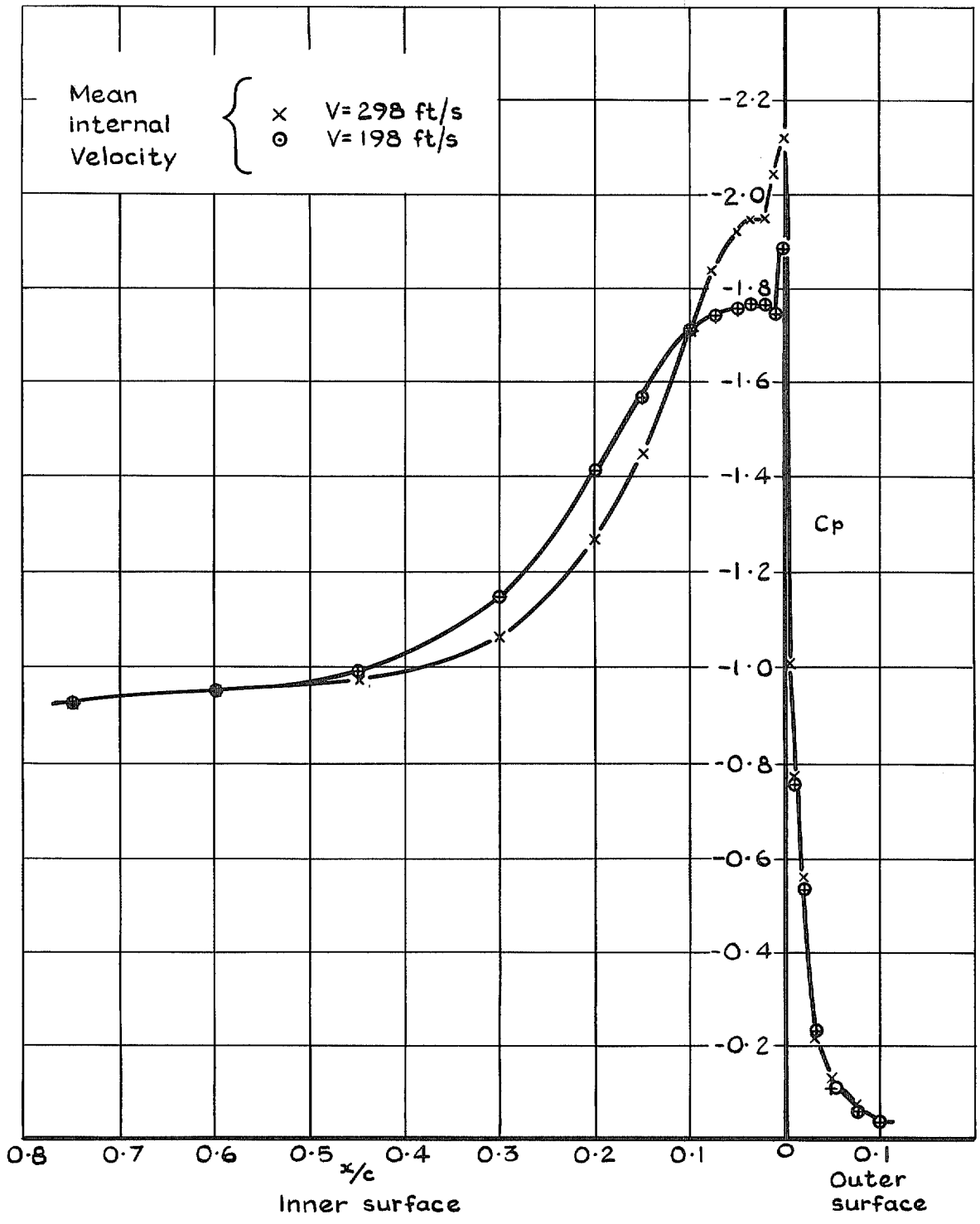

FIG. 52. Static test: cowl 3: surface pressure distribution.

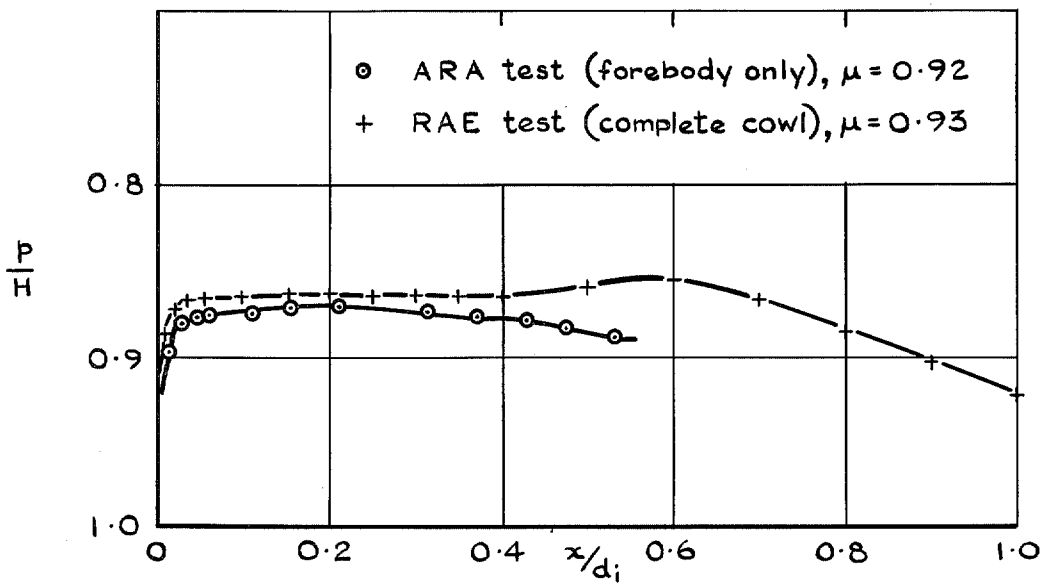

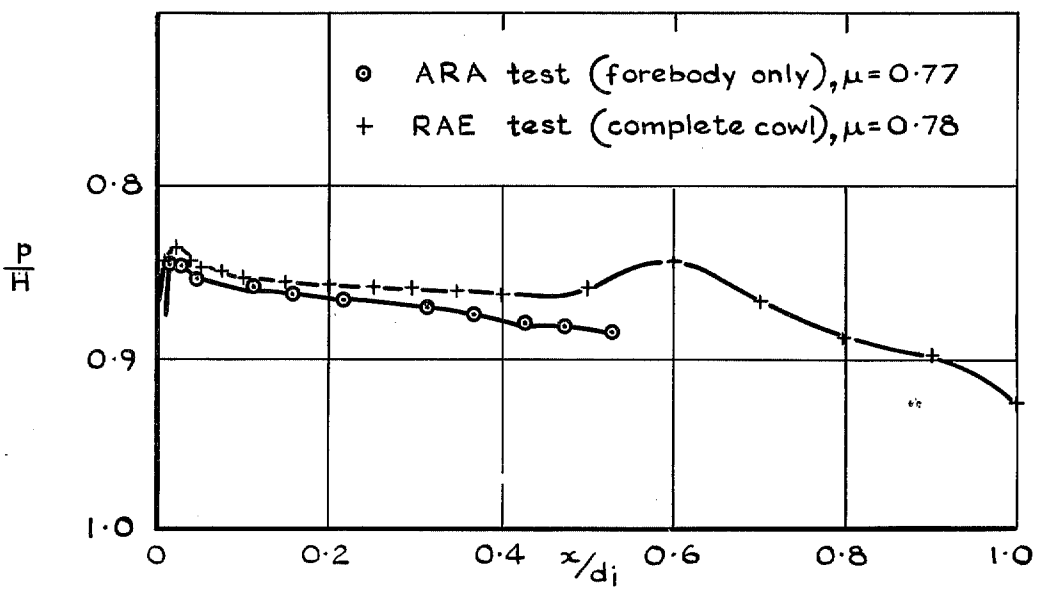

FIG. 53. Comparison between pressure distribution on forebody only and complete cowl: $M = 0{\cdot}4$.

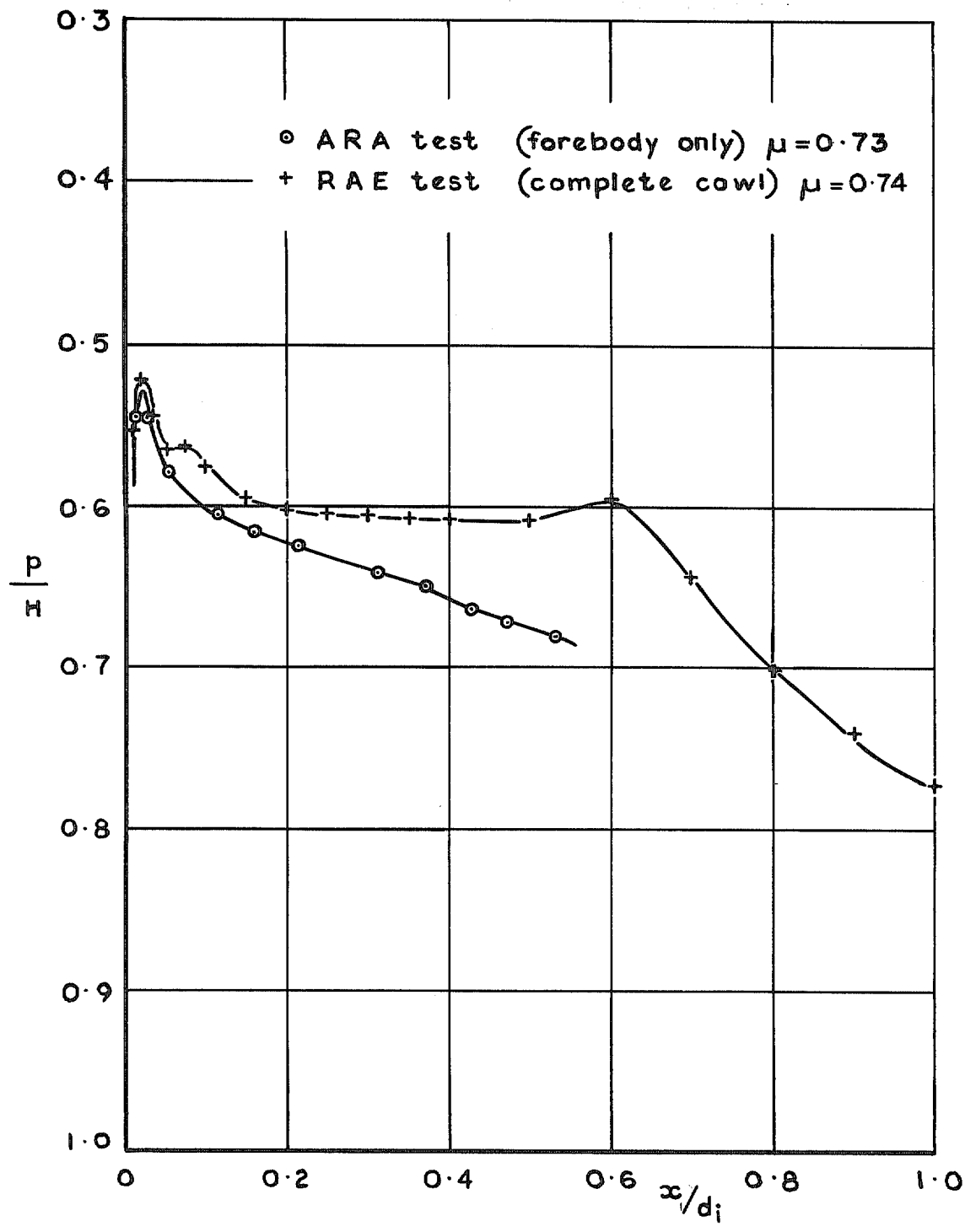

FIG. 54. Comparison between pressure distribution on forebody only and complete cowl: $M = 0{\cdot}70$.

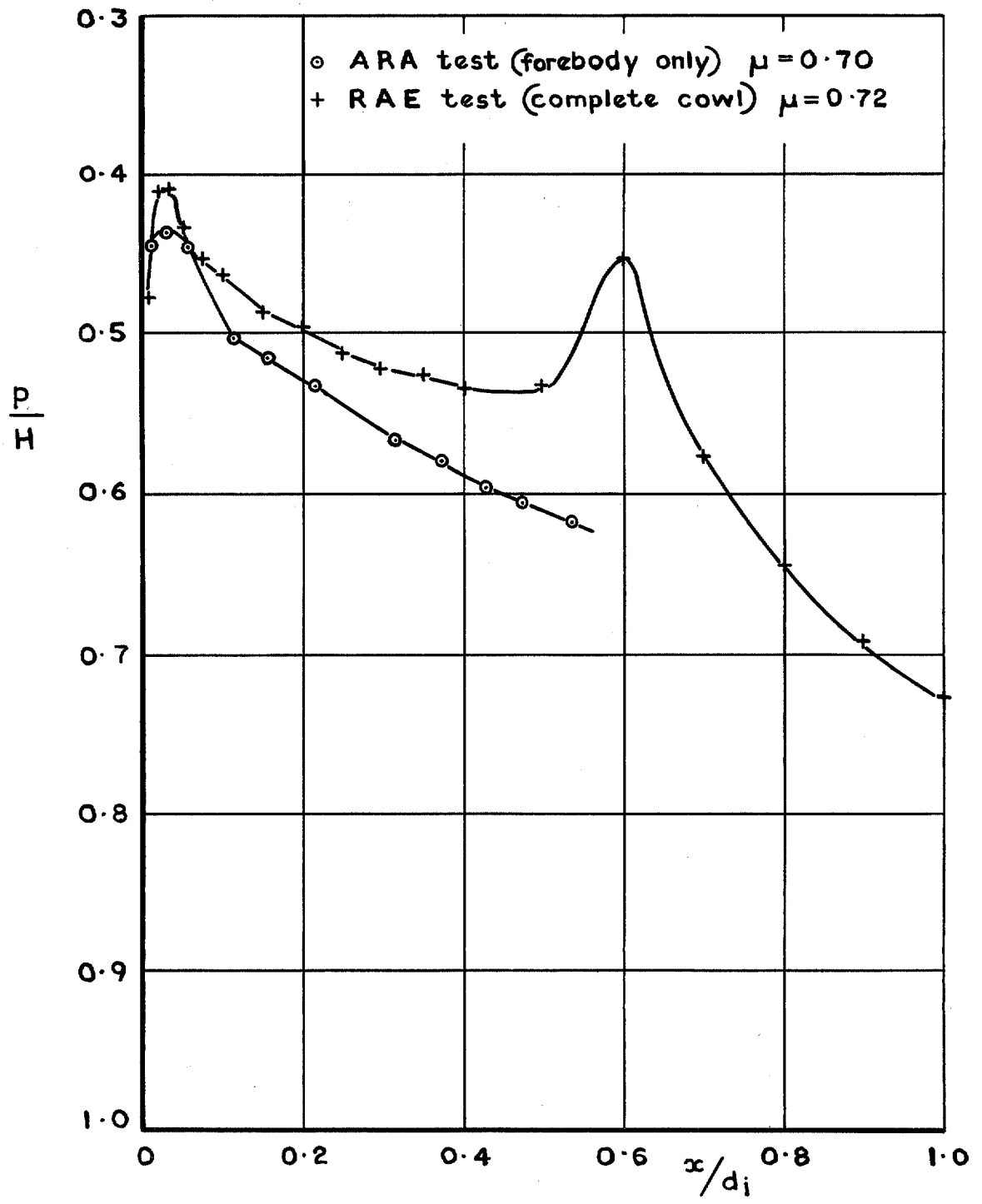

FIG. 55. Comparison between pressure distribution forebody only and complete cowl: $M = 0{\cdot}78$.

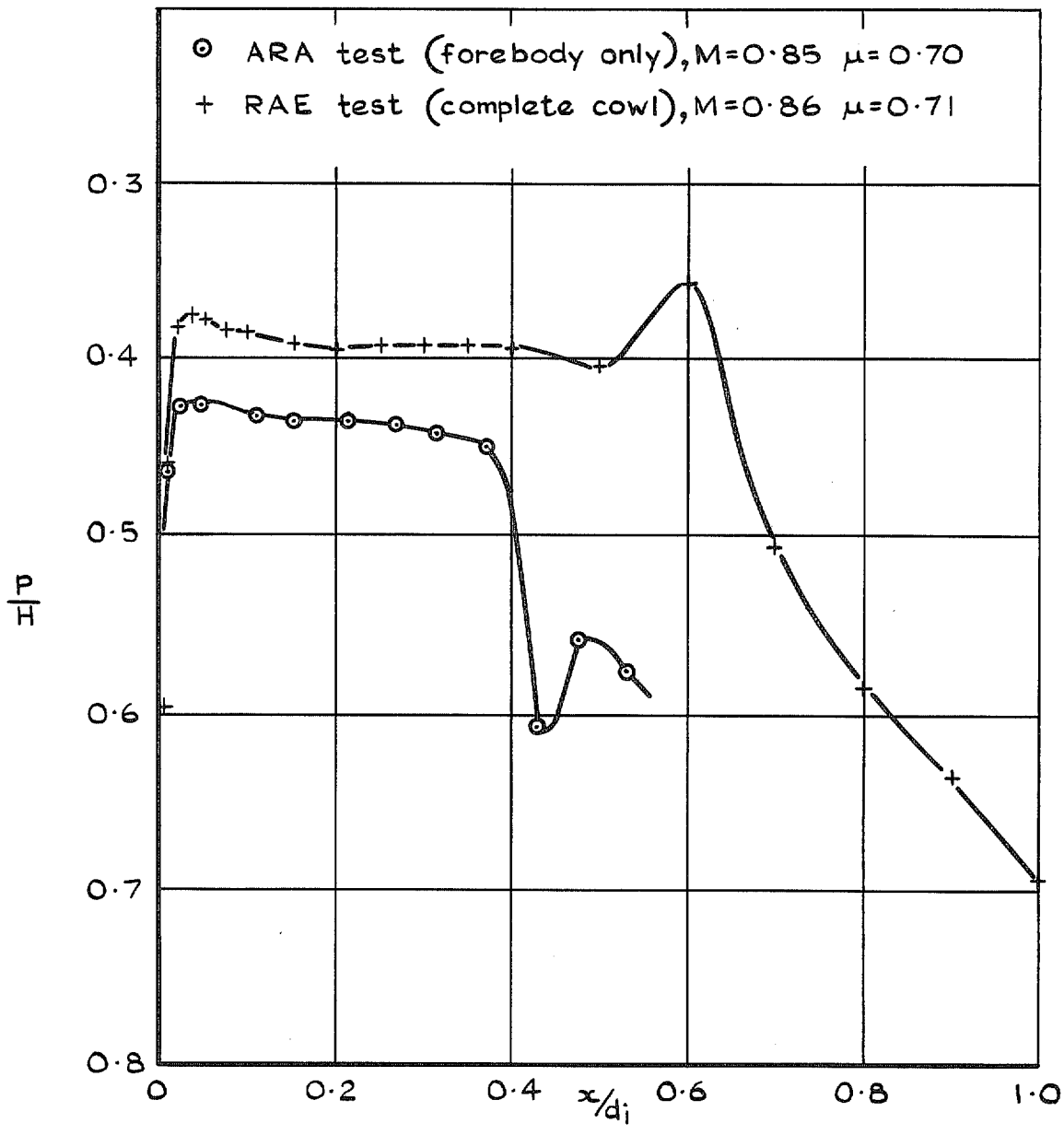

FIG. 56. Comparison between pressure distribution on forebody only and complete cowl: $M = 0{\cdot}85$.

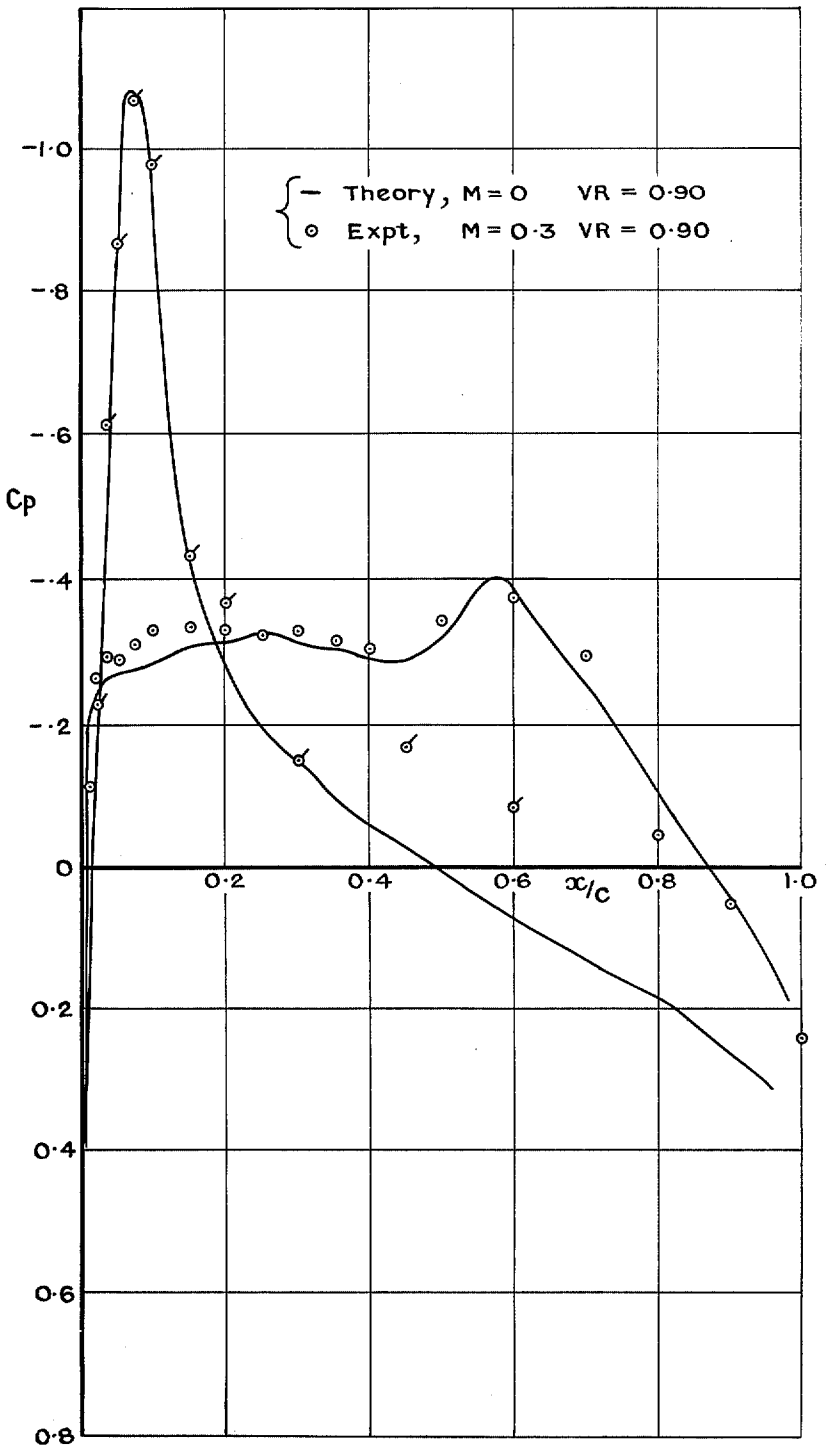

FIG. 57. Comparison with linearised theory: cowl 1.

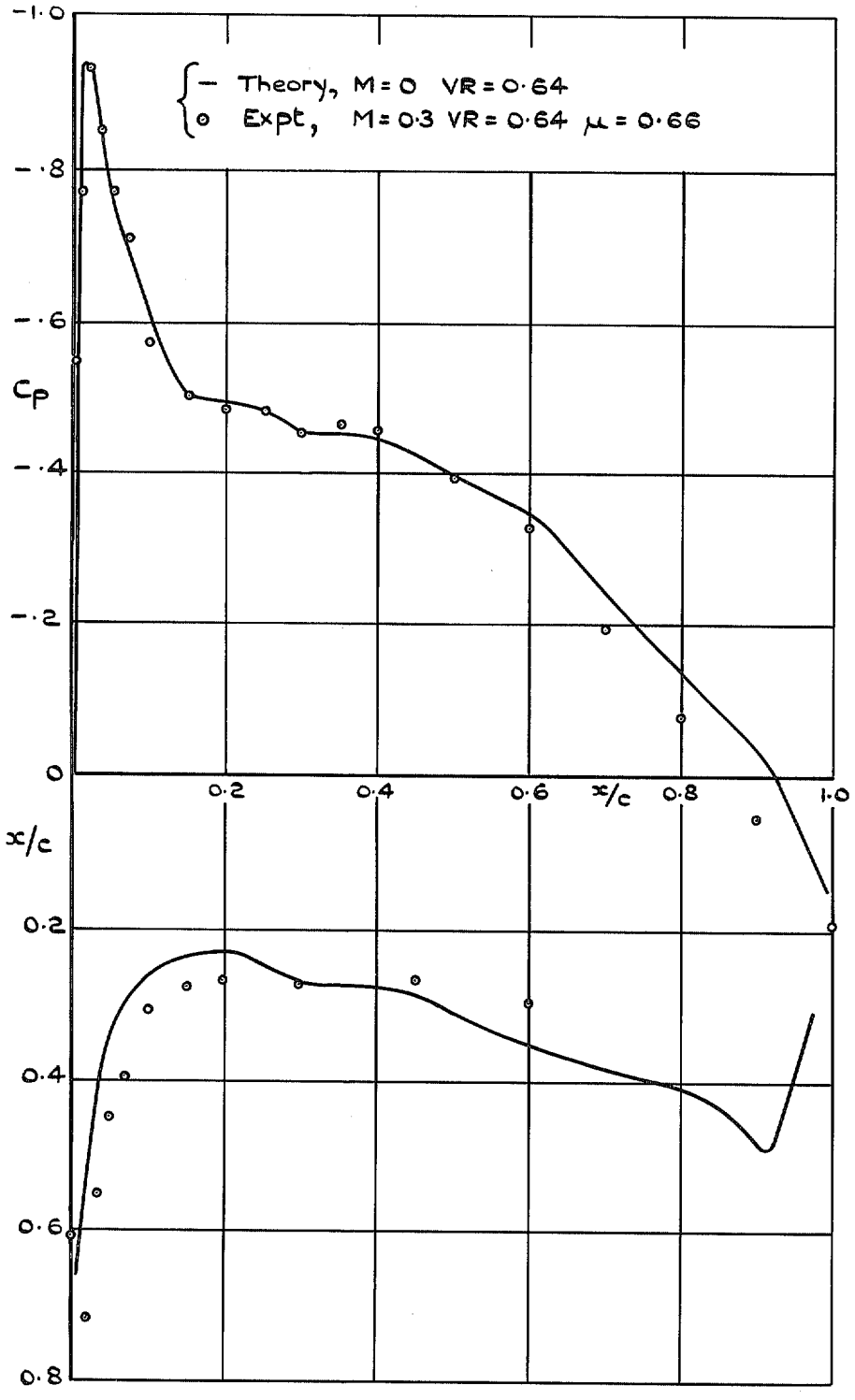

FIG. 58. Comparison with linearised theory: cowl 2.

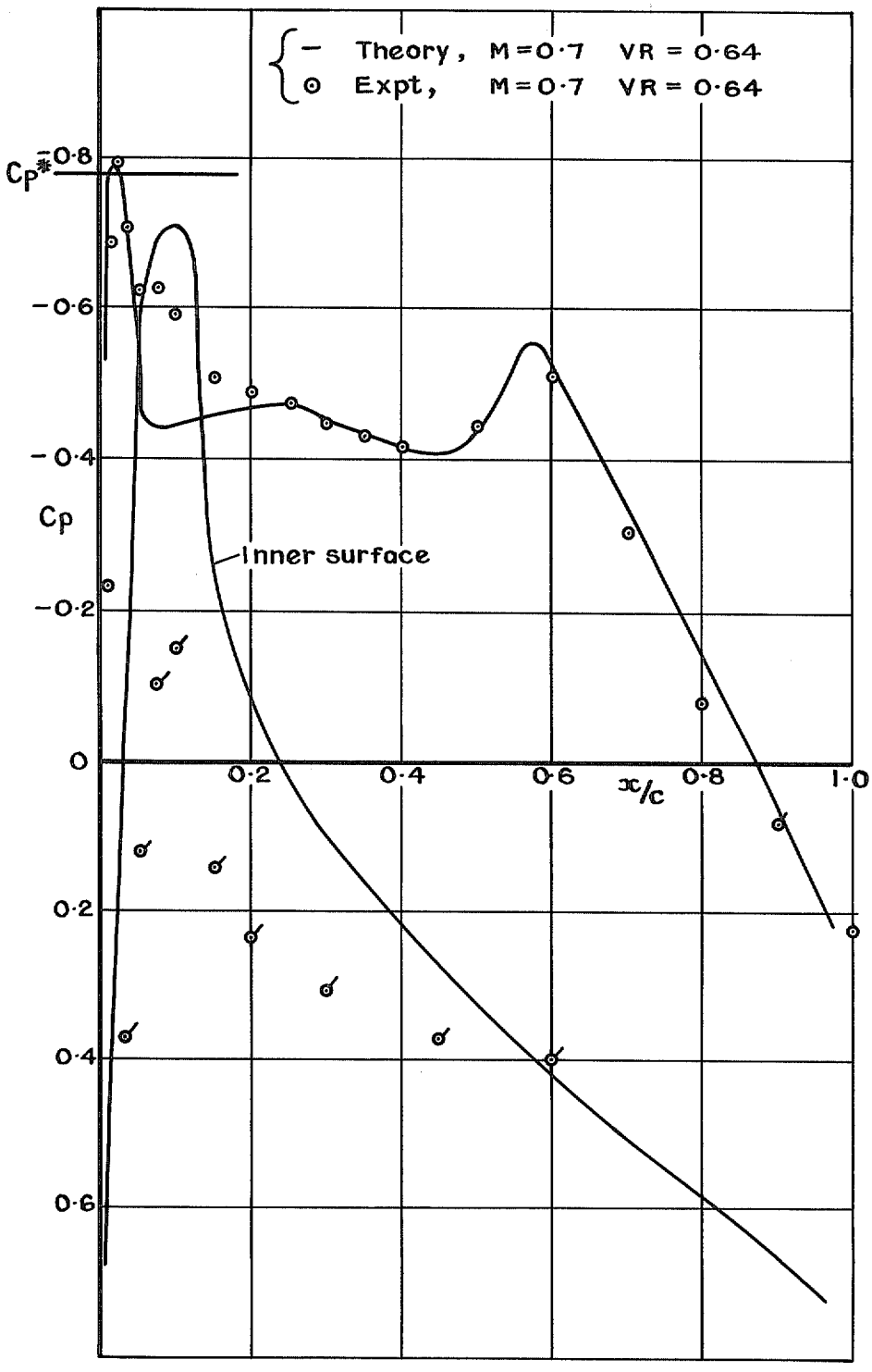

FIG. 60. Comparison with linearised theory: cowl 1.

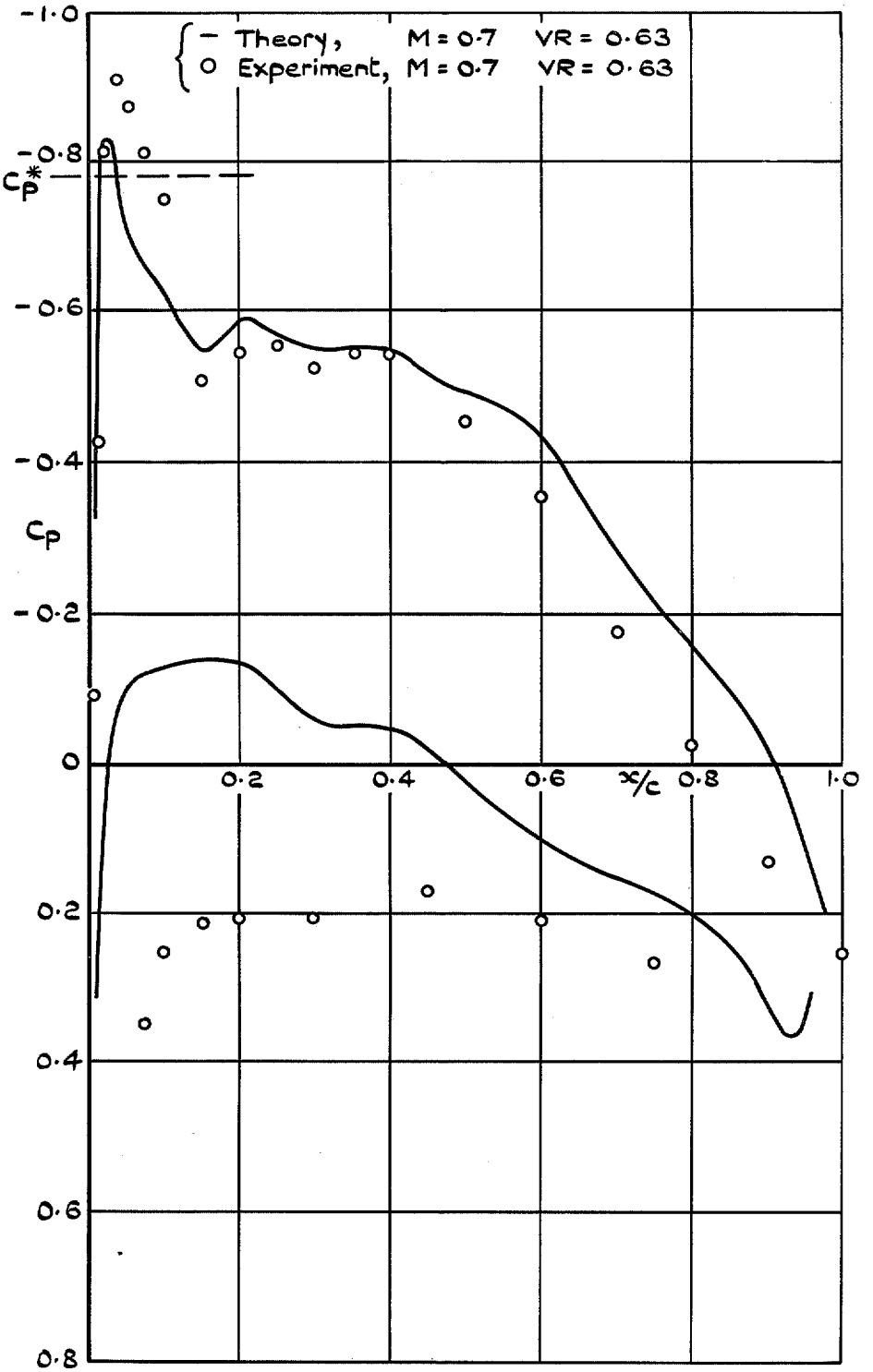

FIG. 61. Comparison with linearised theory: cowl 2.

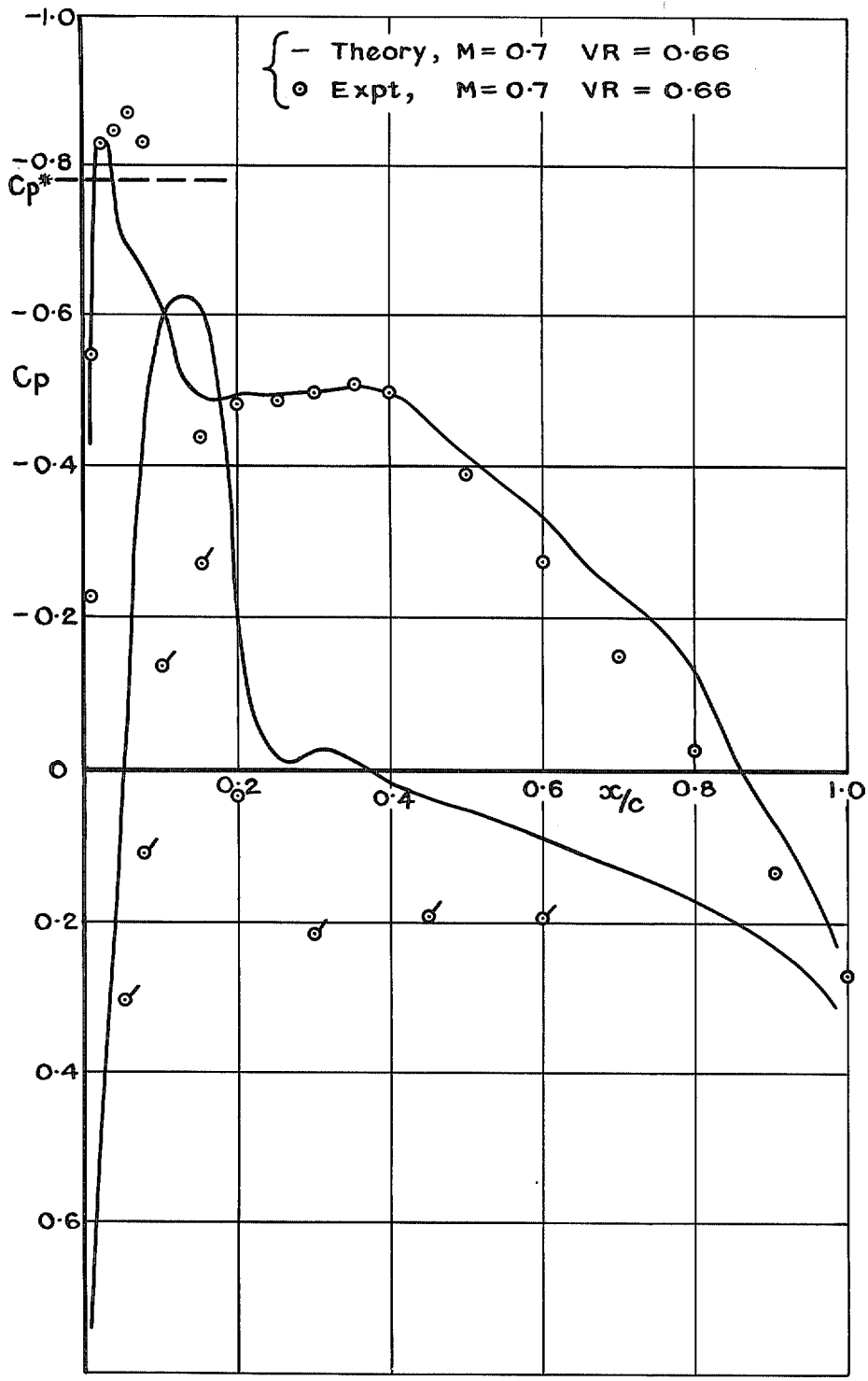

FIG. 62. Comparison with linearised theory: cowl 3.

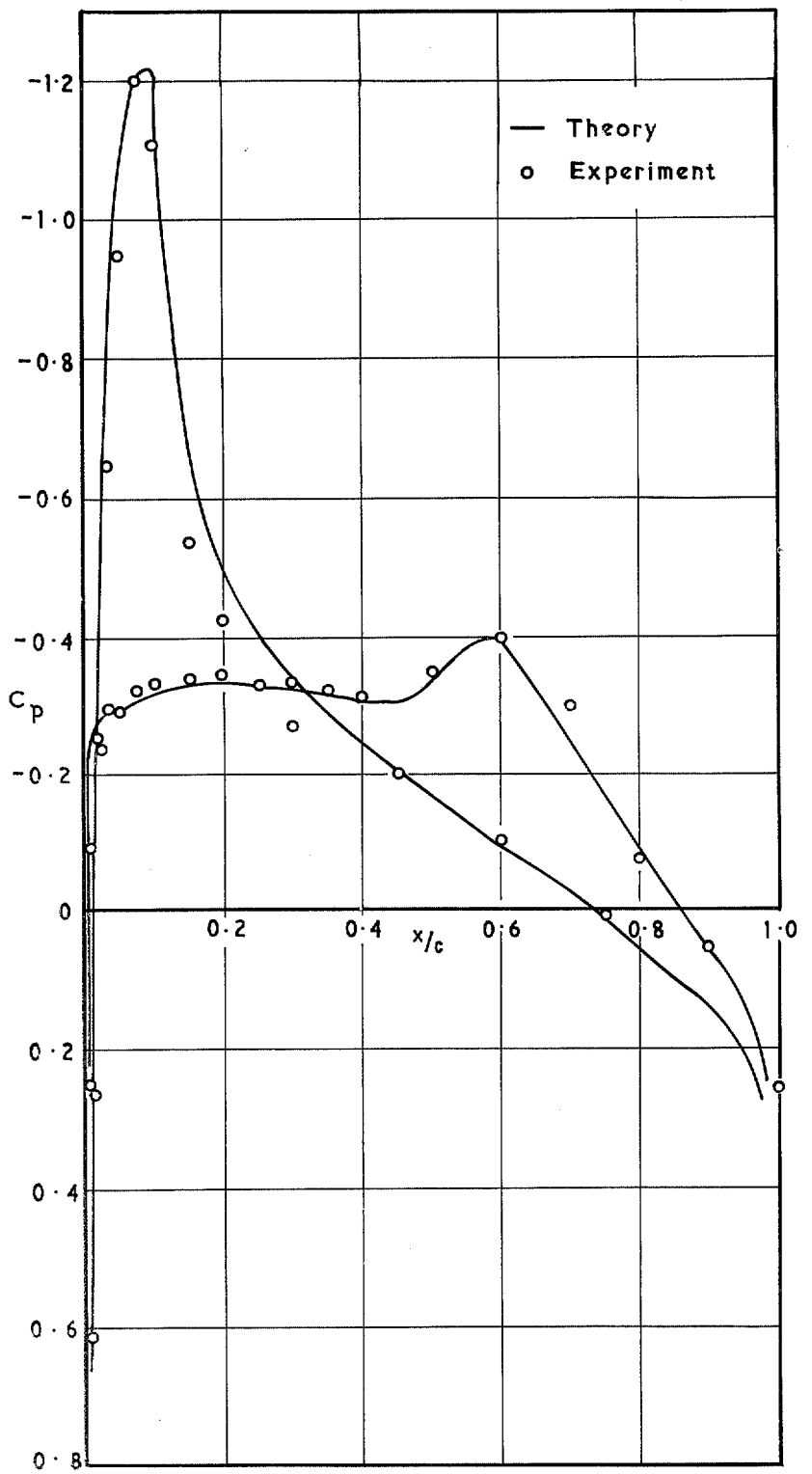

FIG. 63. Comparison with non-linearised theory: cowl 1: $M = 0{\cdot}4$; $\mu = 0{\cdot}93$.

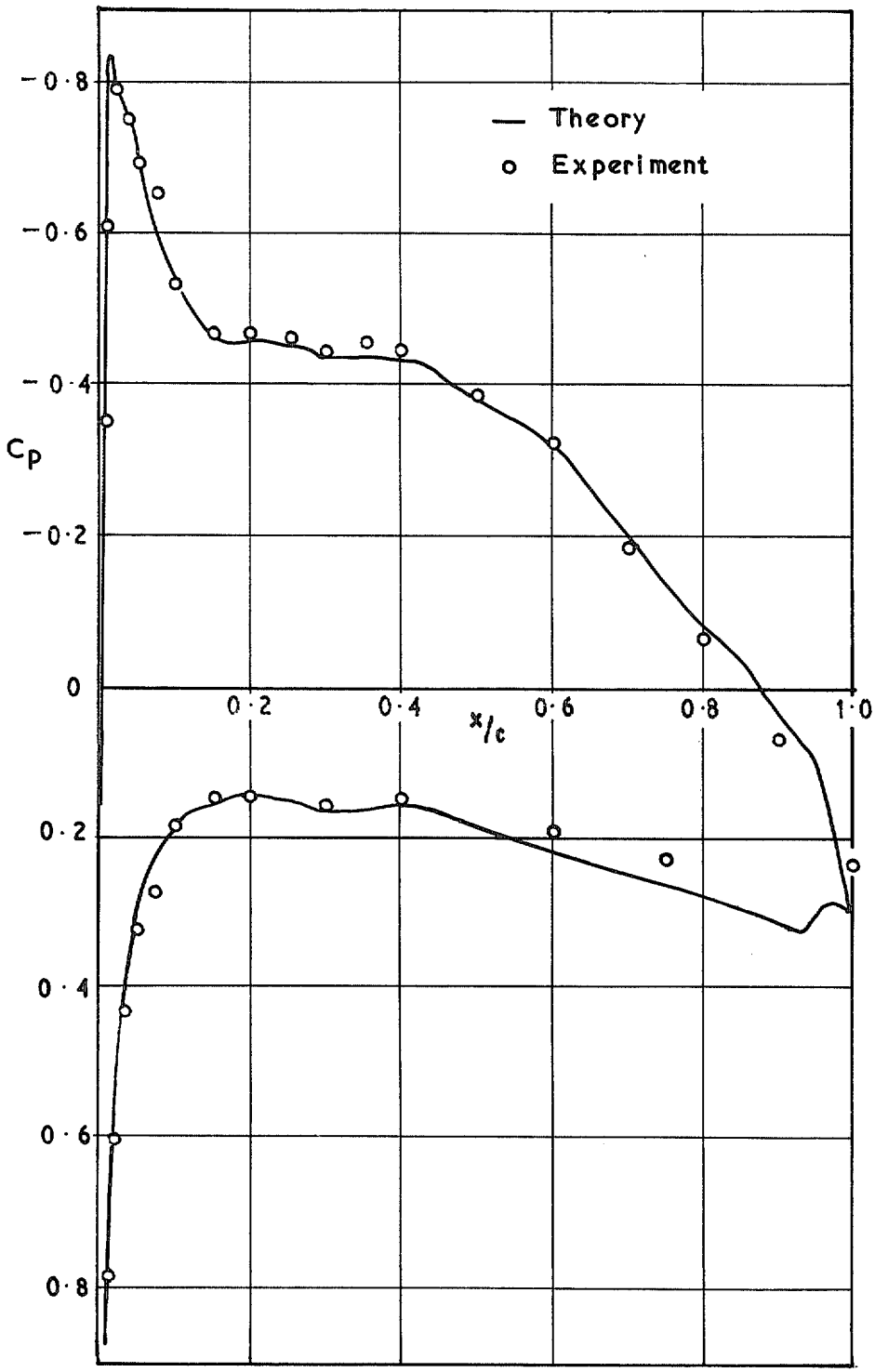

FIG. 64. Comparison with non-linearised theory: cowl 2: $M = 0{\cdot}3$; $\mu = 0{\cdot}72$.

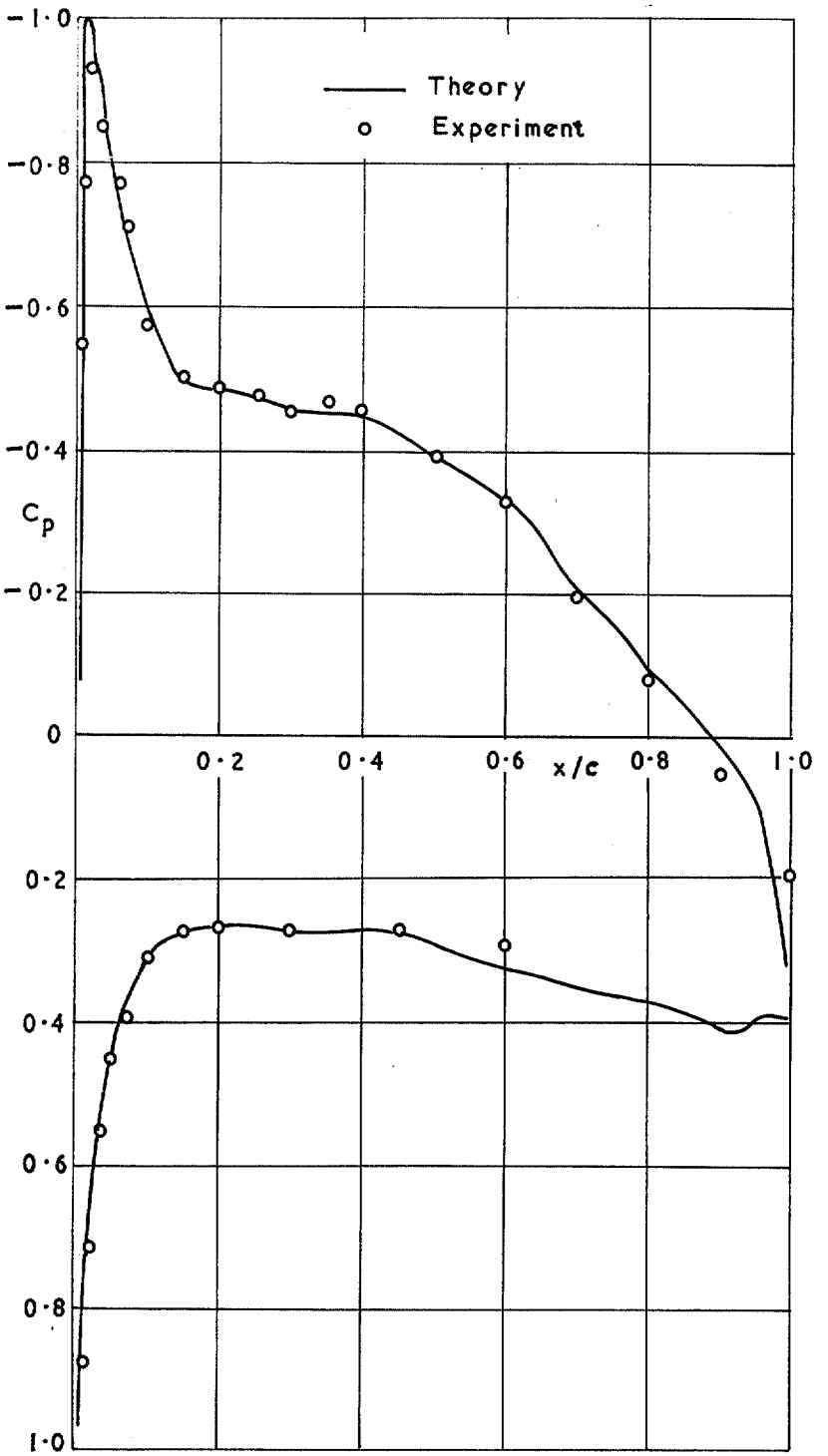

FIG. 65. Comparison with non-linearised theory: cowl 2: $M = 0{\cdot}3$; $\mu = 0{\cdot}68$.

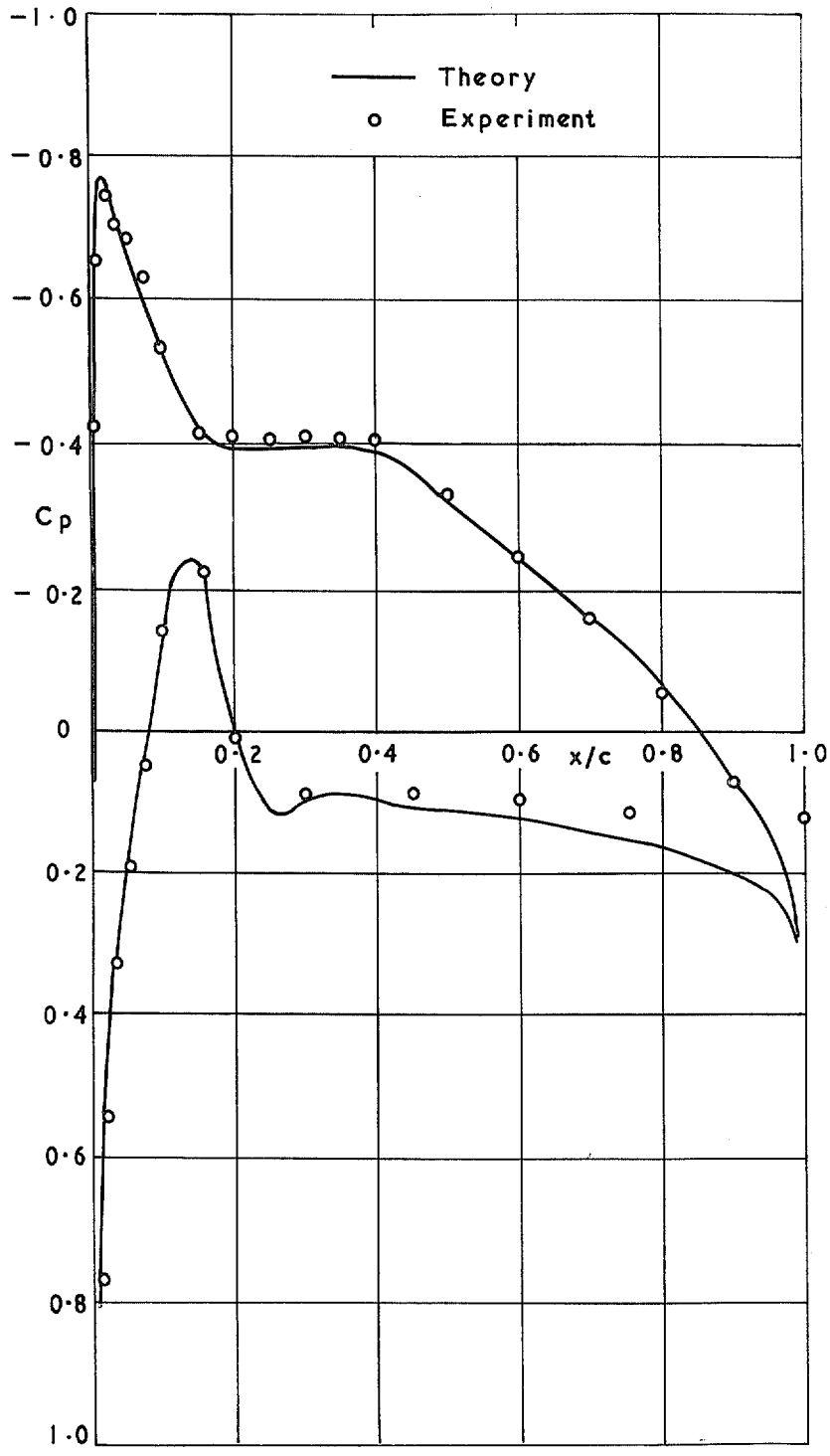

FIG. 66. Comparison with non-linearised theory: cowl 3; $M = 0{\cdot}3$; $\mu = 0{\cdot}76$.

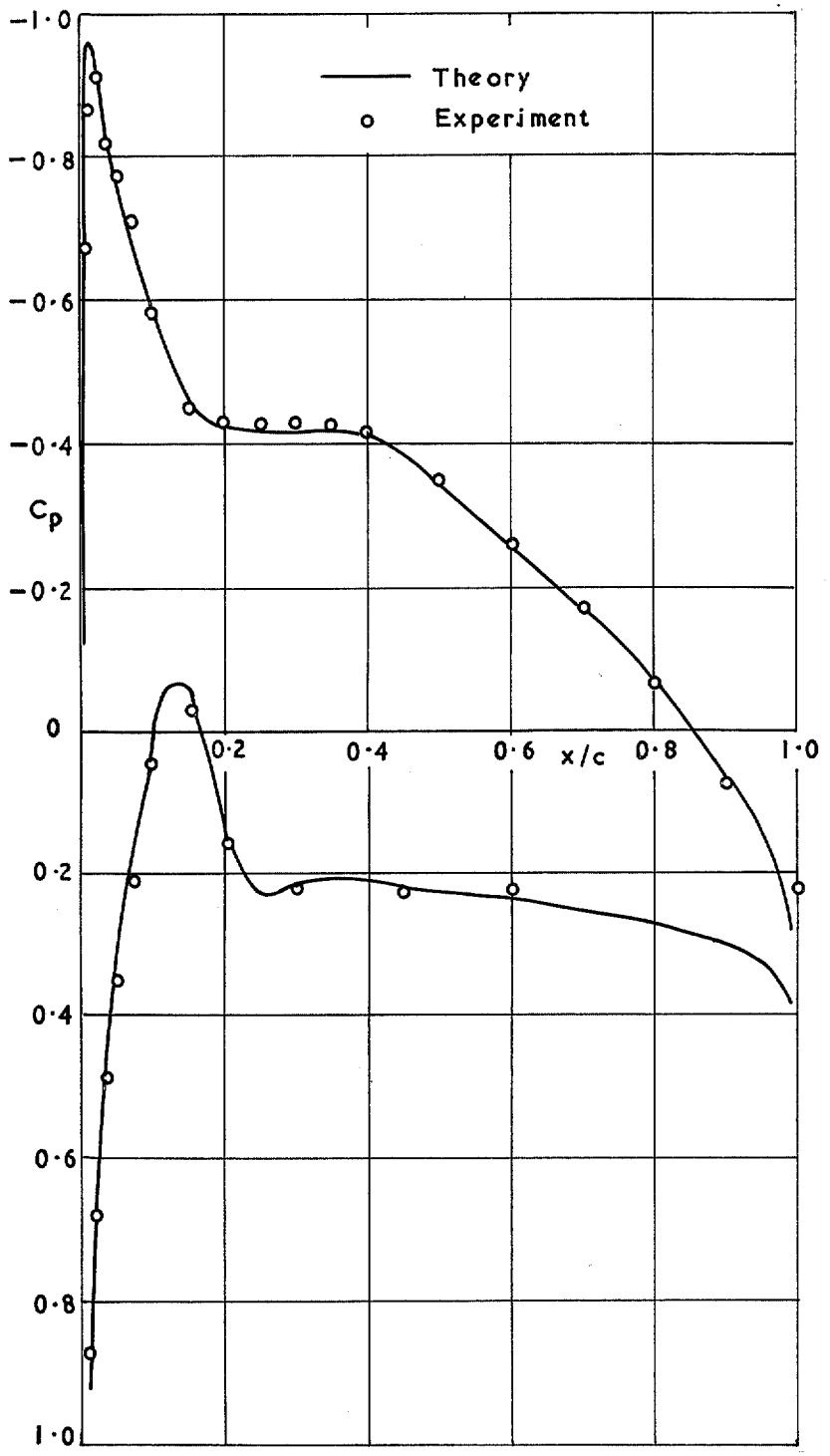

FIG. 67. Comparison with non-linearised theory: cowl 3: $M = 0{\cdot}3$; $\mu = 0{\cdot}71$.

Printed in Wales for Her Majesty's Stationery Office by Allens Printers (Wales) Limited
Dd. 502110 K.5.

Published by
HER MAJESTY'S STATIONERY OFFICE

To be purchased from
49 High Holborn, London WC1V 6HB
13a Castle Street, Edinburgh EH2 3AR
109 St Mary Street, Cardiff CF1 1JW
Brazennose Street, Manchester M60 8AS
50 Fairfax Street, Bristol BS1 3DE
258 Broad Street, Birmingham B1 2HE
80 Chichester Street, Belfast BT1 4JY
or through booksellers

SBN 11 470488 0*